Damage Detection in Reinforcing Steel Bars using Ultrasonic Wave Propagation

A thesis report submitted in the partial fulfillment of the requirements for the award of degree of

MASTERS OF ENGINEERING

IN

STRUCTURAL ENGINEERING

Submitted By

Garima Vermani

Roll No. 80622004

Under the Guidance of

Dr. Abhijit Mukherjee
(*Director, Thapar University*)

Ms. Shruti Sharma
(*Lecturer, CED*)

DEPARTMENT OF CIVIL ENGINEERING

THAPAR UNIVERSITY, PATIALA-147004, INDIA

JANUARY – JUNE (2008)

CERTIFICATE

This is to certify that the work which is presented in this thesis report entitled, "**Damage Detection in Reinforcing Steel Bars using Ultrasonic Wave Propagation** " being submitted by **Garima Vermani** in partial fulfillment of requirements for the award of degree of Master of Engineering in Structural Engineering, at Civil Engineering Department, Thapar University, Patiala, is an authentic record of the initial work carried out by her under the supervision of **Dr. Abhijit Mukherjee , Director,** Thapar University, Patiala and **Ms. Shruti Sharma,** Lecturer, Civil Engineering Department, Thapar University, Patiala.

The matter embodied in this report has not been submitted in part or full to any other university or institute for the award of any degree.

(Dr. Abhijit Mukherjee)
Director , Supervisor
Thapar University, Patiala

24/6/08
(Ms. Shruti Sharma)
Lecturer, CED , Supervisor
Thapar University, Patiala

Countersigned By:

25/6
(Dr. Maneek Kumar)
Professor & Head, CED
Thapar University,
Patiala.

(Dr.R.K.Sharma)
Dean, Academic Affairs
Thapar University,
Patiala.

ACKNOWLEDGEMENT

I take this opportunity to express my sincere gratitude to **Dr. Abhijit Mukherjee, Director**, Thapar University for giving me the opportunity of doing my thesis work under his guidance. I am also thankful to him for his constant supervision and valuable suggestions.

It is my proud privilege to express regards and sincere gratitude to **Ms. Shruti Sharma, Lecturer,** Civil Engineering Department, Thapar University, Patiala, for her patient listening of my ideas and also suggesting new ways for implementing my ideas by her expert guidance throughout my work.

I am also thankful to **Dr. Maneek Kumar, Head Civil Engineering Department,** Thapar University, Patiala, for the motivation and inspiration that triggered me for my thesis work.

I also take this opportunity to thank to the entire faculty and staff of **Civil Engineering Deparment,** Thapar University, Patiala, for their help, inspiration and moral support, which went a long way in successfully completion of this report.

Finally, I want to acknowledge all the little help that I constantly received from my colleagues, T. Raghu Ram, Shailesh and many more.

Garima Vermani

(80622004)

ABSTRACT

In the area of Non destructive testing, ultrasonic testing using wave propagation is an emerging field. Ultrasonic testing uses transmission of high frequency sound waves into a material to detect imperfections or to locate changes in material properties. The most commonly used ultrasonic testing technique is pulse echo and through transmission wherein sound is introduced into a test object and reflections (echoes) are returned to a receiver from internal imperfections. This report presents the use of above two techniques to detect the damage in reinforcing steel bars.

Pulse echo is used to locate the exact position of damage and through transmission is used to know the magnitude of damage in steel rod. Negative spike pulse is used as an input signal to sending transducer at one end of the rod through Pulser/Receiver system and transmitted pulse is received at the other end by receiving transducer. The wave signatures obtained are analysed using mixed-signal oscilloscope and digitizer card. A parametric study is carried out to see the effect of change in location of damage and magnitude of damage on wave propagation through steel rods of variable length. The final results obtained were reported in the form of voltage-time curves.

The characteristics of wave propagation problems are that the frequency content of the exciting force is very high. Therefore, a very fine mesh of finite elements is necessary to adequately model the problem. ABAQUS/Explicit was used as an analytical tool to model the wave propagation through steel rod.

Experimental results obtained are compared with analytical results obtained through ABAQUS/Explicit and are found to be matching with reasonable accuracy.

CONTENTS

LIST OF FIGURES

LIST OF TABLES

CHAPTER 1

INTRODUCTION

1.1 Objectives of the present study

As the design and construction of civil structures continue to evolve, it is becoming imperative that these structures be monitored for their health. In order to meet this need, the discipline of Structural Health Monitoring (SHM) has emerged. It involves the application of wave propagation to civil structures and aims to assist engineers in realizing the full benefits of structural health monitoring. Health of several structures is monitored by recording propagation of stress waves through them. The wave characteristics change due to the deterioration in the structure and they are sensitive to the location, extent and character of damage. However, for a successful monitoring a priori knowledge of the wave characteristic due to different cases is imperative**.**

The overall objectives of the present study are:

- Review of literature on propagation of ultrasonic waves through solids
- Generate and investigate the propagation of ultrasonic waves through the healthy and damaged steel rod specimens using the concept of area reduction.
- Characterize fractures/corrosion in steel and its extent through the analysis and comparison of wave signatures of healthy and damaged steel specimens.
- Acquiring knowledge about ABAQUS/Explicit
- Modeling of wave propagation problem through isotropic medium with and without damage in ABAQUS/Explicit
- Validation of analytical results with experiments.

1.2 Damage detection in steel

1.2.1 Definition of Damage

In the most general terms, damage can be defined as changes introduced into a system that adversely affects its current or future performance. Implicit in this definition is the concept that damage is not meaningful without a comparison between two different states of the system, one of which is assumed to represent the initial, and often undamaged, state. This thesis is focused on the study of damage identification in structural systems; therefore, the definition of damage will be limited to changes to the material and/or geometric properties of these systems, including changes to the boundary conditions and system connectivity, which adversely affect the current or future performance of these systems. As an example, a crack that forms in a mechanical part produces a change in geometry that alters the stiffness characteristics of that part. Depending on the size and location of the crack and the loads applied to the system, the adverse effects of this damage can be either immediate or may take some time before they alter the system's performance. In terms of *length scales*, all damage begins at the material level and then under appropriate loading scenarios progresses to component and system level damage at various rates. In terms of *time scales*, damage can accumulate incrementally over long periods of time such as that associated with fatigue or corrosion damage accumulation.

The process of implementing a damage detection strategy for aerospace, civil, and mechanical engineering infrastructure is referred to as ***Structural Health Monitoring (SHM)***. *Usage monitoring* (UM) attempts to measure the inputs to and responses of a structure before damage so that regression analysis can be used to predict the onset of damage and deterioration in structural condition. *Prognosis* is the coupling of information from SHM, UM, current environmental and operational conditions, previous component and system level testing, and numerical modeling to estimate the remaining useful life of the system.

The damage state is described by answering the following questions:

1) Is there damage in the system (existence)?

2) Where is the damage in the system (location)?

3) What kind of damage is present (type)?

4) How severe is the damage (extent)?

5) How much useful life remains (prognosis)?

The statistical models are used to answer these questions in an unambiguous and quantifiable manner. Experimental structural-dynamics techniques can be used to address the first two questions in either an unsupervised or supervised learning mode. To identify the type of damage, data from structures with the specific types of damage must be available for correlation with the measured features and, hence, a supervised learning approach must be taken. Analytical models are usually needed to answer the fourth and fifth questions unless examples of data are available from the system (or a similar system) when it exhibits varying damage levels. Therefore, the fourth and fifth questions must be addressed in a supervised learning mode.

1.2.2 Damage in Reinforcing steel

Steel reinforced concrete is a widely used and durable construction material. Usually the embedded steel is as durable as the concrete because it is protected by a passivating layer of iron oxide which forms in the alkaline environment prevailing in cement based concrete. But concrete is permeable and if exposed to corrosive agents, these may be able to penetrate through the concrete cover and reach the reinforcing steel. In some cases, this may result in a rapid deterioration in the strength and integrity of the concrete structure. This phenomenon is called ‘Corrosion of reinforcement’ in concrete and is now a feature which figures heavily in the maintenance of existing buildings and has contributed to a number of structural collapses. Besides corrosion, steel embedded in concrete (RC or PSC structures) may be subjected to cracks because of repeated loading or fatigue or overloading though corrosion is the biggest

culprit. The corrosion of reinforcing steel has the following two major detrimental effects on the durability of structures:

(i) Since the rust produced as a result of corrosion has a volume 2–4 times than that of steel, it causes volume expansion developing tensile stresses in concrete, which ultimately results in cracking and spalling of the cover concrete. Due to the loss of cover concrete there may be significant reduction in the load bearing capacity of the structure, and besides this, steel may be more accessible to the aggressive agents leading towards further corrosion at an accelerated rate, and

(ii) Corrosion reduces the cross-sections of the steel and thereby the load carrying capacity of the structure. Pitting (i.e., localized) corrosion of the rebar is more dangerous than uniform corrosion because it progressively reduces the cross-sectional area of rebar to a point where the rebar can no longer withstand the applied load leading to a catastrophic failure of the structure.

Techniques and the methods used presently for damage detection in steel are limited either to visual examination of the state of the structure/members and of the anticorrosive protection applied on their surfaces, the presence of defects/ degradation due to corrosion and the evaluation of changes in the condition of anticorrosive protection or the Non-Destructive Testing or Electrochemical methods.

Table 1.1 gives the list of the various techniques for corrosion assessment of reinforced concrete structures and their specific applications.

Table 1.1: Present Techniques for Corrosion Assessment in Reinforced Concrete

Method	**Detects**
Visual Inspection	Surface cracks
Hammer/Chain	Delamination
Cover meter	Rebar Depth
Phenolphthalein	Carbonation depth
Chloride content	Chloride induced corrosion
Permeability	Diffusion rate
Petrography	Concrete properties
Half Cell	Corrosion risk

Linear polarisation	Corrosion rate
Resistivity	Concrete resistivity
Impact-echo method	Defects/ cracks

All the traditional techniques of corrosion and damage monitoring of steel as described above are either electrochemical in nature or typically fail or encounter problems when applied for in- situ damage monitoring of steel embedded in concrete. They give idea only about the initiation of corrosion but the quantification of corrosion still remains a vital issue.

Hence, there is a need to supplement or replace these methods with an efficient, reliable, in-situ and non-destructive monitoring technique for steel typically for reinforced concrete structures. Present work aims to address the issues discussed above by monitoring state of steel in reinforced concrete using the **ultrasonic wave propagation** principles in conjunction with the use of **piezoelectric transducers as active sensing devices**.

1.3 *Methodology*

Damage detection in steel rods using ultrasonic wave propagation

In the area of structural health monitoring for assessing the damage in reinforced steel bars the wave propagation technique was adopted. Wave Propagation provides an efficient means for characterizing defects in structures. The sudden occurrence of flaws initiated from damage sites in structural solids generates elastic waves which carry important information on the nature of damage. Careful analysis of the waves can reveal the characteristics of the fracture process and damage. Active sensing refers to a regimen which utilizes sensors that are capable of both emitting and sensing signals in order to ascertain the condition of the structure. Knowledge of the condition of the steel in a concrete structure will allow for a more economical condition-based maintenance system rather than traditional schedule-based systems.

1.3.1 Historical Background of wave propagation principles

The history of the study of wave and vibration phenomena goes back hundreds of years. Most early studies were naturally more observational than quantitative and frequently were concerned with musical tones or water waves, two of the most common associations with wave motion. From the time of Galileo onwards, the science of vibrations and wave progressed rapidly in association with developments in the statics of solids. Some of the major developments in the area over the years are chronologically ordered in the following.

Sixth century B.C.: Pythagoras studied the origin of musical sounds and the vibrations of strings.

1636: Mersenne presented the first correct published account on the vibrations of strings.

1638: Galileo described the vibrations of pendulums, the phenomenon of resonance, and the factors influencing the vibrations of strings.

1678: Robert Hooke formulated the law of proportionality between stress and strain for elastic bodies. This law forms the basis for the static and dynamic theory of elasticity.

1686: Newton investigated the speed of water waves and the speed of sound in air.

1700: Sauveur calculated vibrational frequency of a stretched string.

1713: Taylor worked out a completely dynamical solution for the vibrations of a string.

1744: Leonard Euler and Daniel Bernoulli (1751) developed the equation for the vibrations of beams and obtained the normal modes for various boundary conditions.

1747: D'Alembert derived the equation of motion of the string and solved the initial-value problem.

1755: D.Bernoulli developed the principle of superposition and applied it to the vibrations of strings.

1759: Lagrange analyzed the string as a system of discrete mass particles.

1766: Euler attempted to analyze the vibrations of a bell on the basis of the behavior of curved bars. James Bernoulli (1789) also attempted analysis of this problem.

1802: E.F.F. Chladni reported experimental investigations on the vibrations of beams and on the longitudinal and torsional vibrations of rods.

1815: Madame Sophie Germain developed the equations for the vibrations of a plate.

1821: Navier investigated the general equations of equilibrium and vibration of elastic solids. Although not all the developments of the work met with complete acceptance, it represented one of the most important developments in mechanics.

1822: Cauchy developed most of the aspects of the pure theory of elasticity including the dynamical equations of motion for a solid. Poisson (1829) also investigated the general equations.

1828: Poisson investigated the propagation of waves through an elastic solid. He found that two types of waves, longitudinal and transverse, could exist. Cauchy (1830) obtained a similar result. Poisson also solved the problem of the radial vibrations of a sphere.

1828: Poisson developed approximate theories for the vibrations of rods.

1862: Clebsch founded the general theory for the free vibrations of solid bodies using normal modes.

1872: J. Hopkinson performed the first experiments on plastic wave propagation in wires.

1876: Pochhammer obtained the frequency equation for the propagation of waves in rods according to the exact equations of elasticity. Chree (1899) carried out similar studies.

1880: Jaerisch analyzed the general problem of the vibrations of a sphere. The result was obtained independently by Lamb (1882).

1882: Hertz developed the first successful theory for impact.

1883: St. Venant summarized the work on impact of earlier investigators and presented his results on transverse impact.

1887: Rayleigh investigated the propagation of surface waves on a solid.

1888: Rayleigh and Lamb (1889) developed the frequency equation for waves in a plate according to exact elasticity theory.

1904: Lamb made the first investigation of pulse propagation in a semi-infinite solid.

1911: Love developed the theory of waves in a thin layer overlying a solid and showed that such waves accounted for certain anomalies in seismogram records.

1914: B. Hopkinson performed experiments on the propagation of elastic pulses in bars.

1921: Timoshenko developed a theory for beams that accounted for shearing deformation.

1930: Donnell studied the effect of a non-linear stress-strain law on the propagation of stress waves in a bar.

1942: Von Karman, Taylor (1942), and Rakmatulin developed a one dimensional finite-amplitude plastic wave theory.

1949: Davies published an extensive theoretical and experimental study on waves in bars.

1951: Mindlin presented an approximate theory for waves in a plate that provided a general basis for development of higher-order plate and rod theories.

1951: Malvern developed a rate-dependent theory for plastic wave propagation.

1955: Perkeris presented the solution to lamb's problem of pulse propagation in a semi-infinite solid.

Recent developments in the field of wave propagation have dealt with formulating various approximate theories for plates and rods and with the analysis of transient loading situations. In the latter regard, the analysis of pulse propagation in the half-space and in plates and rods has received considerable attention. The application of the digital computer has enabled a number of otherwise intractable problems to be solved.

1.3.2 Applications of Wave Propagation Techniques

In the area of structures, the interest is mainly in the **response to impact or blast loads**. Under transient loads of moderate strength, completely elastic conditions may prevail throughout the structure and elastic wave theory may suffice to predict all aspects of the response. Under more severe loads, local permanent deformation, fracture or perforation of the structure may occur. Studies in this area generally fall in the category of ***anelastic wave propagation***. The waves in a high strength steel rod are used to dynamically load test specimens of weaker materials. Most of the applications are in the area of military and space technology, metal forming processes such as explosive forming, high energy rate forming, or sonic riveting and forging.

Another area in the study of structures involving wave phenomenon is that of **crack propagation** or the interaction of the dynamic stress fields with existing cracks, voids, or inclusions in the material. The concept of a dynamic stress concentration factor finds application in this area.

The field of **ultrasonics** represents another major area of application of wave phenomena. It involves introducing a very low energy level, high frequency stress pulse or 'wave packet' into a material and observing the subsequent propagation and reflection of this energy. The means for introducing and detecting the stress waves are based on the **piezoelectric effect**. By studying the propagation, reflection, and attenuation of ultrasonic pulses, it is possible to determine much fundamental property of materials such as elastic constants and damping characteristics.

Ultrasonic testing is based on time-varying deformations or vibrations in materials, which is generally referred to as acoustics. All material substances are comprised of atoms, which may be forced into vibrational motion about their equilibrium positions. Many different patterns of vibrational motion exist at the atomic level; however, most are irrelevant to acoustics and ultrasonic testing. Acoustics is focused on particles that contain many atoms that move in unison to produce a mechanical wave. When a material is not stressed in tension or compression beyond its elastic limit, its individual particles perform elastic oscillations.

When the particles of a medium are displaced from their equilibrium positions, internal (electrostatic) restoration forces arise. It is these elastic restoring forces between particles, combined with inertia of the particles, that leads to the oscillatory motions of the medium.

Various types of methods based on sound and ultrasound are applied for non destructive testing (NDT). **Acoustic Emission and Ultrasonic Inspection** is the most widely used techniques in industrial applications. The first technique is passive and does not require any external excitation; stress waves are structure-born and produced internally by defects. The second approach requires high- frequency external excitation. The **maturity and proven damage detection** applications are the major advantages of these techniques. The Acousto-Ultrasonic approach combines elements of Acoustic Emission and Ultrasonic inspection.

Acoustic Emission (AE) is one of the first and most widely used NDT techniques for structural damage detection. The technique relies on transient sound waves propagating in the analyzed material. Most of these waves are transient events of significant energy between 100-1000 kHz. The waves can propagate long distances in circles, i.e. in all possible directions. **Therefore AE testing can cover large, often inaccessible, monitored areas**. The distance of propagation depends upon on material properties, geometry, frequency and environment.

Acoustic events at their origin are high-frequency (in MHz), wideband impacts emitted internally by micro cracks and/or inclusion de-cohesion (e.g. Metallic inclusions, bubbles) under external loading applied to monitored specimens. These material defects release elastic energy due to rapid local stress distribution as a result of loading. The energy results from growing cracks, rubbed surfaces of cracks or dislocations. A relatively small number of sensors are required to cover large monitored areas.

Another application of wave propagation is in the field of **Structural Health Monitoring.** Health of several structures is monitored by recording propagation of waves through them. The wave characteristics change due to the deterioration in the structure and they are sensitive to the location, extent and character of damage. However, for a successful monitoring a priori knowledge of the wave characteristic due to different cases is imperative. The forward problem is solved on a numerical model by inflicting different types of damages

on it. The accuracy of the technique depends heavily on the efficacy of the model. Moreover, it is customary to use piezoelectric transducers to generate and record the stress waves. The piezoelectric materials are electromechanically coupled. Therefore, to obtain realistic results it is important to introduce the coupling in the numerical model.

Using wave propagation as a means for monitoring the soundness/ health of structure involves the propagation of acoustic waves through structures. One maps the changes in the wave characteristics to defects. However, to solve the inverse problem one needs a large dataset generated through the solution of forward problems. Wave propagation problems are generally difficult to analyze without resorting to some numerical approaches.

1.3.3 Modes of Wave Propagation

The ultrasonic waves propagate in a number of ways in a medium. On the basis of the mode of particle displacement, these waves can be classified as:

a) Longitudinal or Compression waves(L-waves)
b) Transverse or Shear waves (S-waves)
c) Surface or Rayleigh waves
d) Lamb or Plate waves

- **Longitudinal or Compression waves**

In longitudinal waves, the oscillations occur in the longitudinal direction or the direction of wave propagation. Since compression and dilatational forces are active in these waves, they are also called pressure or compression waves. Compression waves can be generated in liquids, as well as solids because the energy travels through the atomic structure by a series of comparison and expansion (rarefaction) movements. They are also some times called **density waves** because their particle density fluctuates as they move. The velocity of longitudinal ultrasonic waves is about 6000 m/s in steel, 1500 m/s in water and 330 m/s in air approximately.

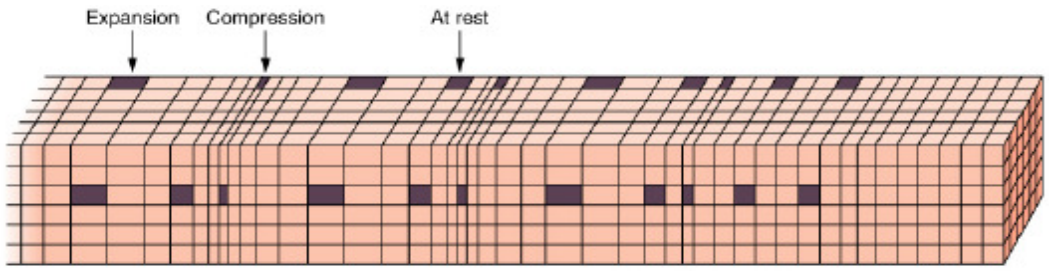

Figure 1.1*: *Propagation of Longitudinal waves

- **Transverse or Shear waves**

In the transverse or shear wave, the particles oscillate at a right angle or transverse to the direction of propagation.

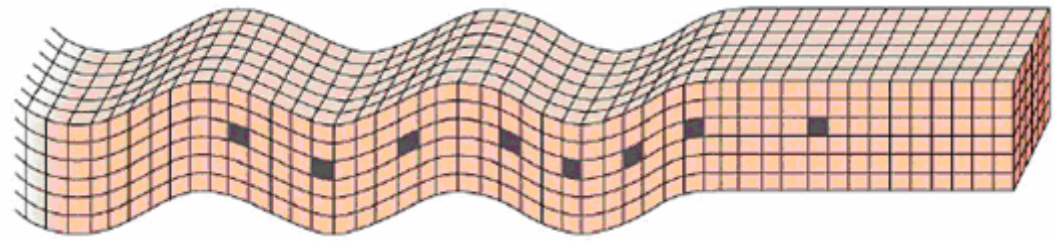

Figure1.2*: *Propagation of Transverse or Shear waves

Shear waves require an acoustically solid material for effective propagation, and therefore, are not effectively propagated in materials such as liquids or gasses. Shear waves are relatively weak when compared to longitudinal waves. S-waves polarized in the horizontal plane are classified as SH-waves. If polarized in the vertical plane, they are classified as SV-waves. When an S- or P-wave strikes an interface at an angle other than 90 degrees, a phenomenon known as **mode conversion** occurs.

- **Surface (or rayleigh) waves**

Surface (or Rayleigh) waves travel the surface of a relatively thick solid material penetrating to a depth of one wavelength. The particle movement has an elliptical orbit as shown in the image and animation below. Rayleigh waves are useful because they are very sensitive to surface defects and they follow the surface around curves. Because of this, Rayleigh waves can be used to inspect areas that other waves might have difficulty reaching.

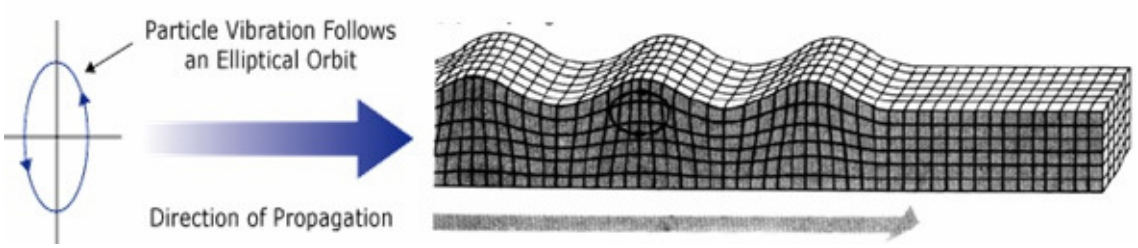

Figure 1.3: Propagation of Surface or Rayleigh Waves

- **Lamb waves or plate waves**

Plate waves can be propagated only in very thin metals. Lamb waves are the most commonly used plate waves in NDT. Lamb waves are complex vibrational waves that travel through the entire thickness of a material. Propagation of lamb waves depends on the density and the elastic material properties of a component. They are also influenced a great deal by the test frequency and material thickness.

With lamb waves, a number of modes of particle vibration are possible, but the two most common are symmetrical and asymmetrical. The complex motion of the particles is similar to the elliptical orbits for surface waves. Symmetrical lamb waves move in a symmetrical fashion about the median plane of the plate. This is sometimes called the extensional mode because the wave is “stretching and compressing” the plate in the wave

motion direction. Wave motion in the symmetrical mode is most efficiently produced when the exciting force is parallel to the plate. The asymmetrical lamb wave mode is often called the "flexural mode" because a large portion of the motion moves in a normal direction to the plate, and a little motion occurs in the direction parallel to the plate. In this mode, the body of the plate bends as the two surfaces move in the same direction.

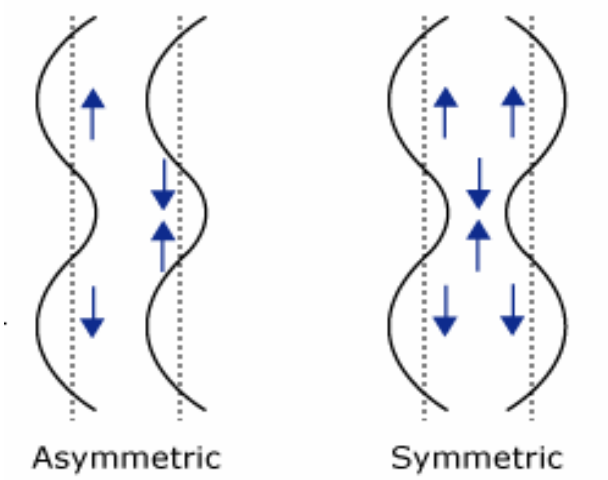

Figure 1.4*: *Lamb Waves Propagation (a) Symmetrical (Dilatational) and (b) Asymmetrical (Bending) waves

1.3.4 Mechanics of wave propagation

Equilibrium Equations

If a body is in equilibrium, then the resultant force and moment on that body must be equal to zero. We have two equilibrium equations:

Force Equilibrium Equation: $$\frac{\partial \sigma_{ji}}{\partial x_j} + f_i = \sigma_{ji} + f_i = 0 \qquad (1.1)$$

Moment Equilibrium Equation: $$\sigma_{ij} = \sigma_{ji} \qquad (1.2)$$

The stress strain relation for isotropic material is given by **Green** as:

$$\boldsymbol{\sigma_{ij} = \lambda\, \delta_{ij}\, \varepsilon_{kk} + 2\, \mu\, \varepsilon_{ij}} \qquad (1.3)$$

where $\lambda = \frac{\nu}{(1-2\nu)(1+\mu)} E$, $\mu = \frac{E}{2(1+\nu)}$ are Lame's first and second constants

$\varepsilon_{ij}=\sigma_{ii}$ (1.4)

Putting the above value of stress strain relationship 1.3 in equilibrium equation 1.1 we get:-

$$(\lambda + \mu)\underline{\nabla}(\underline{\nabla}.u) + \mu\nabla^2 u + f = 0 \quad (1.5)$$

This is the **Navier's Equation**. In index notations it can also be written as:-

$$(\lambda + 2\mu)u_{j,ji} - \mu\varepsilon_{ijk}\varepsilon_{kmn}u_{n,mj} + f_i = 0 \quad (1.6)$$

Where $\varepsilon_{ijk \text{ and}}$ ε_{kmn} are permutation symbols that takes the value 1,-1, or 0. If the subscripts i,j,k have three distinct values of 1,2, and 3 (or 2,3,1 or 3,1,2), respectively then its value is 1; if the values of the subscripts are in the opposite order of 3,2 and 1 then ε_{ijk} is -1.If i,j, and k do not have three distinct values, then $\varepsilon_{ijk}= 0$.

One dimensional problem can be easily solved by Navier's equation where only one component of the problem is nonzero, and this nonzero displacement component is a function of only one variable. But the displacement field in the half space material has two components of displacement, u_1 and u_2, and both of them will be functions of x_1 and x_2 in general. Thus it is very difficult to solve two and three dimensional problems directly from the Navier's equation. Thus ***Stokes- Helmholtz*** decomposition of the displacement field transforms the Navier's governing equation of motion into simple wave equation below.

If ϕ is a scalar function and **A** is a vector function, then any displacement field **u** can be expressed in the following manner:

$$u = \underline{\nabla}\phi + \underline{\nabla} \times A \quad (1.7)$$

The above decomposition is known as the **Stokes-Helmholtz decomposition**. Since the above vector equation has three parameters (u_1, u_2, u_3) on the left-hand side and four parameters (ϕ, A_1, A_2, A_3) on the right-hand side, one can define an additional relation (known as auxiliary condition)

$$\underline{\nabla}.A = 0 \tag{1.8}$$

to obtain unique relations between u_1, u_2, u_3 and ϕ, A_1, A_2, A_3. Substituting Equation 1.8 in the Navier's equation, in absence of a body force, one gets

$$(\lambda + 2\mu)\underline{\nabla}(\underline{\nabla}.u) - \mu\underline{\nabla}\times\underline{\nabla}\times u = \rho\ddot{u}$$

$$\Rightarrow (\lambda + 2\mu)\underline{\nabla}(\underline{\nabla}.\{\underline{\nabla}\phi + \underline{\nabla}\times A\}) - \mu\underline{\nabla}\times\underline{\nabla}\times\{\underline{\nabla}\phi + \underline{\nabla}\times A\} = \rho\{\underline{\nabla}\ddot{\phi} + \underline{\nabla}\times\ddot{A}\}$$

$$\Rightarrow (\lambda + 2\mu)\underline{\nabla}\left(\underline{\nabla}^2\phi + \underline{\nabla}.\{\underline{\nabla}\times A\}\right) - \mu\underline{\nabla}\times\underline{\nabla}\times\{\underline{\nabla}\phi + \underline{\nabla}\times A\} = \rho\{\underline{\nabla}\ddot{\phi} + \underline{\nabla}\times\ddot{A}\} \tag{1.9}$$

However, from the vector identity one can write

$$\underline{\nabla}.(\underline{\nabla}\times A) = 0$$

$$\underline{\nabla}.(\underline{\nabla}\phi) = 0$$

$$\underline{\nabla}\times\underline{\nabla}\times A = \underline{\nabla}(\underline{\nabla}.A) - \nabla^2 A \tag{1.10}$$

Substituting Equation 1.10 and Equation 1.8 into Equation 1.9 one gets

$$(\lambda + 2\mu)\underline{\nabla}(\nabla^2\phi) - \mu\underline{\nabla}\times(-\nabla^2 A) = \rho\{\underline{\nabla}\ddot{\phi} + \underline{\nabla}\times\ddot{A}\}$$

$$\Rightarrow \underline{\nabla}\left[(\lambda + 2\mu)\nabla^2\phi - \rho\ddot{\phi}\right] + \underline{\nabla}\times\left[\mu\nabla^2 A - \rho\ddot{A}\right] = 0$$

Sufficient conditions for the above equation to be satisfied are

$$(\lambda + 2\mu)\nabla^2\phi - \rho\ddot{\phi} = 0$$

$$\mu\nabla^2 A - \rho\ddot{A} = 0$$

or

$$\nabla^2\phi - \frac{\rho}{(\lambda+2\mu)}\ddot{\phi} = \nabla^2\phi - \frac{1}{c_P^2}\ddot{\phi} = 0 \qquad (1.11)$$

$$\nabla^2 A - \frac{\rho}{\mu}\ddot{A} = \nabla^2 A - \frac{1}{c_s^2}\ddot{A} = 0$$

The equations in Equation 1.11 are wave equations that have solutions in the following form:

$$\phi(x,t) = \phi(n.x - c_p t)$$

$$A(x,t) = A(n.x - c_s t) \qquad (1.12)$$

The equations in 1.12 represent two waves propagating in the n direction with the velocity of c_p and c_s, respectively. Note that n is the unit vector in any direction.

When A = 0 and φ = nonzero, then from the above solutions one gets

$$u = \underline{\nabla}\phi = n\phi'(n.x - c_p t) \qquad (1.13)$$

When A is not equal to 0 and ϕ is 0, then from the above solutions one gets

$$u = \underline{\nabla} \times A = \underline{\nabla} \times A(n.x - c_s t) \qquad (1.14)$$

Three components of displacement in the Cartesian coordinate system can be written from Equation 1.14:

$$u_1 = n_2 A_3'(n.x - c_s t) - n_3 A_2'(n.x - c_s t)$$

$$u_2 = n_3 A_1'(n.x - c_s t) - n_1 A_3'(n.x - c_s t) \qquad (1.15)$$

$$u_3 = n_1 A_2'(n.x - c_s t) - n_2 A_1'(n.x - c_s t)$$

Clearly the dot product between n and u is zero; hence, the direction of the displacement vector us is perpendicular to the wave propagation direction n. Displacement fields given in Equation 1.13 and Equation 1.14 correspond to **P- and S-waves**, respectively.

1.3.4.1 P- and S-Waves

Elastic waves in an infinite elastic solid can propagate in two different modes: P-wave mode and S-wave mode. When an elastic wave propagates as the P-wave, then only normal stresses (compression or dilatational) are generated in the solid and the wave propagation speed is

$$c_p \left(= \sqrt{\frac{\lambda + 2\mu}{\rho}} \right)$$

When the elastic wave propagates as the S-wave, then only shear stresses are generated in the solid and the propagation speed is

$$c_s \left(= \sqrt{\frac{\mu}{\rho}} \right).$$

Wave potentials for these two types of waves, propagating in a three-dimensional space in direction n, are given by Equation 1.12. If the problem is simplified to an in-plane problem where the waves propagate in one plane (say $x_1 x_2 - plane$), then the wave potentials, ϕ and ψ, for these two types of waves can be written in the following form:

$$\begin{aligned} \phi(x,t) &= \phi(n.x - c_p t) = \phi(n_1 x_1 + n_2 x_2 - c_p t) = \phi(x_1 \cos\theta + x_2 \sin\theta - c_p t) \\ \psi(x,t) &= \psi(n.x - c_s t) = \psi(n_1 x_1 + n_2 x_2 - c_s t) = \psi(x_1 \cos\theta + x_2 \sin\theta - c_s t) \end{aligned} \qquad (1.16)$$

Equation 1.16 represents waves propagating in direction n in the $x_1 x_2$ - plane.

Note that in any plane normal to the wave propagation direction n the displacement and stress components are identical. In other words, every point on a plane normal to n has the

same state of motion; these planes are called wavefronts, and the propagating P- and S-waves with plane wavefronts are called **plane waves**.

1.3.4.2 P-Wave Incident on a Stress-Free Plane Boundary

First consider the effect of a stress-free boundary on the plane P-wave propagating in the direction as shown in **Figure 1.5**. It will be shown here that the reflected wave from the stress-free boundary will have two components: a P-wave component (denoted by PP) and as S-wave component (denoted by PS). In these notations the first letter indicates the type of wave that is incident on the stress-free surface, and the second subscript indicates the type of wave generated after the reflection at the surface.

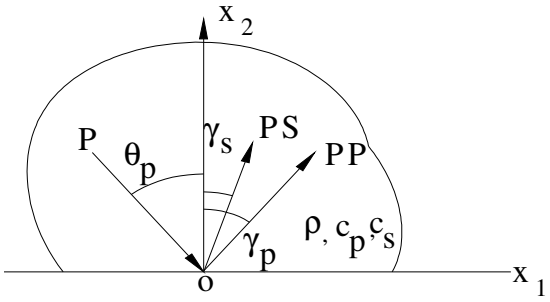

Figure 1.5: Reflection of a plane P- wave by a stress free plane boundary

In the absence of reflected waves PP and PS, let us first investigate if only the incident P-wave can satisfy the stress-free boundary conditions at $x_2 = 0$.

Wave potential for the incident P-wave shown in Figure is given by

$$\phi = \exp\left(ik_p x_1 \sin\theta_p - ik_p x_2 \cos\theta_p - i\omega t\right) = \exp\left(ikx_1 - i\eta x_2 - i\omega t\right) \tag{1.17}$$

where $k = k_p \sin\theta_p$ and $\eta = k_p \cos\theta_p$. Amplitude of the incident wave is assumed to be 1.One can compute the normal and shear stress components at the interface in the following form:

$$\sigma_{22} = \mu\left\{k^2\nabla^2\phi - 2\phi_{,11}\right\} = \mu\left\{-k^2\left(k^2+\eta^2\right)\phi + 2k^2\phi\right\} \tag{1.18}$$

$$\sigma_{12} = \mu\{2\phi_{,12}\} = 2\mu k\eta\phi$$

Clearly, σ_{22} and σ_{12} are not equal to zero at $x_2 = 0$. To satisfy the stress-free boundary conditions at $x_2 = 0$ one needs to include two reflected waves, PP and PS. Inclusion of only PP waves cannot satisfy the stress-free boundary conditions at $x_2 = 0$.

When both PP and PS waves are considered in the reflected field, then their amplitudes in the solid are given by

$$R_{pp} = \frac{4k^2\eta\beta - \left(2k^2 - k_s^2\right)^2}{4k^2\eta\beta + \left(2k^2 - k_s^2\right)^2} \tag{1.19}$$

$$R_{ps} = \frac{-4k\eta\left(2k^2 - k_s^2\right)}{4k^2\eta\beta + \left(2k^2 - k_s^2\right)^2}$$

1.3.4.3 P-Wave Striking an Interface

Figure 1.6 shows a plane P-wave of unit amplitude striking a plane interface between two linear elastic isotropic solids. Both reflected and transmitted waves have P- and SV-wave components and their amplitudes are denoted by $R_{PP}, R_{PS}, T_{PP}, and T_{PS}$.

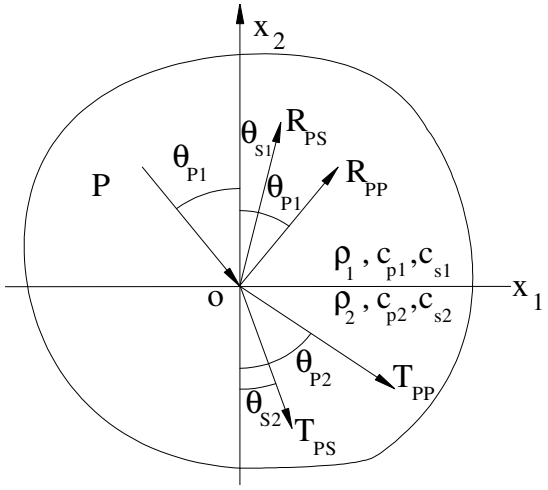

Figure 1.6: Reflected and transmitted waves near an interface for P-wave incidence

The above coefficients can be solved by the solving the following equation set:

$$\begin{bmatrix} k & \beta_1 & -k & \beta_2 \\ \eta_1 & -k & \eta_2 & k \\ 2k\eta_1 & -\left(2k^2 - k_{S1}^2\right) & 2k\eta_2\mu_{21} & \left(2k^2 - k_{S2}^2\right)\mu_{21} \\ \left(2k^2 - k_{S1}^2\right) & 2k\beta_1 & -\left(2k^2 - k_{S2}^2\right)\mu_{21} & 2k\beta_2\mu_{21} \end{bmatrix} \begin{Bmatrix} R_{PP} \\ R_{PS} \\ T_{PP} \\ T_{PS} \end{Bmatrix} = \begin{Bmatrix} k \\ \eta_1 \\ 2k\eta_1 \\ -\left(2k^2 - k_{S1}^2\right) \end{Bmatrix} \quad (1.20)$$

1.3.4.4 Longitudinal waves in thin rods

The governing differential equation for longitudinal wave propagation as given by Graff, (1975) is discussed in this section.

The governing differential equation

Consider a straight, prismatic rod as shown in **figure 1.7**. The rod is assumed to be under a dynamically varying stress field f(x, t), so that adjacent sections are subjected to varying stresses. A body force q(x, t) per unit volume is also assumed to be present. The equation of motion in the x direction then becomes

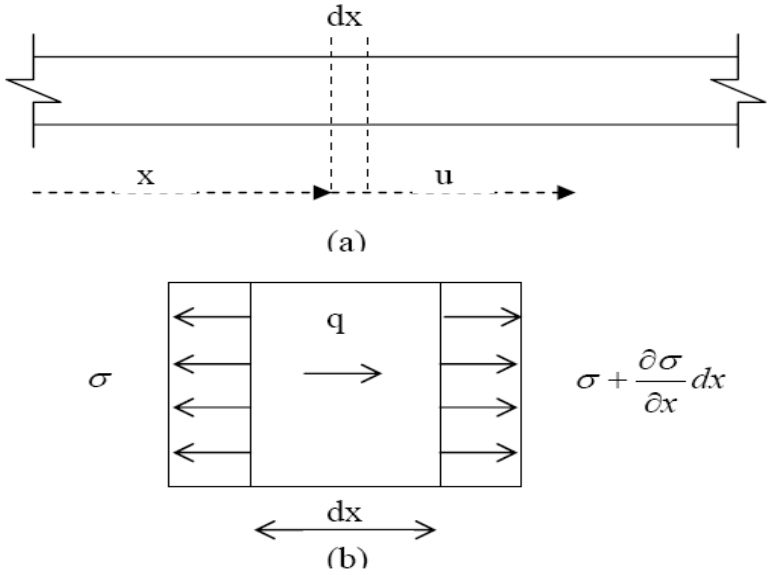

Figure 1.7: A thin rod (a) with coordinate x and displacement u of a section and (b) the stresses acting on a differential element of the rod

$$-\sigma A+\left(\sigma+\frac{\partial\sigma}{\partial x}dx\right)A+qAdx=\rho Adx\frac{\partial^2 u}{\partial t^2} \tag{1.21}$$

where A is the cross-sectional area of the rod. Since A is constant, the above equation reduces to

$$\frac{\partial\sigma}{\partial x}+q=\rho\frac{\partial^2 u}{\partial t^2} \tag{1.22}$$

If the material behaves elastically, then it follows Hooke's law,

$\sigma=E\varepsilon$ and $\varepsilon=\frac{\partial u}{\partial x}$ therefore the final form of the equation becomes,

$$E\frac{\partial^2 u}{\partial x^2}=\rho\frac{\partial^2 u}{\partial t^2} \tag{1.23}$$

which can also be written as,

$$\frac{\partial^2 u}{\partial x^2}=\frac{1}{c_0^2}\frac{\partial^2 u}{\partial t^2} \tag{1.24}$$

Where, $c_0=\sqrt{\frac{E}{\rho}}$

This is the wave equation.

CHAPTER 2

LITERATURE REVIEW

2.1 Status of Wave Propagation Technique for damage detection

This chapter presents a review of literature on propagation of elastic waves through solids. This gives an idea of study carried out in this area up to this stage. This work can be classified based on the theoretical/analytical studies and experimental studies.

In analytical studies the prominent work done is listed here. **Lamb (1904)** made the first investigation of pulse propagation in a semi-infinite solid. **Timoshenko (1921)** developed a theory for beams that accounted for shearing deformation. **Mindlin (1955)** presented an approximate theory for waves in a plate that provided a general basis for development of higher-order plate and rod theories. **Voyiadjis and Baluch (1981)** developed a technical theory for the flexural motions of isotropic elastic plates, taking into account the influence of transverse normal strain and transverse normal stress, together with rotatory inertia and transverse shear.

Doyle and Scala (1978) studied both bulk and surface wave ultrasonic methods for the measurement of the depth of surface-breaking cracks. They presented techniques for measuring crack depth by studying the scattered pulse amplitude, by using time-of-flight methods, or by carrying out ultrasonic spectroscopic analysis.

Abrahams et al. (1992) have examined the scattering of Rayleigh waves by an inclined two-dimensional plane surface breaking crack in an isotropic elastic half-plane.

Lowe et al. (1998) presented the technique of wave propagation and their sensitivity to defects through pipes using pulse echo. Issues of importance were the selection of the

optimum guided wave modes and the establishment of relationships between the defect size and the strength of wave reflection.

Gilchrist (1999) showed how horizontal symmetric crack-like defects can be detected rapidly in thin isotropic plates by using longitudinal ultrasonic waves.

Deng et al. (1999) studied the structural health monitoring using active sensors and wavelet transforms. In these methods, wave propagation signals were collected using arrays of piezoelectric transducers placed on or embedded in a structure. The collected signals were analyzed using appropriate wavelet transforms. The final interpretation of the sensor signals was based on signal patterns uncovered by the wavelet transforms in correlation with elastic wave propagation theory.

Bruck (2000) proposed a simple, one-dimensional model to develop insight into stress wave management issues. This model is initially applied to FGMs with discrete layering, and then extended to continuously graded architectures. The benefit of the FGM over the sharp interface is to introduce a time delay to the reflected wave propagation when stresses approach a peak level which is highly dependent on the composition gradient and the differences in base material properties. The propagation of the lowest-order, antisymmetric a_0 mode through the joint is examined.

Victor et al. (2001) studied the active sensor wave propagation health monitoring of beam and plate structures. Active sensor wave propagation was used for in-situ nondestructive evaluation (NDE). Elastic waves propagating in material carry the information of defects. This information was extracted by analyzing the signals picked up by active sensors. Efficient numerical modeling was used to predict the signal amplitude and time history of elastic waves scattering and diffraction. Wave functions of axial wave, shear wave, flexural wave, Rayleigh wave and Lamb waves were investigated. Finite Element Method was used to simulate and predict the wave propagating through the structure for different excitation and boundary conditions.

Giurgiutiu (2001) investigated the applicability of active sensors for in-situ health monitoring of aging aircraft structures for monitoring the onset and progress of structural damage such as fatigue cracks and corrosion. Wave propagation approach was used for large

area detection.. Finite Element Method was used to simulate and predict the wave propagating through the structure for different excitation and boundary conditions. Aluminum beams and plates were used to get experiment results

Pavlakovic et al. (2001) studied the High-Frequency Low-Loss Ultrasonic Modes in Imbedded Bars. The dispersion relationships of a system comprising a circular bar imbedded in a solid medium having lower acoustic impedance than the bar was predicted.

Wang (2002) investigated shear horizontal (SH) wave propagation in a semi-infinite solid medium surface bonded by a layer of piezoelectric material abutting the vacuum. The dispersive characteristics and the mode shapes of the deflection, the electric potential, and the electric displacements in the thickness direction of the piezoelectric layer are obtained theoretically. **Mal (2002)** analyzed elastic waves generated by localized dynamic sources in structural composites. **Rose (2002)** presented a baseline and vision of ultrasonic guided wave inspection potential.

Victor (2002) studied the Lamb Wave generation with piezoelectric wafer active sensors for structural health monitoring. Theoretical developments and laboratory tests were used to prove that PWAS transducers can satisfactorily perform lamb wave transmission and reception, pulse –echo, pitch-catch, and phased array functions of conventional ultrasonics thus opening the road for embedded ultrasonics.

Sun et al. (2002) presented an effective algorithm for simulating acoustical wave propagation. Example calculations were performed for a semi-infinite duct and a duct with a solid blockage. Numerical accuracy of results were examined and compared with the finite-difference time-domain method. Multiple reflections within the solid blockage and phase changes of the transmitting wave from solid back into air were illustrated through the implementation of this scheme.

Biwa et al. (2003) presented a computational procedure for multiple waves scattering in unidirectional fiber-reinforced composite materials. **Joshi et al. (2003)** discussed the characterization of functionally graded materials. **Lima and Hamilton (2003)** investigated the propagation of finite-amplitude waves in a homogeneous, isotropic, stress-free elastic plate theoretically. **Ahmad (2003)** presented a state of art report on the mechanism of

reinforcement corrosion, techniques utilized to monitor reinforcement corrosion and methodologies that are utilized for the prediction of remaining service life of structures.

Scarpetta and Sumbatyan (2003) studied the wave propagation through elastic solids with a periodic array of arbitrarily shaped defects. By means of a (uniform) approximation slightly stronger than the standard one-mode type, explicit analytical formulas for the scattering parameters were derived. Numerical resolution of the main integral equations for assigned shapes provided some graphs that were reciprocally compared.

Na et al. (2003) studied the delamination between steel bars and concrete using lamb waves. The lamb waves can propagate a long distance along the reinforcing steel bars embedded in concrete as the guided wave and is sensitive to the interface bonding condition between the steel bars and concrete. A special coupler between the steel bar and ultrasonic transducers was used to launch nonaxisymmetric guided waves in the steel bar.

Paul et al. (2004) studied the sensitivity of corrosion and fatigue damage detection using Guided ultrasonic waves. Guided waves have stress distributed through the thickness of the structure and can propagate over large distances. At structural defects, e.g. severe thickness reduction due to corrosion pitting, the guided wave mode is scattered and part of its energy reflected back towards the monitoring location. This allows for the efficient nondestructive testing and monitoring of large technical structures. A guided ultrasonic waves array, consisting of piezoelectric transducer elements for the excitation and reception of the first antisymmetric lamb wave mode A_o was designed and built. Laboratory measurements for a steel plate containing various defects were performed and results compared to theoretical predictions.

Wang and Hashimoto (2004) presented a two-dimensional theory for the analysis of surface acoustic waves in finite elastic solids. To meet the need of a simplified analytical method for surface acoustic waves in finite elastic solids, they used the well-known three-dimensional solutions of semi-infinite elastic solids.

Krawczuk et al. (2004) presented the method of analysis of the wave propagation process in cracked plates. Elastic behavior of the plate at the crack location was considered as a line

spring with a varying stiffness along the crack length. **Rose (2004)** studied the use of ultrasonic guided waves in structural health monitoring.

Siqueira et al. (2004) presented the use of ultrasonic guided waves and wavelets analysis in pipe inspection exploring its one-dimensional geometry which allows inspecting long distances in a short time. **Beard et al. (2004)** studied the use of guided waves in inspection of steel tendons embedded in concrete.

Francesco et al. (2004) dealt with the propagation of ultrasonic guided waves in adhesively bonded lap–shear joints. **Scarpetta and Tibullo (2004)** studied the P- wave propagation through elastic solids with doubly periodic array of cracks.

Suresh et al. (2005) studied the wave propagation approach for NDE using surface bonded piezoceramics. The technique utilizes arrays of surface-bonded piezoceramic (PZT) patches, which serve as transmitters and receivers of elastic waves through the monitored component. The operating frequency was maintained in the order of 100-150 kHz to enable high sensitivity in damage detection. The resulting frequency transfer functions facilitate the identification of the damaged region in the structure.

Giurgiutiu (2005) explored the capability of embedded piezoelectric wafer active sensors (PWAS) to excite and detect tuned Lamb waves for structural health monitoring.

Reis et Al. (2005) studied the corrosion damage in steel reinforced mortar using guided waves. Reinforced mortar specimens with seeded defects were used to simulate corrosion damage and monitored using ultrasonic approach. Advantage was taken of the lower frequency (<250 KHz) fundamental flexural propagation mode because of its relatively large displacements at the interface between the reinforcing steel and the surrounding mortar.

Zak et al. (2006) present certain results of the analysis of wave propagation in an isotropic panel with damage in the form of a fatigue crack.

Yang et al. (2006) studied some aspects of numerical simulation for Lamb wave propagation in composite laminates. Because of its unique characteristics such as long-range propagation, sensitivity to internal flaws, through-thickness interrogation, etc., Lamb wave can be used as an effective mechanism to interrogate plate-like structures for damage identification. Some

aspects of numerical simulation of Lamb wave propagation in composite laminates using the finite element models with explicit dynamic analysis were addressed in the study. To correctly and efficiently describe the guided-wave excited/received by piezoelectric actuators/sensors, effective models of surface-bounded flat PZT disks based on effective force, moment and displacement were developed. Different finite element models for Lamb wave excitation, collection and propagation in isotropic plate and quasi-isotropic laminated composite were evaluated using continuum elements (3-D solid element) and structural elements (3-D shell element), to elaborate the validity and versatility of the proposed actuator/sensor models.

Mukherjee et al. (2006, a) investigated piezoelectric transducers to produce a broadband frequency spectrum. However, the interference produced from the sympathetic pulses generated by the transducer limits the duration of waveform to a very short time. The work discussed the grading of transducer as a means of alleviating the sympathetic pulses**.**

Mukherjee et al. (2006, b) studied the use of acoustic wave propagation for the characterization of discretely graded materials. In this research work, a simple one-dimensional model was proposed to study the stress waves in discretely graded media. The model used spectral approach to determine the stresses due to the incident and reflected waves in FGMs.

He et al. (2006) studied the delamination present in load bearing rock bolts using semi analytical FEM model to calculate the theoretical wave structures for a rod embedded in concrete. A qualitative relationship between percent delamination and wave reflection energy was demonstrated.

Aggelis and Shiotani (2007) studied repair evaluation of concrete cracks using surface and through-transmission wave measurements. Rayleigh waves demonstrate the filling condition of the material into the shallow layer near the surface while tomography using longitudinal waves through the thickness yields information about the area inside the structure. Wave propagation dispersion features are exploited by the proposed tomography at different frequencies, demonstrating that higher frequencies lead to more accurate characterization.

Sekhar (2007) studied the effect of double/multi-cracks their influences and identification methods in vibration structures such as beams, rotors, pipes etc.

2.2 Status of damage detection in steel

Reinforcement corrosion and damage detection in steel has been widely reported in the literature over the last two or three decades. A wide range of techniques have been reported in the literature that may be suitably employed for the monitoring of steel in concrete structures for the purpose of diagnosing the cause and extent of damage in the form of fractures and corrosion. A brief account on recent developments for corrosion monitoring in structures and in general, damage detection in steel is presented below:

Scheel et al. (1995) discussed the capacity of the remnant magnetism methods to detect fractures of steel in tendons embedded in prestressed concrete.

Baranio et al. (1996,a) studied steel corrosion monitoring using potential measurements in normal and light-weight concretes exposed to chloride and sulphate solutions. Baranio et al. (1996,b) studied steel corrosion monitoring using polarization resistance measurements in normal and light-weight concretes exposed to chloride and sulphate solutions.

Glass et al. (1997) monitored the passivation of steel in concrete induced by cathodic protection. The work examined the applicability of mixed potential theory to predict the corrosion rate of steel in concrete using the negative potential shift induced by a known cathodic current density.

Gullikers (1997) developed corrosion monitoring probe to improve service life prediction of RC structures w.r.t to reinforcement corrosion**. A**n integrated probe for monitoring the corrosion rate of steel was designed for use in a range of aggressive, chloride containing or carbonated, concrete environments. The probe measured the variation with time of polarizing galvanic current, corrosion potential, concrete resistance and temperature.

Rens et al. (2000) discussed acoustic tomographic imaging of concrete infrastructure to detect anomalies in concrete. Although this technology has been used with great success to

image fluid-rich media like biological tissue, the complex behavior of stress waves in solids complicates the imaging of concrete, masonry and other heterogeneous materials such as those used to construct concrete structures.

Zivica (2000) discussed utilization of electrical resistance method for the evaluation of the state of steel reinforcement in concrete and the rate of its corrosion. In this research work, the applications of an electrical resistance method for monitoring the state of steel reinforcement in concrete and its rate were described.

Giurgiutiu et al. (2001) proposed active sensor wave propagation for health monitoring of beam and plate structures.

Matt (2001) discussed some techniques of non-destructive evaluation and monitoring of post-tensioning tendons like Reflectometrical Impulse Measurement (RIMT) and Acoustic Monitoring and their specific applications and drawbacks

Broomfield (2002) studied corrosion monitoring systems consisting of linear polarization, concrete resistivity and other probes were installed in new structures to monitor durability and in existing structures to evaluate rehabilitation strategies such as corrosion inhibitor application and patch repairs. The type of sensors used and the data collected and its interpretation was discussed.

Elsener (2002) investigated macro cell corrosion of steel in concrete with a local anode and a large cathode which frequently occurs in chloride induced corrosion of rebars in concrete and is responsible for very high local corrosion attacks and reduction in cross-section found e.g., in bridge decks or substructures.

Iyer et al. (2002) proposed ultrasonic C-scan imaging to detect corrosion and voids in post-tensioning tendons. Investigations on post-tensioned specimens using ultrasound C-scan imaging technique have proved this method to be promising for future applications in the evaluation of corrosion and voids in post-tensioned tendons. But the study recommends further investigations to upgrade the technique from bench-top to a field-ready instrument.

Park et al. (2005) developed a galvanic sensor system for detecting the corrosion damage of the steel embedded in concrete structure. The correlation between sensor output and the corrosion rate of steel bar was confirmed in concrete environment. Open-circuit potential, linear polarization resistance (LPR) measurement and electrochemical impedance spectroscopy (EIS) were used to evaluate the corrosion behaviour of steel bar embedded in concrete.

Li et al. (2006) discussed the application of steel thin film electrical resistance sensor for in situ corrosion monitoring. The corrosion sensor should have high sensitivity enough to measure the corrosion rate in mild corrosive environments and the ability to detect the corrosion mechanism. Therefore, the goal of this research was to develop and apply a steel thin film electrical resistance (TFER) sensor based on the measurement of changes in electrical resistance of the sensing elements in order to follow the corrosion of steel in a wide range of environments.

Parthiban et al. (2006) developed a Data Acquisition System for simultaneous measurement of potential of steel from different points in a concrete slab using NI-DAQ card. Suitable software was developed for interpreting the measured data based on ASTM C-876 to assess the condition of embedded steel. Software was developed using Visual Basic 6.0 and NI-DAQ driver software.

Sathiyanarayanan et al. (2006) discussed the corrosion monitoring of steel in concrete by galvanostatic pulse technique. Corrosion rate values obtained by weight loss method and linear polarization techniques were compared with the values obtained from galvanostatic pulse technique for steel reinforced in M15, M20, M30 and M35 grade concrete containing 0-5%bNaCl. It was found that this technique gave reliable corrosion rate values.

CHAPTER 3

BASIC PRINCIPLES OF ULTRASONIC TESTING

3.1 Non Destructive Testing

The field of Nondestructive testing (NDT) is a very broad, interdisciplinary field that plays a critical role in assuring that structural components and systems perform their function in a reliable and cost effective fashion. The term is generally applied to investigations of material integrity. These tests are performed in a manner that does not affect the future usefulness of the object or material. Because it allows inspection without interfering with a product's final use, NDT provides an excellent balance between quality control and cost-effectiveness.

Non Destructive Evaluation: Nondestructive evaluation (NDE) is a term that is often used interchangeably with NDT. However, technically, NDE is used to describe measurements that are more quantitative in nature. For example, a NDE method would not only locate a defect, but it would also be used to measure something about that defect such as its size, shape, and orientation. NDE may be used to determine material properties such as fracture toughness, formability, and other physical characteristics.

3.1.1 NDT or NDE methods

Non destructive methods used for condition assessment of steel in concrete are given in **Table 3.1.**

Table 3.1: Present Techniques for Condition Assessment of steel in concrete

Method	**Detects/Features**
Impact-echo	Defects/ cracks
Radiography	X- Ray image
Remanent Magnetism	Fractures in steel
Reflectometrical Impulse Measurement (RIMT)	Anomalies in steel
Acoustic Monitoring	General defects
Thermography	Delamination/ Debonding
Acoustic Tomography	Imaging of concrete

Although a number of different NDT methods have been developed, but following methods are most commonly used.

- **Impact Echo Method-** The impact-echo method is a technique for flaw detection in concrete. It is based on monitoring the surface motion resulting from a short-duration mechanical impact. The method overcomes many of the barriers associated with flaw detection in concrete based on ultrasonic methods. It can be used to check a tendon for prestressed grout voids but is a delicate operation requiring skilled personnel. The presence of cracks and other concrete defects as often found in real structures influences significantly the test results and can make the evaluation impossible at times.

- **Remnant Magnetism Method:** This method developed in Germany detects fractures in steel. The magnetizing and recording equipment has to be moved along the tendon path on auxiliary guidance rails and scaffolding fixed to the concrete surface in order to measure a magnetic leakage field generated by the formation of magnetic dipole distribution around the fracture area. Fracture patterns have typical signatures that are matched and interpreted by experienced personal or pattern recognition (PR) software. The method is suitable to locate fractures of steel strands and to detect real corrosion. But the major constraint of this method is the difficulty in coping with the disturbing magnetic signals originating from other embedded steel elements such as normal reinforcement, anchorage elements, duct couplers, steel plates, nails, etc.

- **Reflectometrical impulse measurement (RIMT):** RIMT employs time-domain reflectometry to locate anomalies such as corrosion, breakage of wires or whole tendons. It involves the sending of a high-frequency impulse along a tendon or anchor and allows *in-situ* measurement of the integrity of steel and rock/soil anchors. This method is expensive and incomplete because it requires the destruction and restoration of a part of the structure. Also the recorded signals do not contain information on the condition of the tendon but are artifacts of the measurement procedure. Thus, Matt disregards it as a diagnostic technique for grouted tendons.

- **Visual and Optical Testing-**Visual inspection involves using an inspector's eyes to look for defects. The inspector may also use special tools such as magnifying glasses or mirrors gain access and more closely inspect the subject area.

- **Penetrant Testing-** Test specimens are coated with visible or fluorescent dye solution. Excess dye is then wiped out from the surface, and a developer is applied. The developer acts as blotter, drawing trapped penetrant out of imperfections open to the surface. With visible dyes, vivid colour contrasts between the penetrant and developer make “bleedout" easy to see.

- **Magnetic Particle Testing (MT)** – In this method a magnetic field in a ferromagnetic material is induced and then dusting the surface with iron particles (either dry or suspended in liquid) is done. Surface and near-surface imperfections distort the magnetic field and concentrate iron particles near imperfections, previewing a visual indication of the flaw.

- **Electromagnetic Testing (ET) or Eddy Current Testing-** Eddy currents are generated in a conductive material by an induced alternating magnetic field and they flow in circles at just below the surface of the material. Interruptions in the flow of eddy currents, caused by imperfections, dimensional changes, or changes in the materials conductive and permeability properties, can be detected with the proper equipment.

- **Radiography (RT) -** Radiography involves the use of penetrating gamma or X-radiation to examine parts and products for imperfections. An X-ray generator or radioactive isotope is used as a source of radiation. The resulting shadowgraph shows the dimensional features of the part. Possible imperfections are indicated as density changes on the film in the same manner as medical X-ray shows broken bones.

- **Thermography:** All objects naturally emit infrared radiation in proportion to their surface temperature. Thermography measures the emitted radiation and displays the information as a visual image. By combining infrared and computer technologies, it is possible to generate thermo grams (heat pictures), having up to 256 colors, that clearly show thermal profiles and temperature measurements. A combination of thermography and natural heating/cooling

cycle allows areas of delaminated concrete and debonded tendons to be detected. The advantages of this technique are that it is a remote operation and is nondestructive.

- **Tomography:** Acoustic tomographic imaging of concrete is a developing nondestructive evaluation technology and has a potential to assess the condition of concrete structures.Although this technology has been used with great success to image fluid-rich media like biological tissue, the complex behavior of stress waves in solids complicates the imaging of concrete, masonry and other heterogeneous materials such as those used to construct concrete structures.

- **Ultrasonic Testing (UT) -** ultrasonic testing use transmission of high-frequency sound waves into a material to detect imperfections or to locate changes in material properties. The most commonly used ultrasonic testing technique is pulse echo, wherein sound is introduced into a test object and reflections (echoes) are returned to a receiver from internal imperfections or from the part's geometrical surfaces.

- **Acoustic Emission Testing (AE) -** when a solid material is stressed, imperfections within the material emit short bursts of acoustic energy called "emissions." as in ultrasonic testing; acoustic emissions can be detected by special receivers. Emission sources can be evaluated through the study of their intensity, rate, and location.

- **Leak Testing (LT) -** Several techniques are used to detect and locate leaks in pressure containment parts, pressure vessels, and structures. Leaks can be detected by using electronic listening devices, pressure gauge measurements, liquid and gas Penetrant techniques, and/or a simple soap-bubble test.

Wave propagation provides an efficient means of characterizing defects in structures. For this purpose it is necessary to analyze scattering of waves by such defects. The sudden occurrence of small flaws initiated from damage sites in structural solids generates elastic waves that carry important information on the nature of damage.

3.2 Ultrasonic Testing

3.2.1 Basic Principle of Ultrasonic Testing:

Ultrasonic nondestructive testing introduces high frequency sound waves into a test object to obtain information about the object without altering or damaging it in any way. A typical UT inspection system consists of several functional units, such as the pulser/receiver, transducer, and display devices. A pulser/receiver is an electronic device that can produce high voltage electrical pulses. Driven by the pulser, the transducer generates high frequency ultrasonic energy. The sound energy is introduced and propagates through the materials in the form of waves. When there is a discontinuity (such as a crack) in the wave path, part of the energy will be reflected back from the flaw surface. The reflected wave signal is transformed into an electrical signal by the transducer and is displayed on a screen.

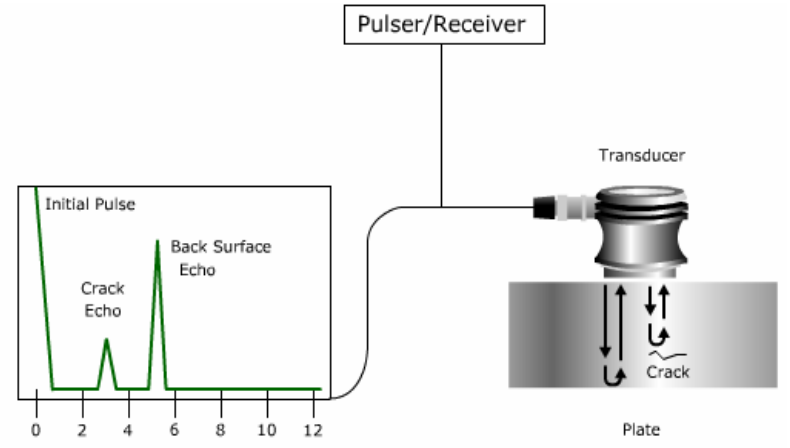

Figure 3.1: General ultrasonic Inspection Principle (pulse echo method)

Two basic quantities are measured in ultrasonic testing; they are time of flight or the amount of time for the sound to travel through the sample, and amplitude of received signal. Based on velocity and round trip time of flight through the material the material, thickness can be calculated as follows:

$$T = \frac{ct}{2}$$

T = Material Thickness

c = Material Sound Velocity

t = Time of Flight

Measurements of the relative change in signal amplitude can be used in sizing flaws or measuring the attenuation of a material. The relative change in signal amplitude is commonly measured in decibels. Decibel values are the logarithmic value of the ratio of two signal amplitudes. This can be calculated using the following equation.

$$dB = 20\ log_{10}\left(\frac{A_1}{A_2}\right) \tag{3.1}$$

dB = Decibels

A1 = Amplitude of signal 1

A2 = Amplitude of signal 2

3.2.2 Sound Field

The sound field of a transducer is divided into two zones; the near field and the far field. The near field is the region directly in front of the transducer where the echo amplitude goes through a series of maxima and minima and ends at the last maximum, at distance N from the transducer.

The location of the last maximum is known as the near field distance (N or Y0+) and is the natural focus of the transducer. The far field is the area beyond N where the sound field pressure gradually drops to zero. Because of the variations within the near field it can be difficult to accurately evaluate flaws using amplitude based techniques. The near field distance is a function of the transducer frequency, element diameter, and the sound velocity of the test material as shown by Equation 3.2:

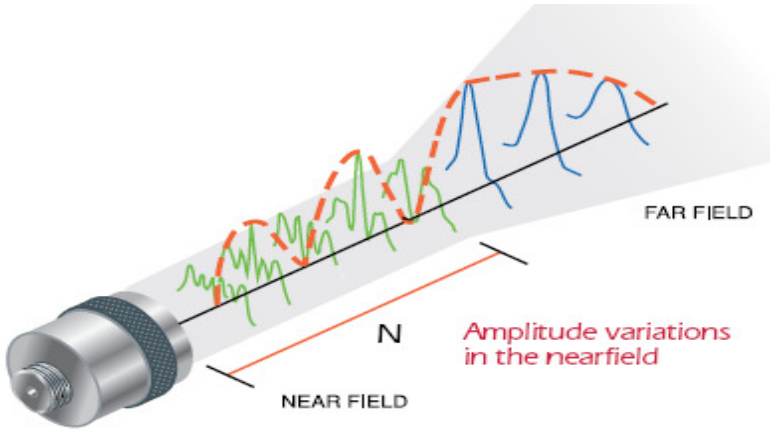

$$N = \frac{D^2 f}{4c} \tag{3.2}$$

$$N = \frac{D^2}{4\lambda} \tag{3.3}$$

N = Near Field Distance

D = Element Diameter

f = Frequency

c = Material Sound Velocity

l = Wavelength

3.2.3 Beam Spread and Half Angle

All ultrasonic beams diverge. In other words, all transducers have beam spread. Figure 3.2 gives a simplified view of a sound beam for a flat transducer. In the near field, the beam has a complex shape that narrows. In the far field the beam diverges.

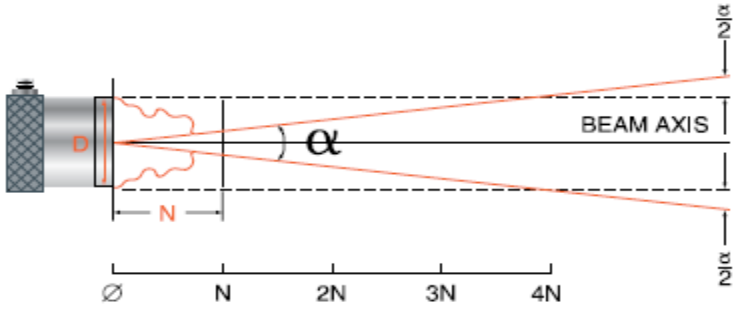

Figure 3.2: Sound beam for a flat transducer

For flat transducers as shown in Figure 3.2, the - 6 dB pulse-echo beam spread angle is given by Equation 3.4:

$$\mathbf{Sin}\left(\alpha/_{2}\right) = 0.\frac{514c}{fD}$$

α/2 = Half Angle Spread between -6 dB points

It can be seen from this equation that beam spread from a transducer can be reduced by selecting a transducer with a higher frequency or a larger element diameter or both.

3.2.4 Design characteristics of transducers

A transducer is any device that converts one form of energy to another. An ultrasonic transducer converts electrical energy to mechanical energy, in the form of sound, and vice versa.

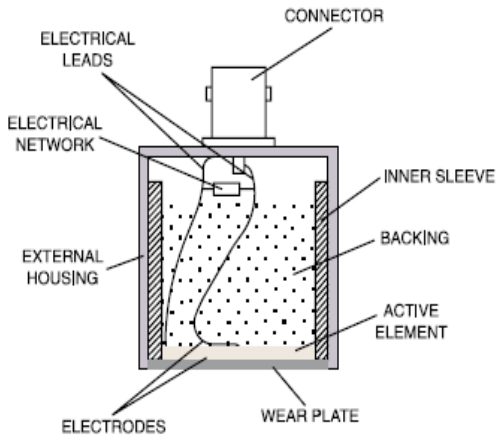

The main components are the active element, backing, and wear plate.

- **The Active Element**

The active element, which is piezo or ferroelectric material, converts electrical energy such as an excitation pulse from a flaw detector into ultrasonic energy. The most commonly used materials are polarized ceramics which can be cut in a variety of manners to produce different wave

modes. New materials such as piezo polymers and composites are also being employed for applications where they provide benefit to transducer and system performance.

- **Backing**

The backing is usually a highly attenuative, high density material that is used to control the vibration of the transducer by absorbing the energy radiating from the back face of the active element. When the acoustic impedance of the backing matches the acoustic impedance of the active element, the result will be a heavily damped transducer that displays good range resolution but may be lower in signal amplitude. If there is a mismatch in acoustic impedance between the element and the backing, more sound energy will be reflected forward into the test material. The end result is a transducer that is lower in resolution due to longer waveform duration, but may be higher in signal amplitude or greater in sensitivity.

- **Wear Plate**

The basic purpose of the transducer wear plate is to protect the transducer element from the testing environment. In the case of contact transducers, the wear plate must be a durable and corrosion resistant material in order to withstand the wear caused by use on materials such as steel. The choice of the wear surface thickness is based upon the idea of superposition that allows waves generated by the active element to be in phase with the wave reverberating in the matching layer as shown in Figure 3.2. When signals are in phase, their amplitudes are additive, thus a greater amplitude wave enters the test piece. Figure 3.3 shows the active element and the wear plate, and when they are in phase. If a transducer is not tightly controlled or designed with care and the proper materials, and the sound waves are not in phase, it causes a disruption in the wavefront.

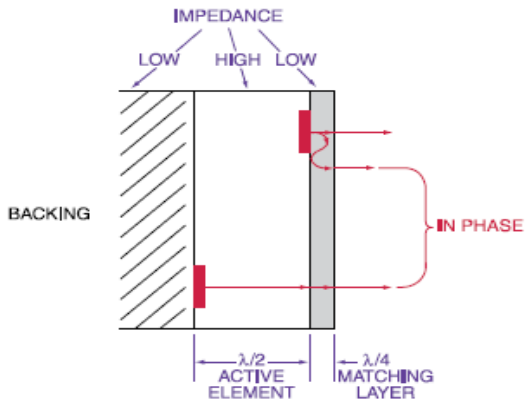

Figure 3.3: In phase active element and wear plate of transducer

3.3 Methods of ultrasonic testing

1. Pulse echo method
2. Through transmission method
3. Two transducer method

- **Pulse echo method:**

In the pulse-echo method, a piezoelectric transducer with its longitudinal axis located perpendicular to and mounted on or near the surface of the test material is used to transmit and receive ultrasonic energy. The ultrasonic waves are reflected by the opposite face of the material or by discontinuities, layers, voids, or inclusions in the material, and received by the same transducer where the reflected energy is converted into an electrical signal. The electrical signal is computer processed for display on a video monitor or TV screen. The display can show the relative thickness of the material, depth into the material where flaws are located, and (with proper scanning hardware and software), where the flaws are located in the X-Y plane.

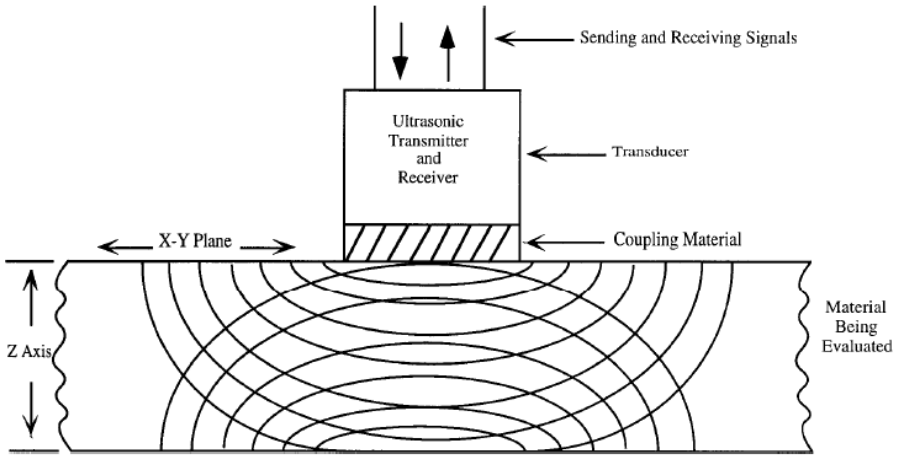

Figure 3.4: Principle of pulse echo method of inspection

- **Through transmission method:**

In the through-transmission method, an ultrasonic transmitter is used on one side of the material while a detector is placed on the opposite side. One unit acts as transmitter and the other unit as receiver. The beam from the transmitter T travels through the material to its opposite surface where the receiving transducer R is placed. Scanning of the material using this method will result in the location of defects, flaws, and inclusions in the X-Y plane.

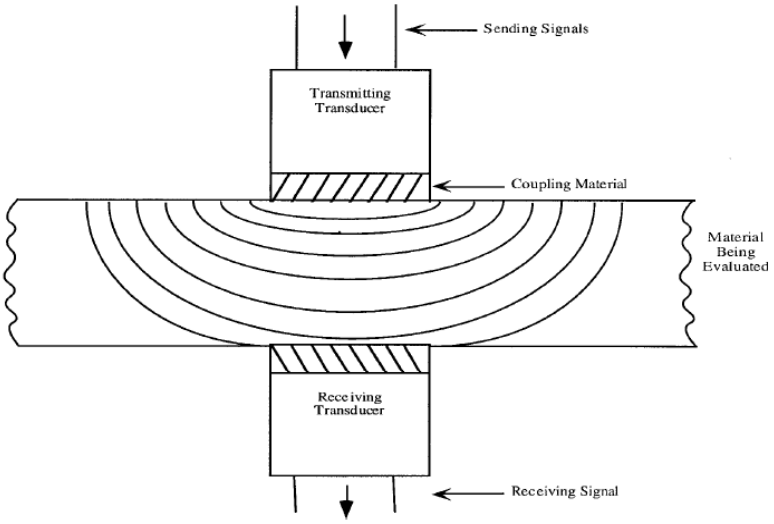

Figure 3.4: Principle of through transmission of ultrasonic testing

- **Two transducer method**

The pulse echo method can be used with either single or double crystal unit in single transducer unit the probe acts as both transmitter and receiver .In two transducer arrangement ,one transmits and other receives the ultrasonic waves .These are placed on same side of specimen .pulse wave is send in to the specimen by the transducer T. And the echoes reflected from the back surface or any defect .Are received by the transducer R and displayed on the flaw detector screen. For specific applications like wall thickness measurement special type of transducers in which the transmitting and the receiving crystals are housed in a single unit are also used .These transducers are popularly known as 'twin' or T-R probes .

CHAPTER 4

NUMERICAL TECHNIQUES TO MODEL WAVE PROPAGATION

There are various methods for numerical modeling of wave propagation problems. These methods either use time based approach or frequency based techniques. Some of them are hybrid or extended from them using certain manipulations. The characteristics of wave propagation problems are that the frequency content of the exciting force is very high. As we know that, at very high frequencies the system becomes mass dominated where inertial effects need to be very accurately modeled. Some popular methods of modeling wave propagation are:

1. Ray tracing method
2. Spectral Approach
3. Finite Element Method
4. Distributed Point Source Method (DPSM)

4.1 Ray tracing method

A simple elegant, one-dimensional model based on ray tracing the path of wave movement was proposed by Bruck (2000) to develop insight into stress wave management issues. Ray Tracing is a unique method working independent of time or spectral approach.

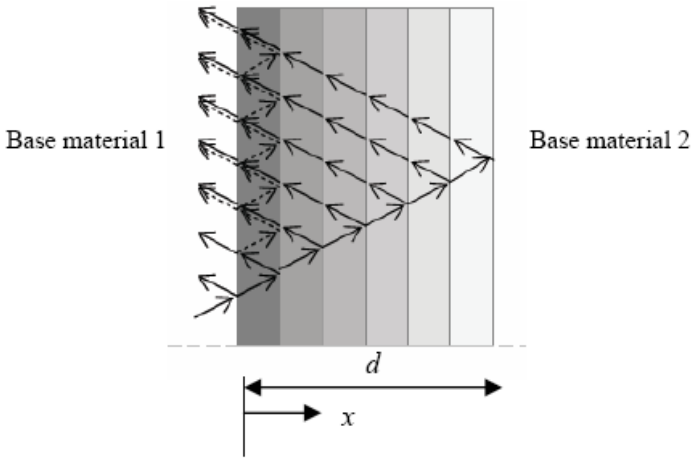

Figure 4.1: 1-D stress wave propagation through discretely layered FGM

Ray tracing method has wide applications in characterization of materials. So, it is used as a very promising means for characterization of functionally graded materials (FGMs).The method adopted by Bruck (2000), to characterize the discretely graded FGM, is a simple reflection-transmission method. When the stress waves come across an interface, some part of it is reflected and the remaining is transmitted in the next layer. The behavior of these waves, moving across the FGM is traced and hence it is called as the ray-tracing method. In this method, the path of waves emerging out of a point or a group of points is traced as rays through all interfaces. Ray tracing is useful when only a few trains of wave emerge and they traverse through simple interfaces **(Figure 4.1)**. The amount of stress wave reflection and transmission can be given by simple laws of physics.

$$f_t = \frac{2}{1+\alpha} f_i \tag{4.1}$$

$$f_r = \left(\frac{1-\alpha}{1+\alpha}\right) f_i \tag{4.2}$$

where f_i is the amount of stress in the incident wave, f_t is the amount of stress in the transmitted wave, f_r is the amount of stress in the reflected wave, and α is the ratio of the acoustic impedance of base material 1 to the acoustic impedance of base material 2.Acoustic impedance can be defined as the ratio of pressure across the material to the flow through it. It is defined as ρ*c/A*. For unit area it becomes the characteristic impedance which is the material property.

If *d* is the thickness of the graded layer and *m* is the number of graded layers, then the thickness of each layer is *d/m*, and the total time, *t*, it takes for the incident wave to travel through a layer and then get reflected back is:

$$t = \frac{2d}{cm} \tag{4.3}$$

where, *c* is the longitudinal wave speed of the layer.

Disadvantages in this method

- This method is limited only up to 1-dimension wave propagation and cannot be extended to 2 or 3 dimensions.

- It cannot be used under arbitrary forcing functions.

4.2 Spectral approach

One of the shortcomings of Ray Tracing Method is its difficulty in extending it to two-dimensional wave propagation. Also another problem faced in modeling of wave propagation was that the frequency content of the exciting force is very high. Therefore, a very fine mesh of finite elements is necessary to adequately model the problem. This problem can be alleviated if we use frequency-based methods, such as the spectral method instead of the time-based techniques. It has many advantages over time-based approaches like it takes very less time for running simulation models. In addition, the inertial effects are exactly represented in it and hence often-exact solutions are obtained for the transformed partial differential equation. In this method, the governing partial differential wave equation is reduced to a set of ordinary differential equations. Their solution is easier than the original differential equation. However, often-approximate solutions are sought. The transformation occurs as a result of Fast Fourier transformation (FFT). These solutions to the governing equations are used as shape functions for spectral element formulation. In addition, often the resulting element is super convergent and very few elements are required to model the system.

Spectral analysis method (Doyle, 1989) is a means of solving wave propagation problems in structures. While it is possible to solve structural dynamics problems by starting with partial differential equations of motion and integrating, the task is horrendously large even for the biggest computer available. It has been known long back that an arbitrary time signal can be thought of as the superposition of many sinusoidal components. This is the basis of Fourier (or spectral) analysis. In wave analysis, the time domain for the disturbance is from minus infinity to plus infinity and thus the components have a continuous distribution (known as Continuous Fourier transform). However, the numerical evaluation of the transform requires discretizing the distribution in some manner, and the one chosen here is by the way of discrete Fourier transform (DFT). This has two advantages. First, many of the ideas and methods of time series analysis can be borrowed and used for present purposes. Second, it allows the use of the very efficient Fast Fourier Transform (FFT) computer algorithm.

Spectral analysis of differential equations

The key to the spectral description of waves is to be able to express the phase changes incurred as the wave propagates from location to location. This is done conveniently through the use of the governing differential equations for particular structural models (although other schemes are possible).The idea of representing the time variation of a function by a summation of harmonic functions is to represent arbitrary functions of time and positions resulting from solution to wave equation. The approach is to remove the time variation by using the spectral representation of the solution. This leaves a new differential equation for the coefficients, which in many cases can be integrated directly.

General functions of space and time

The solutions in wave propagation are general functions of space and time. If the time variation of the solution is focused on at a particular point in space, then it has the spectral representation

$$u(x_1, y_1, t) = f_1(t) = \sum C_{1n} e^{i\omega t} \tag{4.4}$$

At another point, it behaves as a time function $f_2(t)$ and is represented by the Fourier coefficients. That is, the coefficients are different at each spatial point. Thus, the solution at any arbitrary position has the following spectral representation

$$u(x, y, t) = \sum \hat{u}_n(x, y, \omega_n) e^{i\omega_n t} \tag{4.5}$$

where u are the spatially dependent Fourier coefficients.

Derivatives

The differential equations have terms of both space and time derivatives. Now apply the spectral representation to each differential term appearing in the differential equation. Thus the spectral representation for the time derivatives is

$$\frac{\partial u}{\partial t} = \frac{\partial}{\partial t} \sum \hat{u}_n e^{i\omega_n t} = \sum i\omega_n \hat{u}_n e^{i\omega_n t} \tag{4.6}$$

In fact, time derivatives of general order have the representation

$$\frac{\partial^m u}{\partial t^m} \Rightarrow i^m \omega_n{}^m \hat{u}_n \quad or \quad i^m \omega^m{}_n \hat{u}_n \tag{4.7}$$

Herein lays the advantages of the spectral approach to solving differential equations. The algebraic expressions in the Fourier coefficients replace the time derivatives. That is, there is a reduction in the number of derivatives occurring.

Similarly, the spatial derivatives are represented by,

$$\frac{\partial u}{\partial x} = \frac{\partial}{\partial x}\sum \hat{u}_n e^{i\omega t} = \sum \frac{\partial \hat{u}_n}{\partial x} e^{i\omega t} \tag{4.8}$$

And in shorthand notation, it becomes

$$\frac{\partial u}{\partial x} \Rightarrow \frac{\partial \hat{u}_n}{\partial x} \quad or \quad \frac{\partial \hat{u}_n}{\partial x}$$

Spectral relation

Linear differential equations with constant coefficients have solutions of the form, where λ is obtained by solving algebraic characteristics equation

$$A_1 + A_2\lambda + A_3\lambda^2 + ... = 0 \tag{4.9}$$

It is usual in wave analysis, however to assume that λ is complex to begin with, that is, that the solutions are of the form.

$$\hat{u}(x) = Ce^{ikx}$$

For example, consider the differential equation

$$au + \frac{d\hat{u}}{dx} = 0 \Rightarrow \left[a - k^2\right]C = 0$$

This gives *k* and the solution as

$$k = -a \quad and \quad \hat{u}(x) = Ce^{-ax}$$

where C is a constant of integration. Similarly, following second-order differential equation

$$au + \frac{d^2\hat{u}}{dx^2} = 0 \Rightarrow \left[a - k^2\right]C = 0$$

gives k and the solution as,

$$k = \pm\sqrt{a} \quad and \quad \hat{u}(x) = C_1e^{i\sqrt{a}x} + C_2e^{-i\sqrt{a}x}$$

There are two solutions (and constant of integration) because occurred to the power of two. Note that, even if the coefficients in the differential equation are real, it is possible for to be complex. In general, then, the characteristics equation becomes

$$A_1 + (ik)A_2 + (ik)^2A_3 + ... = 0$$

and this has many values of k that satisfies it. That is, *k*

$$k_{mn} = f_m(A_1, A_2, A_3, ..., \omega_n)$$

This relation between the exponent *k* (called the wave number) and frequency ω is called the spectral relation and is fundamental to the spectral analysis of waves. The different values of *m* correspond to the different modes. The solution is given as the superposition of modes in the form,

$$u(x) = C_1 e^{ik_1 x} + C_2 e^{ik_2 x} + ... + C_{mn} e^{ik_m x}$$

There are as many modes (or solutions) are there are roots of the characteristics equation and these should be confused with the number of solutions at each frequency. To reinforce this, the solution in total form is written as,

$$u(x) = \sum_n \left\{ C_1 e^{ik_1 x} + C_2 e^{ik_2 x} + ... + C_{mn} e^{ik_m x} \right\} e^{i\omega t} \tag{4.10}$$

The exponential form for each term is due to the coefficients of the differential equation being constant; however, the solution for any problem can be always be expressed as

$$u(x,t) = \sum F_n G(K_{mn} x) e^{i\omega t} \tag{4.11}$$

where F_n is the amplitude spectrum and G (which may be combination of modes) is the system transfer function. Analysis of the partial differential equation combined with the boundary conditions determines the particular forms for *G* and in fact, G determines the phase shifts with respect to space. Further, it is noted that the wave number *k* acts as a scale factor on the position variable in the same way that the frequency acts on the time. The analysis of the scaling done by *k* provides a good deal of insight into the solution before the actual solution is obtained.

Propagating and Reconstructing waves

The significance of the spectral approach to waves coupled with the use of the differential equations is that once the signal is characterized at one space position then it is known at all positions, therefore propagating it becomes a fairly simple matter. This section illustrates the basic algorithm for doing this.

- **Basic Algorithm**

In its simplest terms, the solutions to a waves problems is represented as,

$$u(x) = \sum_n \left\{ C_1 e^{ik_1 x} + C_2 e^{ik_2 x} + ... + C_{mn} e^{ik_m x} \right\} e^{i\omega t} = \sum \hat{F}_n G(K_{mn} x) e^{i\omega t} \tag{4.12}$$

where G is the analytically known transfer function of the problems. It is a function of position x and has different numerical values at each frequency. $\hat{F}$ is the amplitude spectrum; this is known from the input conditions or from some measurement. This $\hat{F}_n G$ is recognized as the Fourier transform of the solution. Of course it is different at each position but once it is evaluated at a particular position then its inverse immediately gives the time history of the solution at that point**. Figure.4.2** is a flow diagram for its evaluation. Briefly, the time input $F(t)$ is converted to its spectrum $\hat{F}_n$ through a use of the forward FFT. The transform solution is the obtained by evaluating the product, at each frequency.

$$\hat{u}_n = \hat{F}_n G(k_{mn}) \tag{4.13}$$

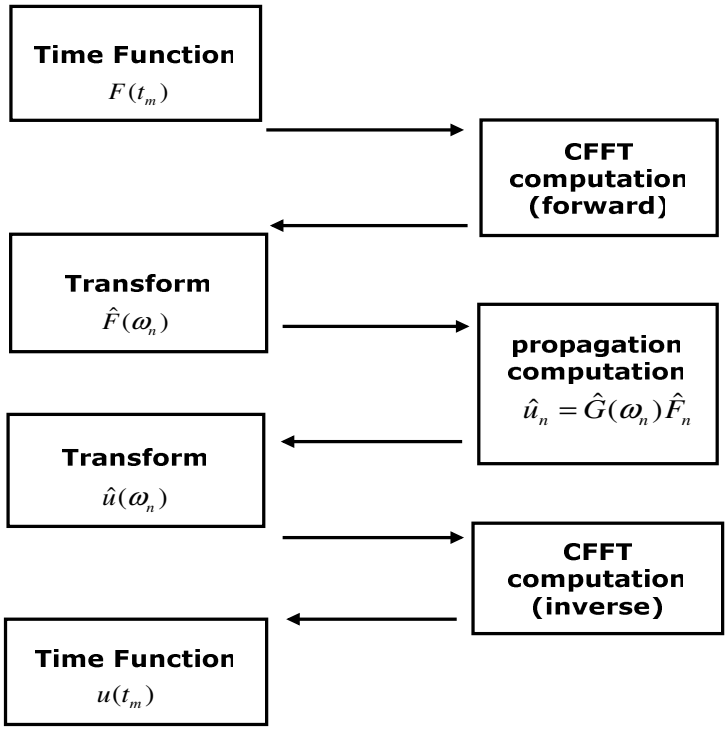

Figure 4.2: Flow diagram for wave reconstruction program

This is finally reconstructed in the time domain by the use of the inverse FFT. In the process, it is necessary to realize (when using the FFT to perform the inversion) that $\hat{F}_n G$ is evaluated only up to the Nyquist frequency and the remainder is obtained by imposing that it must be complex conjugate of the initial part, This ensures that reconstructed time history is real only.

Disadvantages of Spectral element method

- Exact solutions for complex differential equations are difficult to obtain, hence this method becomes inefficient in this case
- Non-linear problems are difficult to solve using this approach.

4.3 Finite element approach

As already discussed, Ray tracing method is limited to 1-D wave propagation and cannot be applied to 2 or 3 dimensions. Spectral approach is a frequency based method and involves decomposition of the applied impulse into its many sinusoidal components (Fourier components). In this method, the governing partial differential wave equation is reduced to a set of ordinary differential equations whose solution is easier than the original differential equation. The transformation is effected by Fast Fourier Transform (FFT) Algorithm. But the disadvantage of this method is exact solutions for complex differential equations are difficult to obtain and hence this method becomes inefficient in this case. Also non-linear problems are difficult to solve using this approach. The above two methods seem to be very useful to determine stress wave propagation in the 1-D models, however they prove to be futile when complex models are to be analyzed. In order to analyze linear and non-linear problems, conventional FEM proves to be more useful.

A coordinated theoretical and experimental program was carried out by Deepti et al. (2006) in an effort to develop the knowledge base required for the design of a damage monitoring system in structures consisting of distributed surface mounted sensors. The behavior of isotropic was studied numerically and experimentally for undamaged and damaged conditions. Study aimed at detection of the damage in beam/plate using wave propagation technique. The experimental and numerical investigations were being made to locate the position and extent of crack approximately with single actuator and several surface mounted sensors. Numerical modeling of wave propagation was done using ABAQUS/EXPLICIT through isotropic and isotropic medium with damages. Now a days so many solvers for solving FEM problems are

coming among them ABAQUS/EXPLICIT is superior in solving wave propagation problems so a brief introduction is given in this chapter about it.

4.3.1 Finite element method for explicit dynamics

This section contains a conceptual and an algorithmic description of the ABAQUS/Explicit analysis product as well as a discussion on the advantages of the method.

4.3.1.1 Stress wave propagation illustrated

This section attempts to provide some conceptual understanding of how forces propagate through a model when using the explicit dynamics method. In this illustrative example we consider the propagation of a stress wave along a rod modeled with three elements, as shown in **figure.4.3.** We study the state of the rod as we increment through time.

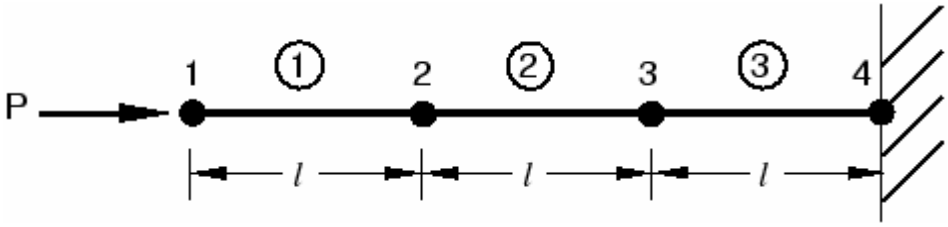

Figure 4.3: Initial configuration of a rod with a concentrated load, P, at the free end.

In the first time increment node 1 has acceleration, $\ddot{u}_1$ as a result of the concentrated force, *P*, applied to it. The acceleration causes node 1 to have a velocity, $\dot{u}_1$ which, in turn, causes a strain rate, $\dot{\varepsilon}_{el1}$ in element 1. The increment of strain, d_{el1} in element 1 is obtained by integrating the strain rate through the time of increment 1. The total strain, ε_{el1} , is the sum of the initial strain, ε_0 , and the increment in strain. In this case the initial strain is zero. Once the element strain has been calculated, the element stress σ_{el1} is obtained by applying the material constitutive model. For a linear elastic material the stress is simply the elastic modulus times the total strain. This process is shown in **figure 4.4.** Nodes 2 and 3 do not move in the first increment since no force is applied to them.

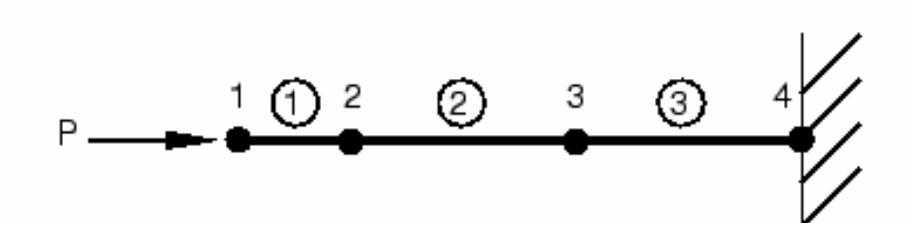

Figure 4.4: Configuration at the end of increment 1 of a rod with a concentrated load, P, at the free end.

$$\ddot{u}_1 = \frac{P}{M_1} \Rightarrow \dot{u}_1 = \int \ddot{u}_1 dt \Rightarrow \dot{\varepsilon}_{el1} = \frac{\ddot{u}_1}{l} \Rightarrow d\varepsilon_{el1} = \int \dot{\varepsilon}_{el1} dt \Rightarrow \varepsilon_{el1} = \varepsilon_0 + d\varepsilon_{el1} \Rightarrow \sigma_{el1} = E\varepsilon_{el1} \quad (3.30)$$

In the second increment the stresses in element 1 apply internal, element forces to the nodes associated with element 1, as shown in **figure 4.5.** These element stresses are then used to calculate dynamic equilibrium at nodes 1 and 2.

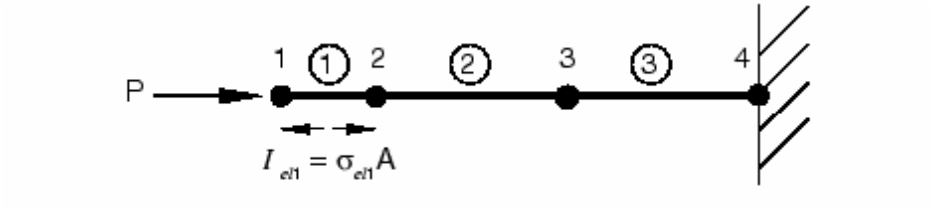

Figure 4.5: Configuration of the rod at the beginning of increment 2.

$$\ddot{u}_1 = \frac{P - I_{el1}}{M_1} \Rightarrow \dot{u}_1 = \dot{u}_1^{old} + \int \ddot{u}_1 dt \quad (4.14)$$

$$\ddot{u}_2 = \frac{I_{el1}}{M_2} \Rightarrow \dot{u}_2 = \int u_2 dt \quad (4.15)$$

$$\dot{\varepsilon}_{el1} = \frac{\dot{u}_2 - \dot{u}_1}{l} \Rightarrow d\varepsilon_{el1} = \int \dot{\varepsilon}_{el1} dt \Rightarrow \varepsilon_1 + d\varepsilon_{el1} \Rightarrow \sigma_{el1} = E\varepsilon_{el1} \quad (4.16)$$

The process continues so that at the start of the third increment there are stresses in both elements 1 and 2, and there are forces at nodes 1, 2, and 3, as shown in **figure 4.6**. The process continues until the analysis reaches the desired total time.

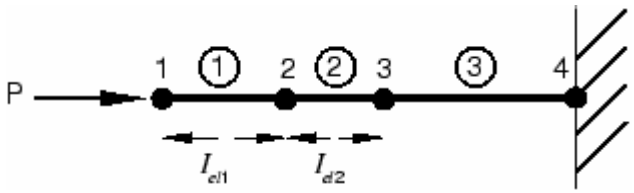

Figure 4.6: Configuration of the rod at the beginning of increment 3

4.3.1.2.1 Time integration

ABAQUS/Explicit uses a central difference rule to integrate the equations of motion explicitly through time, using the kinematic conditions at one increment to calculate the kinematic conditions at the next increment. At the beginning of the increment the program solves for dynamic equilibrium, which states that the nodal mass matrix, *M*, times the nodal accelerations, $\ddot{u}$, equals the total nodal forces (the difference between the external applied forces, P, and internal element forces, I):

$$M\ddot{u} = P - I \tag{4.17}$$

The accelerations at the beginning of the current increment (time) are calculated as

$$\ddot{u}\,|_{(t)} = (M)^{-1}.(P-I)\,|_{(t)} \tag{4.18}$$

Since the explicit procedure always uses a diagonal, or lumped, mass matrix, solving for the accelerations is trivial; there are no simultaneous equations to solve. The acceleration of any node is determined completely by its mass and the net force acting on it, making the nodal calculations very inexpensive.

The accelerations are integrated through time using the central difference rule, which calculates the change in velocity assuming that the acceleration is constant. This change in velocity is added to the velocity from the middle of the previous increment to determine the velocities at the middle of the current increment:

$$\dot{u}\,|_{\left(t+\frac{\Delta t}{2}\right)} = \dot{u}\,|_{\left(t-\frac{\Delta t}{2}\right)} + \frac{\left(\Delta t\,|_{(t+\Delta t)} + \Delta t\,|_{(t)}\right)}{2}\ddot{u}\,|_{(t)} \tag{4.19}$$

The velocities are integrated through time and added to the displacements at the beginning of the increment to determine the displacements at the end of the increment:

$$u|_{(t+\Delta t)} = u|_{(t)} + \Delta t|_{(t+\Delta t)}\ \dot{u}|_{\left(t+\frac{\Delta t}{2}\right)} \tag{4.20}$$

Here is a summary of the explicit dynamics algorithm:

1. Nodal calculations.

   a. Dynamic equilibrium.

$$\ddot{u}_{(t)} = \left(M\right)^{-1}.(P_{(t)} - I_{(t)}) \tag{4.21}$$

   b. Integrate explicitly through time.

$$\dot{u}|_{\left(t+\frac{\Delta t}{2}\right)} = \dot{u}|_{\left(t-\frac{\Delta t}{2}\right)} + \frac{\left(\Delta t|_{(t+\Delta t)} + \Delta t|_{(t)}\right)}{2}\ddot{u}|_{(t)} \tag{4.22}$$

$$u|_{(t+\Delta t)} = u|_{(t)} + \Delta t|_{(t+\Delta t)}\ \dot{u}|_{\left(t+\frac{\Delta t}{2}\right)} \tag{4.23}$$

2. Element calculations.

   a. Compute element strain increments, $d\varepsilon$, from the strain rate, $\dot{\varepsilon}$.

   b. Compute stresses, σ, from constitutive equations.

$$\sigma_{(t+\Delta t)} = (\sigma_{(t)}, d\varepsilon) \tag{4.24}$$

   c. Assemble nodal internal forces, $I_{(t+\Delta t)}$

3. Set $t + \Delta t$ to t and return to Step 1.

4.4 Distributed point source method

Introduction

This method is used specifically for modeling of ultrasonic field .The main originality of DPSM method is that it is not necessary to mesh the totality of the computation volume, but only the surface of interest, in the contrary to a classical finite elements method. The implementation of the model simply requires discretization of the active surface of the transducer or the interfaces to obtain an array of point sources, so that the initial complexity is changed into a superposition of elementary problems. The active surfaces like transducers, emitters, or interfaces reflecting a part of an incident field are discretized into a finite number of elementary surfaces, a point source being placed at the centroid of every elemental surface. DPSM technique for ultrasonic field modeling was first developed by Placko and Kundu (2001). They successfully used this technique to model ultrasonic fields in a homogeneous fluid, and in a non-homogeneous fluid with one interface (Lee et al. 2002, Placko et al. 2002) and multiple interfaces (Banerjee, Kundu and Placko, 2005). The interaction between two transducers, for different transducer arrangements and source strengths, placed in a homogeneous fluid has been studied by Ahmad et al.(2003).

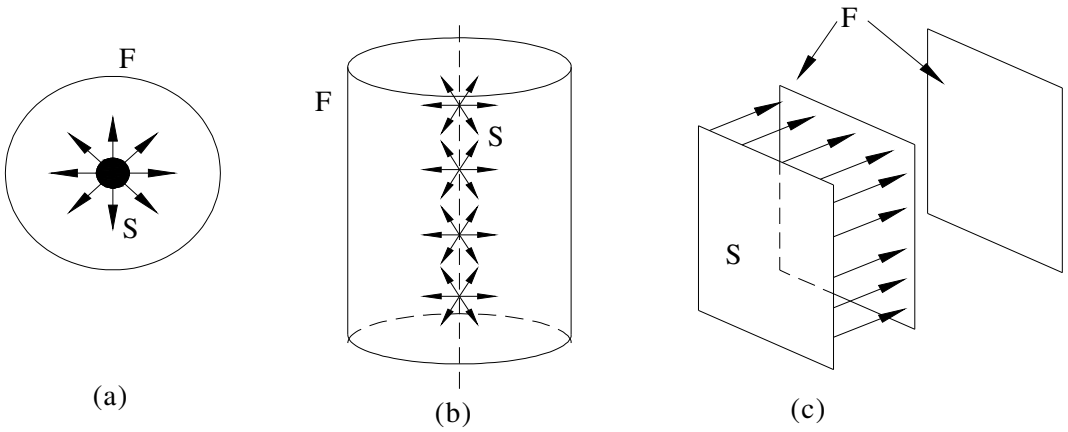

Figure 4.7: (a) Point source generating spherical wavefront

(b) Line source generating cylindrical wavefront

(c) Infinite plane source generating plane wavefront

The scattered ultrasonic field generated by a solid scatterer of finite dimension placed in a homogeneous fluid has also been modeled by the DPSM technique (Placko et al. 2003). Recently the method has been extended to model the phased array transducers (Ahmad et. al. 2005). All these works modeled the ultrasonic field in a fluid medium. The ultrasonic field generated inside the solid half-space or the leaky waves in the fluid produced by guided waves propagating along the fluid-solid interface have not been modeled yet. ***Figure (4.7) shows*** spherical waves generated by a point source in an infinite medium, cylindrical waves generated by a line source and plane waves generated by an infinite plane. The pressure field due to a finite plane source can be assumed to be the summation of pressure fields generated by a number of point sources distributed over the finite source as shown in ***Figure 4.8***. The finite source can be the front face of the transducer. A harmonic point source, which expands and contracts alternately, can be represented by a point and a sphere as shown in ***Figure 4.9(a)***. The point represents the contracted position and the sphere represents the expanded position. When a large number of point sources are placed side by side on a plane surface, then the contacted and expanded positions are shown in ***Figure 4.9(b)***. The combined effect of a large number of point sources placed side by side is shown in ***Figure 4.9(c)***. From this figure it is clear that the combined effect of a large number of point sources distributed on a plane surface is the vibration of particles in the direction normal to the plane surface. Non-normal components of motion at a point on the surface generated by neighboring source points cancel each other as shown in ***Figure 4.9(d).*** However, non normal components do not vanish along the edge of surface. The particles not only vibrate normal to the surface but also expand to a hemisphere and contract to a point on the edge as shown.

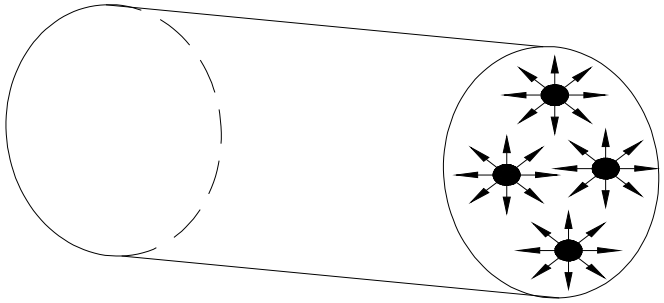

Figure 4.8: Four point sources distributed over a finite surface

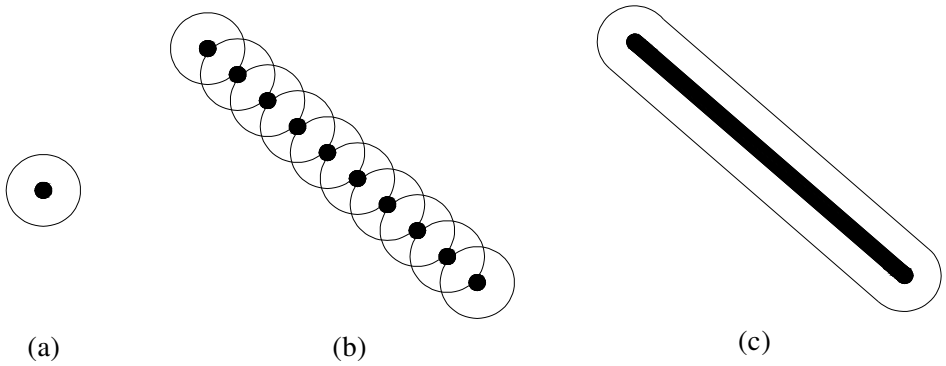

(a) (b) (c)

Source expanded - Thin line Source contracted - Dark point

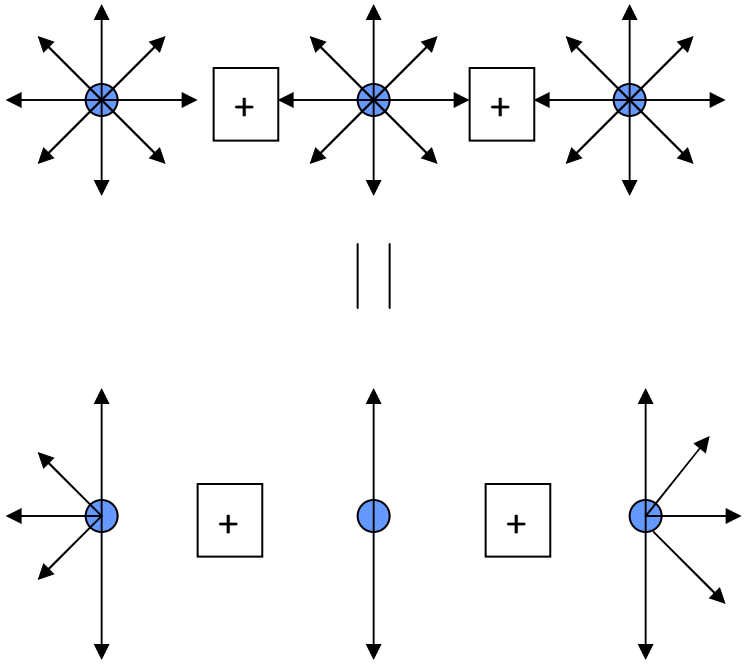

(d)

Figure 4.9: Position of particles for (a) Point source (b) Distributed finite number of points (c) Large number of point sources (d) components of motion of multiple point sources

CHAPTER 5

DAMAGE DETECTION IN BARS-EXPERIMENTAL SETUP

5.1 General

The main effects of corrosion degradation in reinforced concrete result from rust formation at the outer surface of the reinforcing steel with the corresponding steel cross-sectional loss. Rust product is widely accepted as being more voluminous than steel, with reports ranging from twice to six times the volume. An increase in rust product accumulation at the interface, results in a reduction of the reinforcing steel cross-section as shown in **figure 5.1**. The eventual cracking caused by the pressure induced from the rust product accumulation causes a loss of bond between the steel and concrete.

Cracking of the surrounding concrete caused by the continuing pressure buildup from corrosion product is the main form of degradation to the surrounding concrete. Cracking, spalling, and rust staining are usually the earliest indications of corrosion in the concrete. Cracking usually occurs at small percentages of loss of steel mass, usually around a rust thickness of 0.1 to 0.2 mm.

In the laboratory, uniform corrosion is relatively easier to achieve than localized corrosion. However, uniform corrosion is virtually nonexistent in a realistic situation. Instead, pits (crevices) of corrosion are generally found scattered along the rebar.

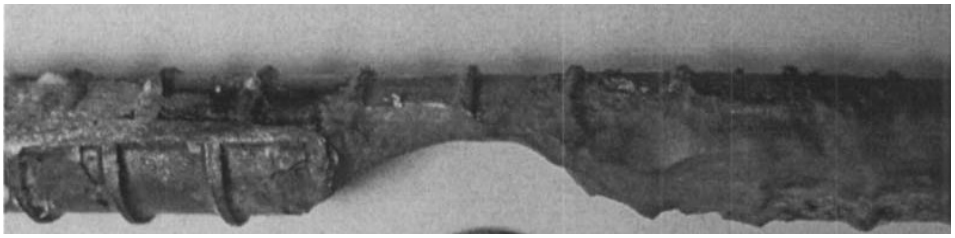

Figure 5.1: Reduction of cross-sectional area caused by pitting corrosion of the reinforcing steel bar

Pitting of the steel causes reflections of the wave form and mode conversions leading to the overall attenuation of the signal strength of the transmitted mode. In an infinite isotropic solid medium only two types of independent wave propagation exist, i.e., compressional and shear waves. Both waves propagate with constant velocities and are nondispersive. The effect of area reduction on wave propagation through extruded mild steel bar was studied experimentally and is discussed in detail in this chapter.

5.2 Experimental Details

The extruded mild steel bars of 12 mm diameter and variable length were used for experiments. The damage in the form of area reduction was introduced at the centre of the bar. Four sets of specimens with 0%, 20%, 40% and 60% area reduction were prepared as shown in **figure 5.2**. The location of damage was also varied along the length of the bar. Four sets of specimen length were manufactured with 0.81 m, 1.0 m, 1.5m and 2.0 m bar length.

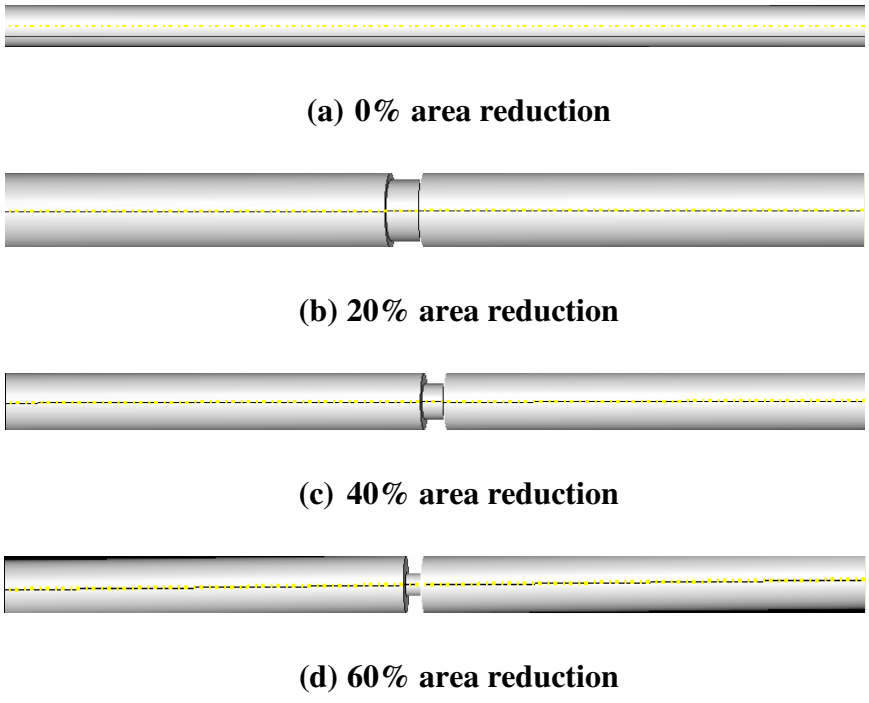

(a) 0% area reduction

(b) 20% area reduction

(c) 40% area reduction

(d) 60% area reduction

Figure 5.2: Steel bars with (a) 0%, (b) 20%, (c) 40% and (d) 60% area reduction at the centre

Two type of experimental setup were used. In first setup the oscilloscope was used for capturing the wave signatures and in second setup digitizer card was used for analyzing the wave signal as

shown in **figure 5.3** and **figure 5.4** below. Two contact transducers were used for sending and receiving the waveforms in through transmission method. Pulser/Receiver was used for generating the negative spike pulse. Personal computer was used for storing the data received.

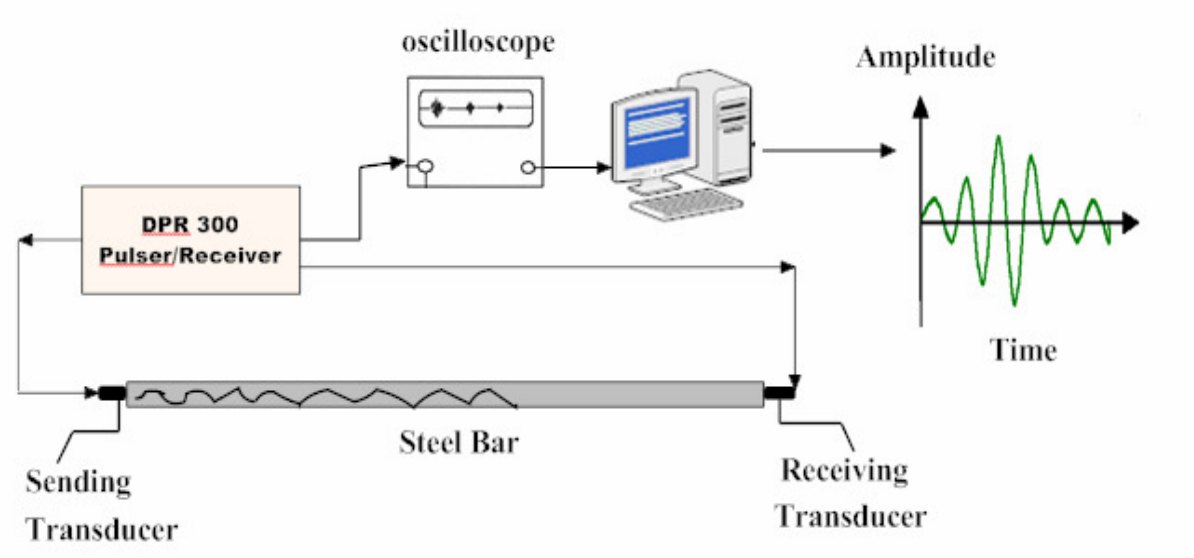

Figure 5.3: Experimental setup with oscilloscope used for capturing the wave signatures

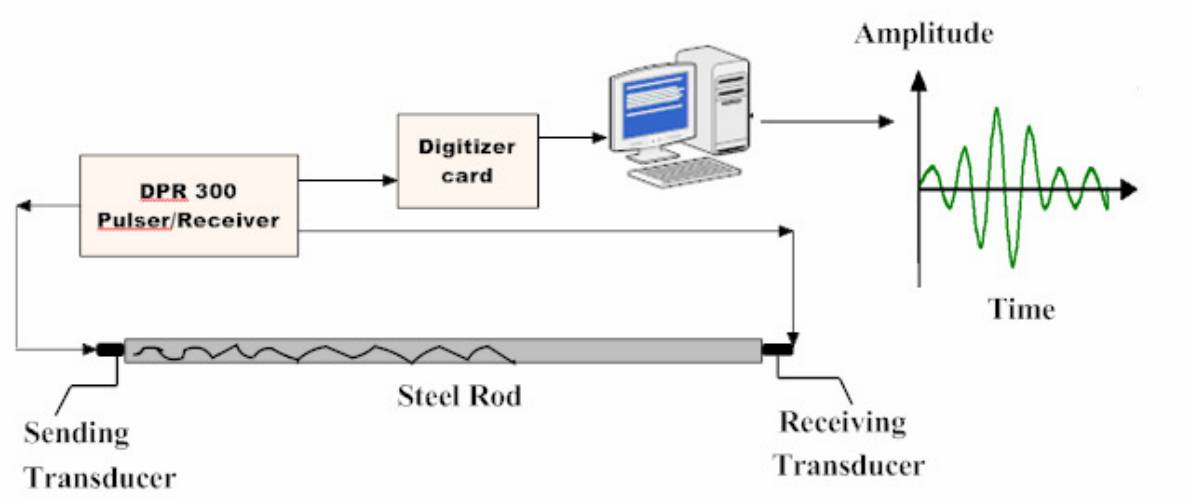

Figure 5.4: Experimental setup with digitizer card used for capturing the wave signatures

Following are the salient features of the equipments used:

- **Transducer**

A contact transducer is a single element longitudinal wave transducer intended for use in direct contact with a test piece. It can be used in straight beam flaw detection and thickness gauging, detection and sizing of delamination, material characterization and sound velocity measurements, inspection of plates, billets, bars, forgings castings, extrusions, and a wide variety of other metallic and non-metallic components. ACCUSCAN "S" series have longer wave form duration and a relatively narrow frequency bandwidth.

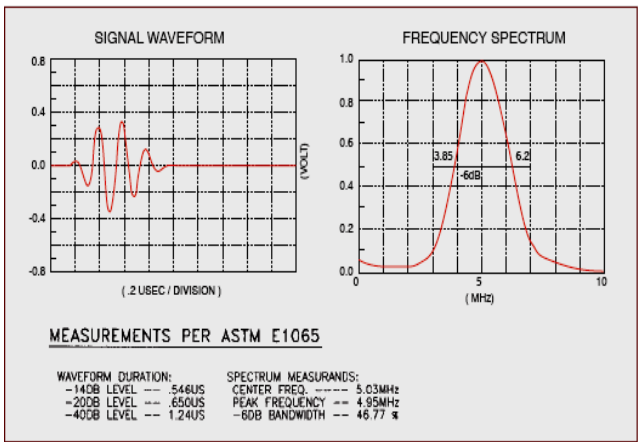

A182S-RB Standard contact transducer of 3.5 Mhz frequency and 13mm diameter was used.

- **Agilent Function 6000 Series Oscilloscope**

A 100 MHz, 2-channel + 16 Logic Channels MSO with maximum sampling rate of 2 GSa/s was used. The analog input impedance of the 100 MHz oscilloscopes is fixed at 1 MΩ.

- **JSR Ultrasonics DPR 300 Pulser/ Receiver System**

DPR300 pulser produces a high voltage electrical excitation pulse and applies this pulse to the instrument's T/R connector. An ultrasonic transducer connected to the T/R connector via a length of 50 Ω coaxial cable is then employed to convert the electrical energy of the excitation pulse into an ultrasonic pulse that is propagated into a test material or medium.

With the DPR300 configured for pulse-echo mode operation, acoustic echoes reflected from interfaces or defects within the test material are converted by the transducer into electrical signals that are presented to the T/R connector of the DPR300. The low-noise DPR300 receiver amplifies these electrical signals, and the signals then pass through adjustable high pass and low

pass filters. The DPR300 receiver gain is adjustable between -13 dB and 66 dB, and there are six high pass and six low pass filter settings for band-limiting the receiver frequency response. The amplified and filtered signals are available on the instrument's Receiver Output connector.

The DPR300 may also be used in transmission mode operation wherein a separate receiving transducer is used to detect acoustic pulses that have propagated through a test material or medium.

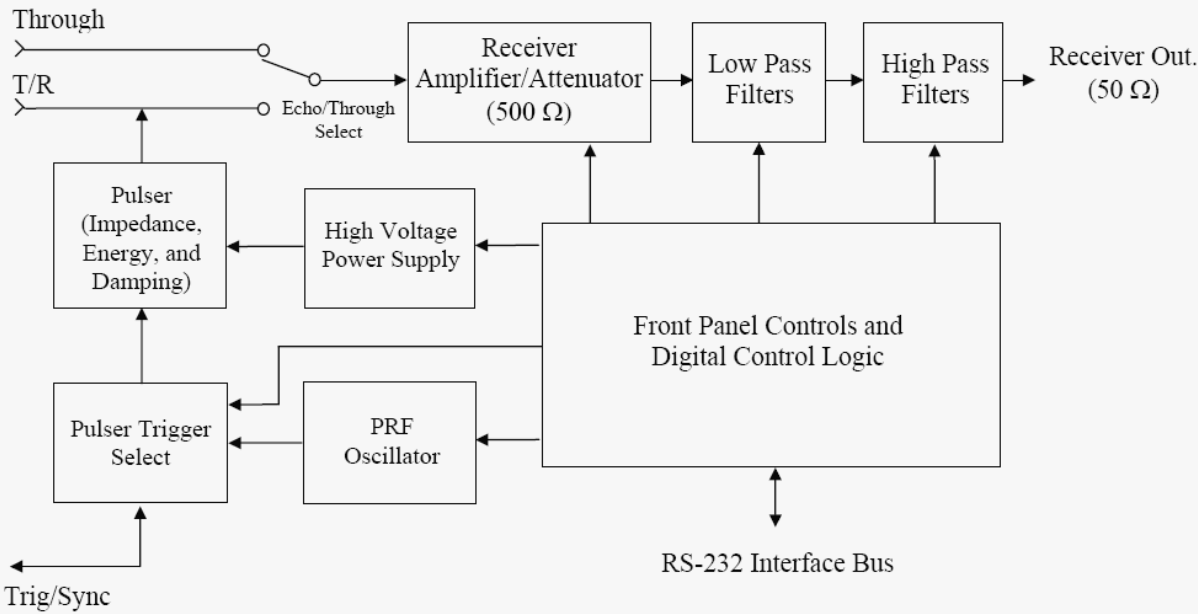

Figure 5.5: Detail circuit diagram of Pulser/Reciever system

PRF Oscillator & Pulser Trigger control: The internal PRF oscillator generates repetitive trigger pulses for the pulser subsystem under the control of the PRF control. Pulser Trigger control selects between the internal PRF oscillator or an external source applied to the Trig/Sync connector as trigger sources for the DPR 300 Pulser.

Pulser (Impedance/Energy/Damping): The pulser generates an excitation pulse upon receiving a trigger event from a selected source. There are four energy and two impedance values, and the single Energy and impedance control adjusts the pulse energy and the pulser impedance.

Receiver amplifier: It controls the amplification or attenuation of signals processed by the DPR300 receiver. The receiver gain can be varied from -13dB to 66 dB.

Low Pass and High Pass filters: Low filters are available for reducing the bandwidth of the DPR300 receiver. High Pass filters are available for eliminating undesirable low frequency energy from the DPR300 receiver signal. High pass filtering can be used as a means of providing faster receiver recovery from strong signals such as the excitation pulse or strong interface echoes.

Pulser	
Pulse Type	Negative Spike Pulse
High Voltage Supply	100V to 475V
Initial Transition (Fall Time)	<5 ns (10-90%) typical for 475V pulsers
Pulse Amplitude	-475V peak. Amplitude depends on Energy, Impedance, Damping control settings, and pulser type
Pulse Energy	1.55 µJoules minimum, 304 µjoules maximum for 475V pulsers. Dependent upon energy and voltage setting
Pulse Duration	Typically 10-70 ns FWHM for 50 Ω load. Function of the Energy, Impedance, and Damping controls
Damping	16 Damping values: 331, 198, 142, 110, 92, 77, 67, 59, 52, 47, 43, 39, 37, 34, 32, and 30Ω.
Mode	Pulse-echo or through transmission
Through Mode Isolation	Typically 80 dB at 10 MHz
Pulser Repetition rate	Internal: 100 Hz - 5 kHz for 475V pulsers. External: 0 - 5 kHz for 475V pulsers.
Sync Output	Maximum +5 V, tr < 30 ns, tw = 50 ns. min. TTL and CMOS compatible. Minimum value of load impedance is 50 Ω
Pulser Trigger Source	Selectable by computer between internal oscillator and external source
External Trigger Input	3 - 5 V positive going pulse. Triggering will occur synchronously with leading edge of trigger signal. TTL and CMOS compatible
Receiver	
Gain	-13 to 66 dB in 1 dB steps controlled by the host computer
Phase	0^o (noninverting)
Input Impedance	500Ω (through transmission)
Bandwidth	.001-35 MHz (-3 dB) or .001-50 MHz

High Pass Filter	DC,1, 2.5, 5, 7.5 and 12.5 MHz
Low Pass Filter	3,7.5,10,15,22.5 (35 MHz BW) or 5,10,15,22.5,35 (50 MHz BW)
Receiver Noise	Typically 49 μV pk-pk input referred(measured at 60dB,35 MHz bandwidth)
Output Impedance	50Ω
Output Voltage	± 0.5 V into 50Ω

- **Dual-Channel High-Resolution Waveform Digitizer**

Model DC438 Dual-channel, 12-bit, 100 MHz, 200 MS/s, 4 M point acquisition memory card was used to capture the waveform. Waveforms are transferred directly into the digitizer large acquisition memories so that complex signals can be stored over very long time periods. Large memories are essential for maintaining fast sampling rates and therefore timing resolution.

Model DC438	
Bandwidth (-3 dB)	DC to 100 MHz
Full Scale Range (FSR)	250 mV, 500 mV, 1 V, 2 V, 5 V and 10 V
Impedance	50 Ω ± 1% @ DC
Connector	BNC, gold-plated
Channels	Two
Coupling	DC
Maximum Input Voltage	±10 V DC (2 W) or 10 V RMS at 50 Ω
Bandwidth Limit Filter	35 MHz 2-pole Bessel filter (DC438)
Minimum Amplitude	1 V pk-pk
Impedance	50 Ω

5.3 Mode of Excitation Signal

Transducers with center frequencies of 2.25 MHz, 3.5 MHz and 5 MHz were used for the experiments. The transducers were driven by a Pulser/receiver system with maximum gain of 66 dB and maximum input voltage of 475V. An external PC and Digitizer card was used to capture the received signal and for further processing. The transducer was mounted in a holder and coupled using a industrial coupling gel. The excitation signal consisted of a negative spike pulse with pulse duration ranging from 10-70 ns. The results illustrate that different frequencies and modes have different dispersion characteristics with a trend toward higher frequencies having slower energy transport velocities**.**

5.4 Experimental Method

To simulate corrosion damage area reduction was done at three different locations along the length of the bar. The magnitude of the defect was also varied at a particular location. Pulse echo and through transmission method were used for characterizing the damage. To find the location of crack, Pulse Echo method was used and to find the extent of damage Through Transmission was used. The depth of the crack is the measurement of the transit time of the wave diffracted by the tip of the crack. Longitudinal wave was generated by placing the transducers normal to the cross section of the bar. The nature of these waves is non- dispersive meaning that their propagation along a surface of a semi-infinite and homogeneous medium would not alter their frequency content and velocity would not be frequency dependent. In through transmission method, two probes were used one as an actuator for sending the waves at one end and another as a receiver for receiving the waves at the other end of the bar.

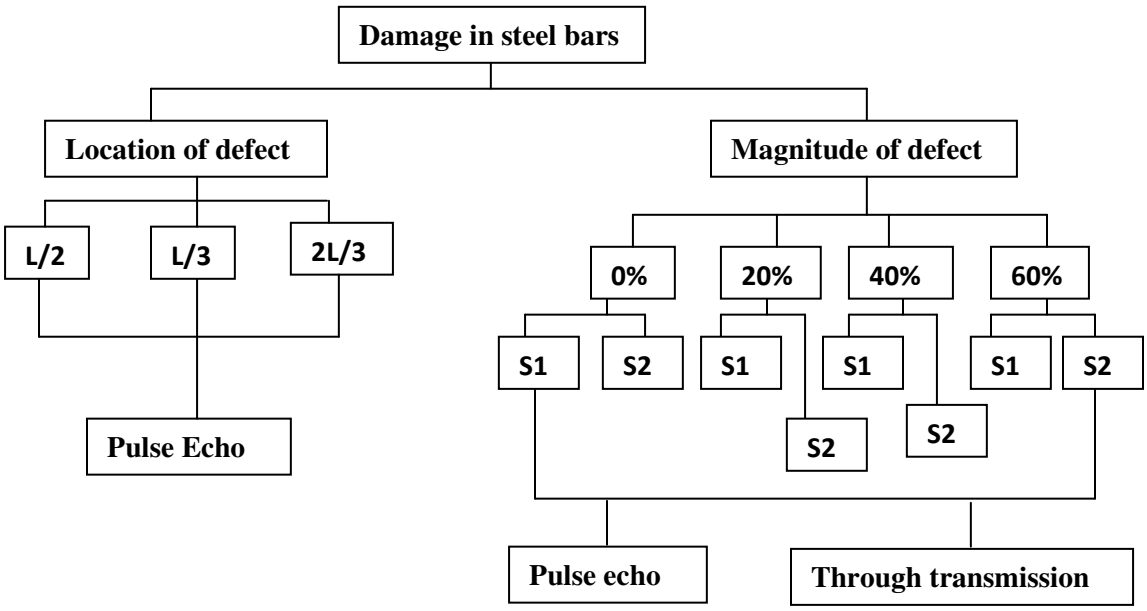

Figure 5.6: Methodology of damage detection in bars

Type of transducer, input parameters like voltage, gain, PRF rate and transducer central frequency are few important parameters for ultrasonic testing. To decide one particular ultrasonic frequency of broadband transducers for testing, three sets of transducers were used of frequency 2.25 MHz, 3.5 MHz and 5 MHz .All the specimens were tested on these frequencies and based

on the results the best frequency was decided. A parametric study was carried out to ascertain the location and magnitude of damage. **Figure 5.7** defines the procedure of study in brief.

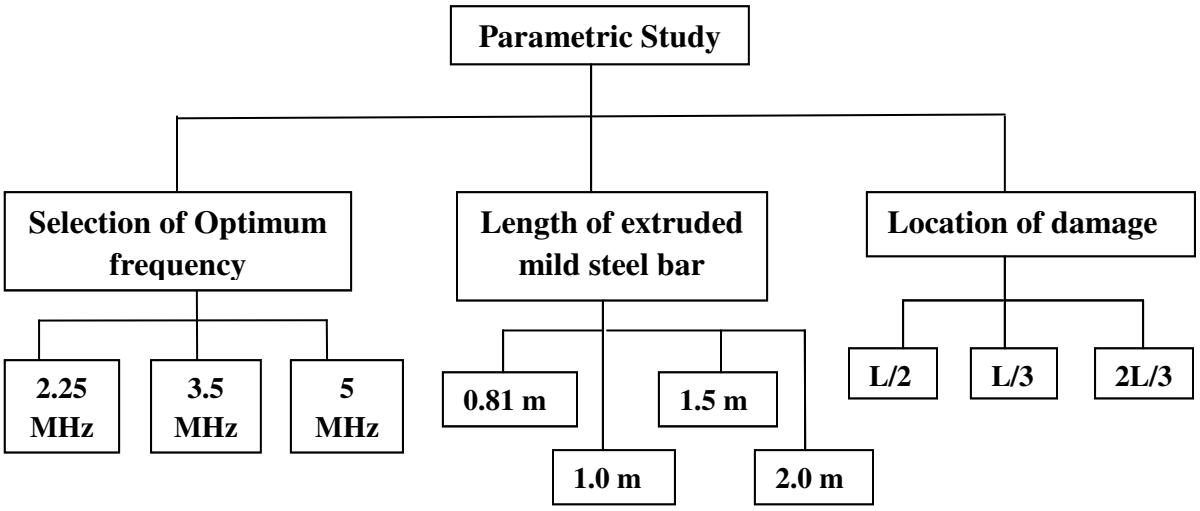

Figure 5.7: Flow chart showing the layout of the study carried for damage detection in bars.

- **Pulse Echo Method**

In nondestructive testing of metals, the *ultrasonic pulse-echo* (UP-E) technique has proven to be a reliable method for locating cracks and other internal defects. An electro-mechanical transducer is used to generate a short pulse of ultrasonic stress waves that propagates into the object being inspected. Reflection of the stress pulse occurs at boundaries separating materials with different densities and elastic properties. The reflected pulse travels back to the transducer that also acts as a receiver. The received signal is displayed on an oscilloscope, and the round trip travel time of the pulse is measured electronically. By knowing the speed of the stress wave, the distance to the reflecting interface can be determined.

5.5 Experiments

5.5.1 Selection of optimum frequency

Steel bars of 1 m length and 12 mm diameter were tested using pulse echo and through transmission method using 2.25 MHz, 3.5 MHz and 5MHz frequency transducers. The signals or waveforms were captured on Agilent MSO and transferred to PC where signals were processed using suitable software. The results illustrate that 3.5 MHz frequency broad band transducers gave best results with the same input parameters and hence were further used in experiments for carrying out the parametric study.

- **2.25 MHz Transducer, 1m long steel bar, Fault Location-L/2, Pulse Echo**

JSR DPR 300 Pulser/Receiver settings	
Receiver	
Bandwith	35
Gain [-12 dB-67 dB]	47 dB
High Pass Filter [Out-12.5 MHz]	1 MHz
Low Pass Filter [3 MHz-35 MHz]	10 MHz
Pulser	
Damping [331 ohms-30 ohms]	59 ohms
Energy [1-4]	1
PRF [100 Hz-5 KHz]	100 Hz
Voltage [100V-400V]	300 V
Impedance [Low-High]	Low

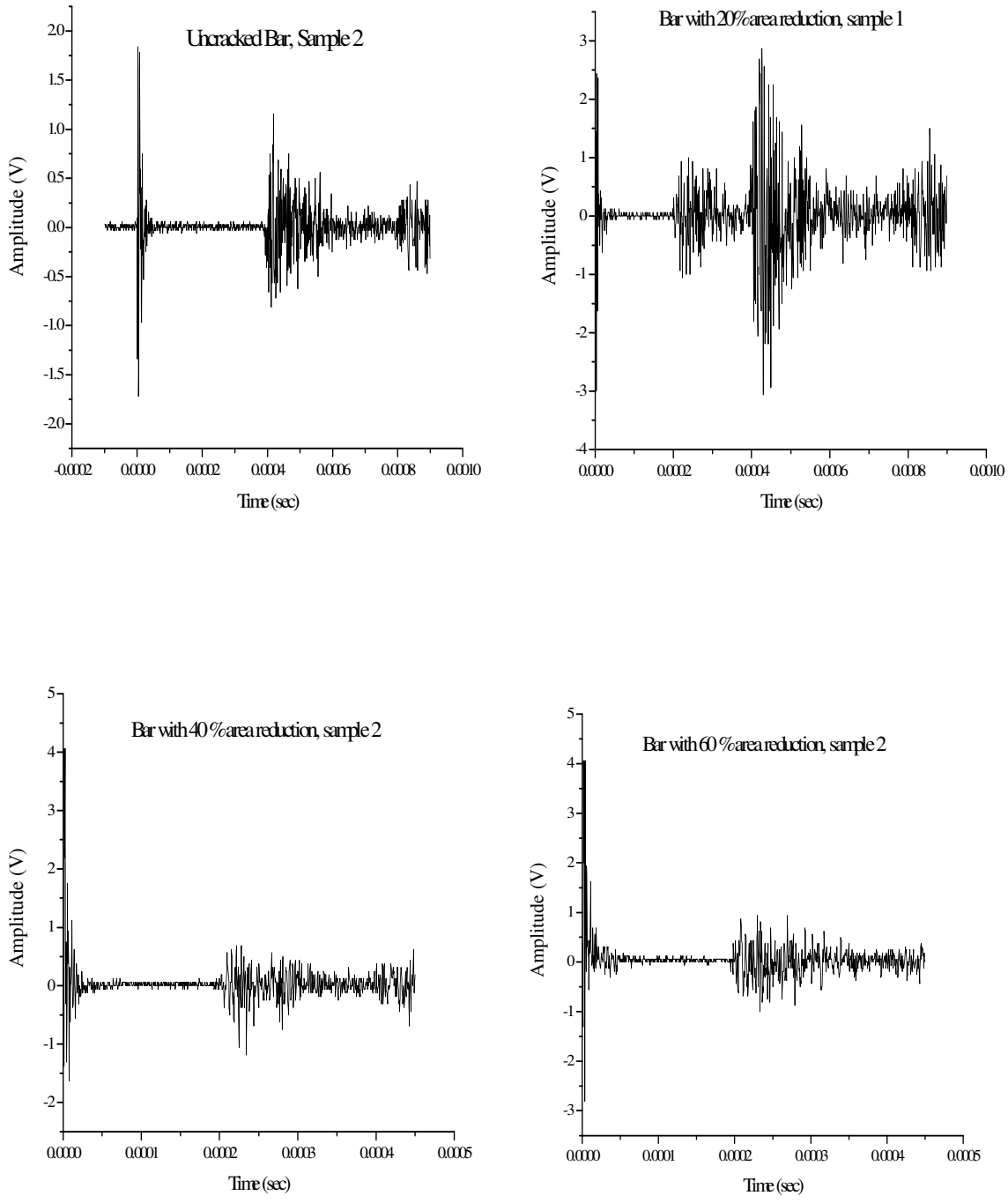

Figure 5.8: Pulse Echo through bar with 0%, 20%, 40% and 60% area reduction at the centre respectively at 2.25 MHz frequency

- **2.25 MHz Transducer, 1m long steel bar, Fault Location-L/2, Through Transmission**

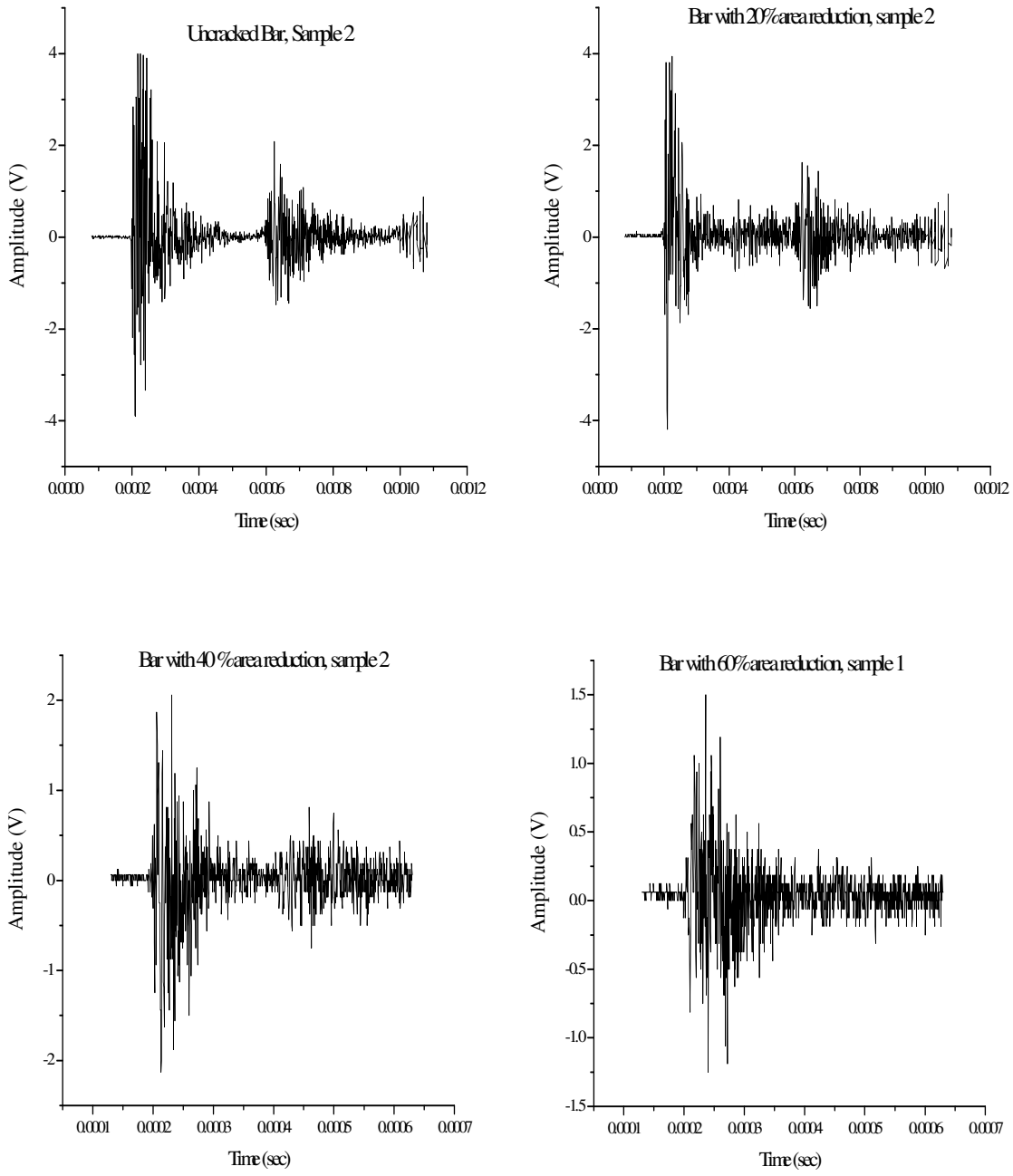

Figure 5.9: Through Transmission in bar with 0%, 20%, 40% and 60% area reduction at the centre respectively at 2.25 MHz frequency

- **5.0 MHz Transducer, 1m long steel bar, Fault Location-L/2, Pulse Echo**

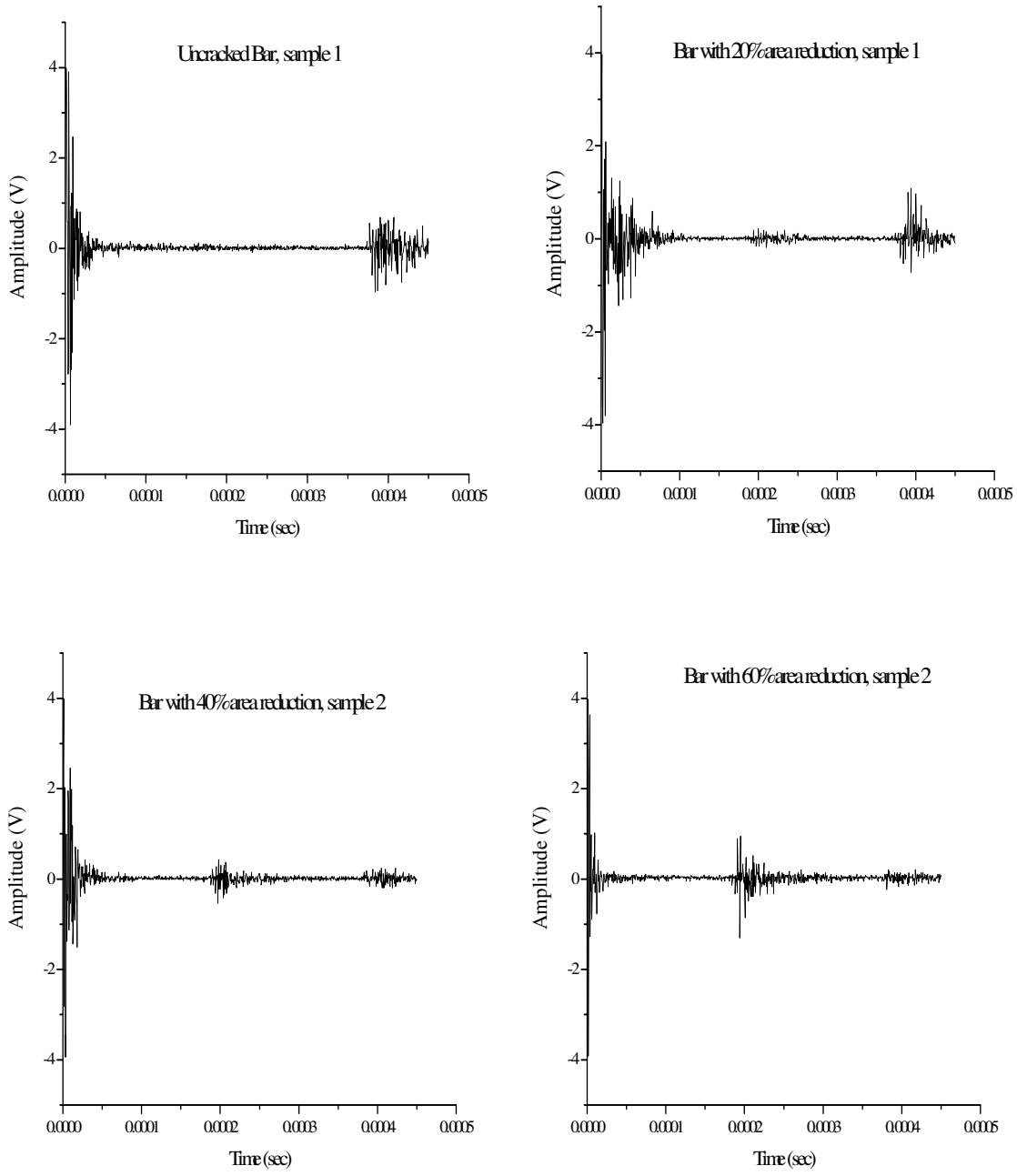

Figure 5.10: Pulse Echo through bar with 0%, 20%, 40% and 60% area reduction at the centre respectively at 5 MHz frequency

- **5.0 MHz Transducer, 1m long steel bar, Fault Location-L/2, Through Transmission**

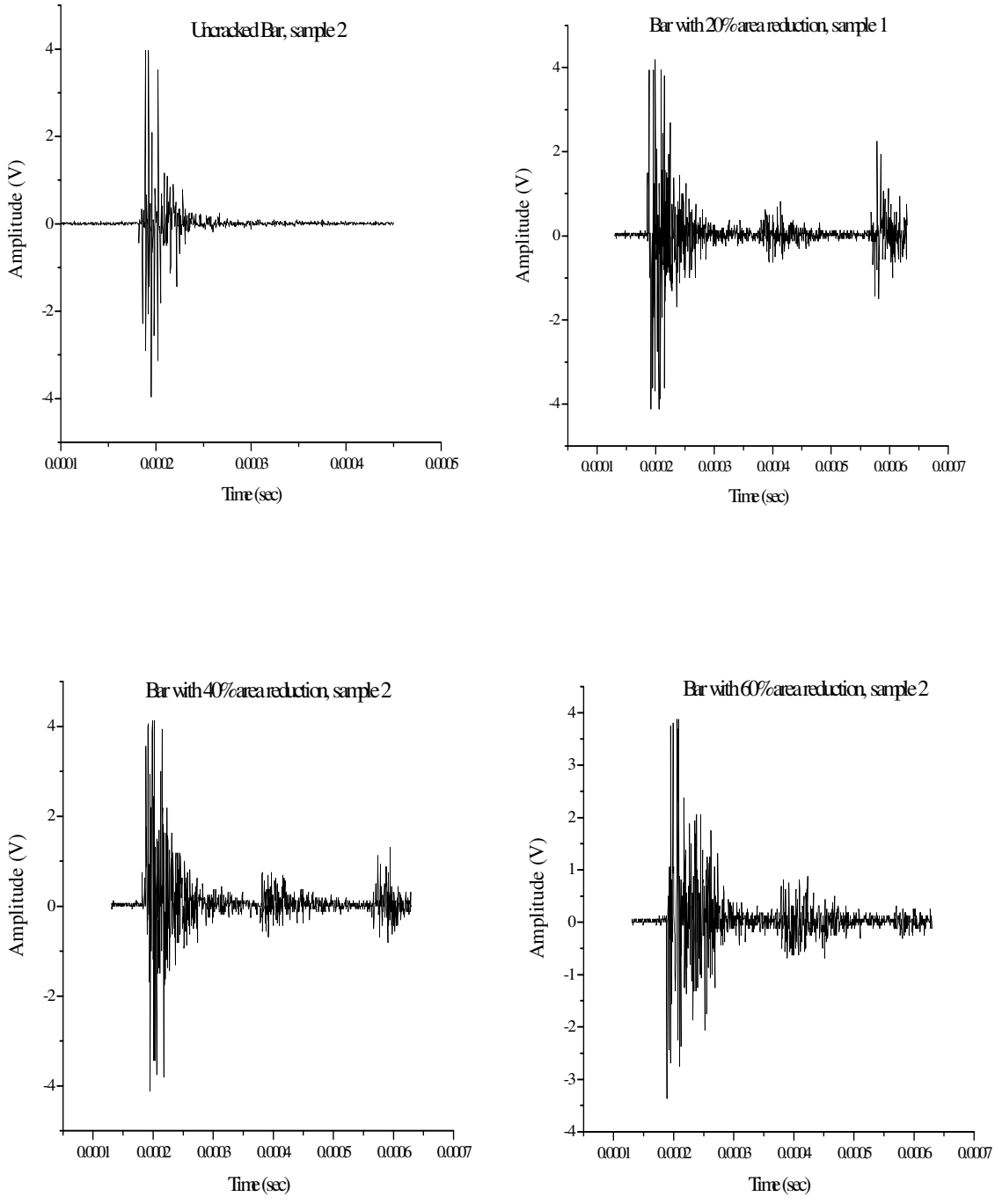

Figure 5.11: Through Transmission in bar with 0%, 20%, 40% and 60% area reduction at the centre respectively at 5 MHz frequency

- **3.5 MHz Transducer, 1m long steel bar, Fault Location-L/2, Through Transmission**

JSR DPR 300 Pulser/Receiver settings	
Receiver	
Bandwith	35
Gain [-12 dB-67 dB]	30 dB
High Pass Filter [Out-12.5 MHz]	1 MHz
Low Pass Filter [3 MHz-35 MHz]	10 MHz
Pulser	
Damping [331 ohms-30 ohms]	67 ohms
Energy [1-4]	4
PRF [100 Hz-5 KHz]	600 Hz
Voltage [100V-400V]	450 V
Impedance [Low-High]	High

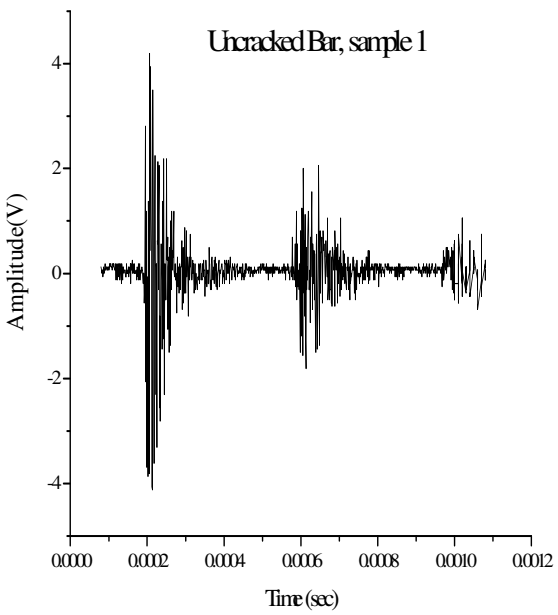

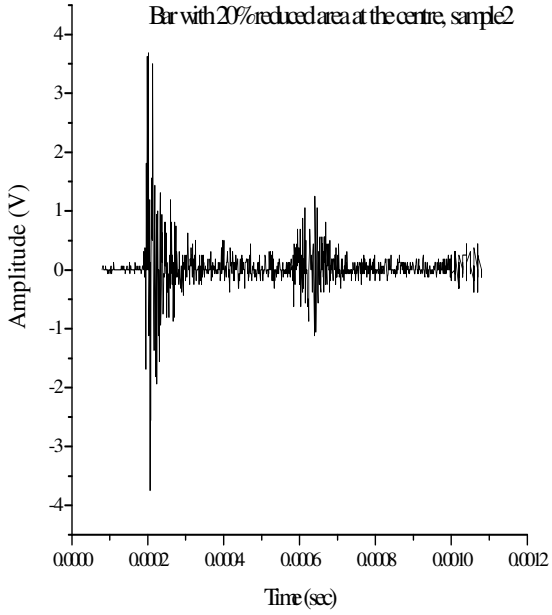

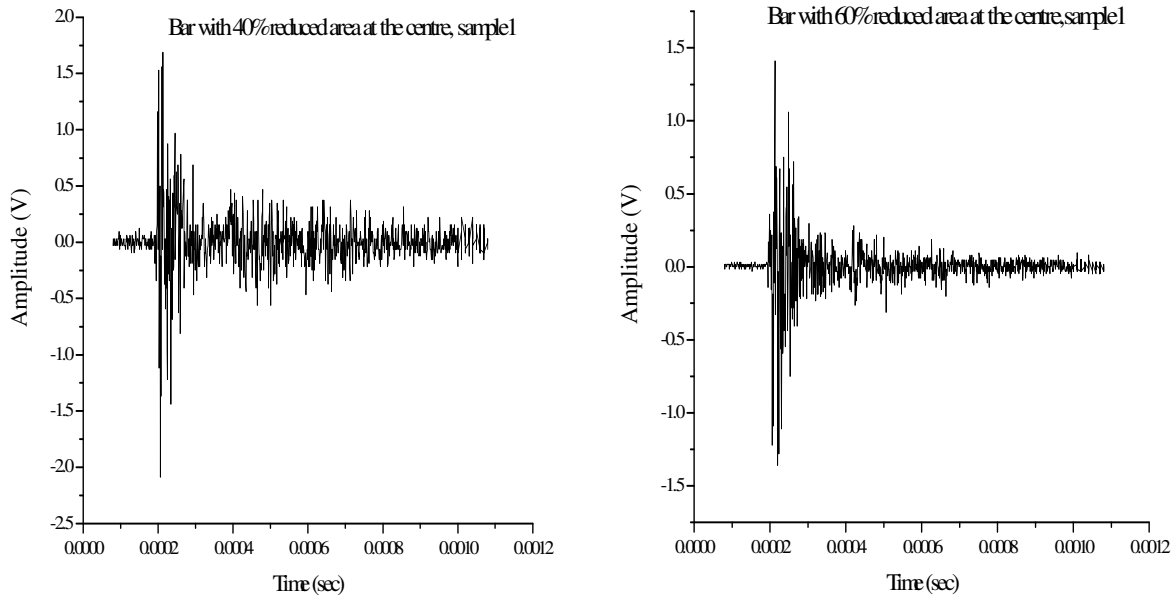

Figure 5.12: Through Transmission in bar with 0%, 20%, 40% and 60% area reduction at the centre respectively at 3.5 MHz frequency

- **3.5 MHz Transducer, 1m long steel bar, Fault Location-L/2, Pulse Echo**

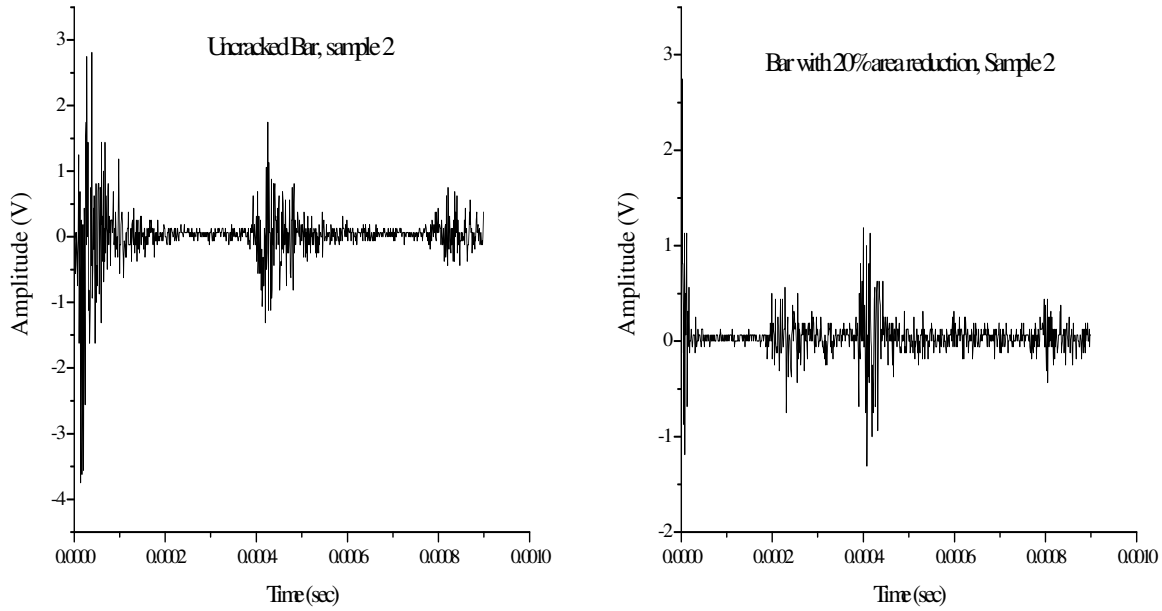

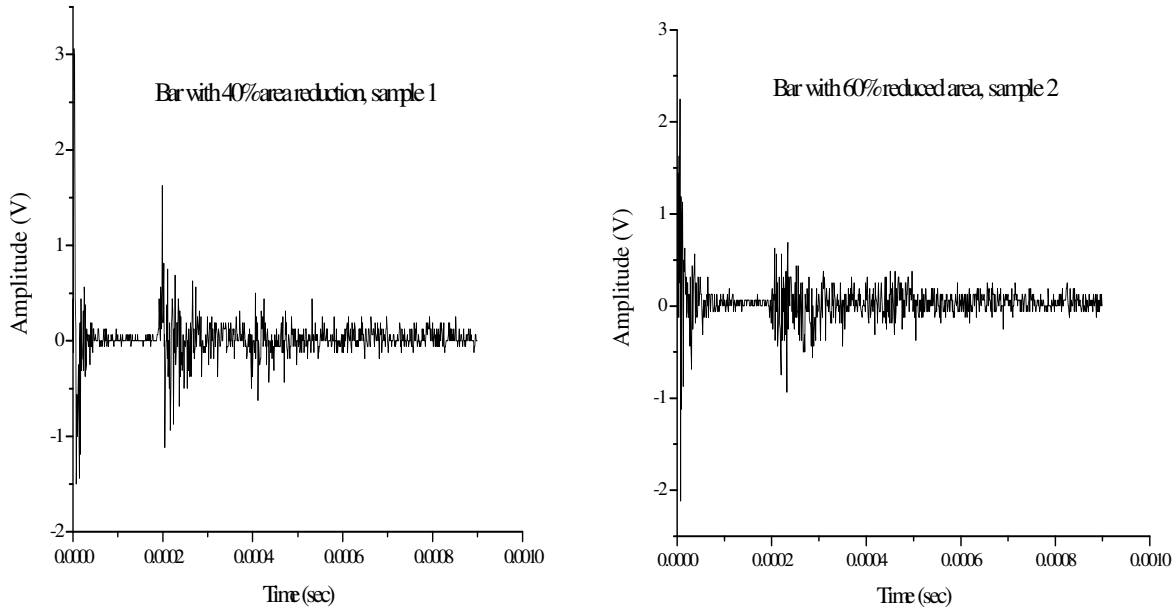

Figure 5.13: Pulse Echo through bar with 0%, 20%, 40% and 60% area reduction at the centre respectively at 3.5 MHz frequency

Conclusion

As seen from the results above (**figure 5.12 and figure 5.13**) of pulse echo and through transmission, it was concluded that 3.5 MHz frequency gives the best result or wave signatures in locating the fault location and hence is best suited for ultrasonic testing through steel bars of 12mm diameter. All the further experiments were carried out with 3.5 MHz frequency transducers only.

5.5.2 Location of damage

As a further study the location of crack was changed from L/2 location to L/3 and 2L/3 locations along the length of the rods. Signals received from all the specimens (two samples each for % area reduction) was analysed and compared with the healthy specimen. It was found that time of flight of peak from the crack was same as it comes out to be theoretically hence validating the results.

Application of 3.5 MHz frequency to steel rod with fault at L/3 location

- **3.5 MHz Transducer, 1m long steel bar, Fault Location-L/3, Pulse Echo**

JSR DPR 300 Pulser/Receiver settings	
Receiver	
Bandwith	35
Gain [-12 dB-67 dB]	38 dB
High Pass Filter [Out-12.5 MHz]	1 MHz
Low Pass Filter [3 MHz-35 MHz]	7.5 MHz
Pulser	
Damping [331 ohms-30 ohms]	43 ohms
Energy [1-4]	4
PRF [100 Hz-5 KHz]	100 Hz
Voltage [100V-400V]	475 V
Impedance [Low-High]	Low

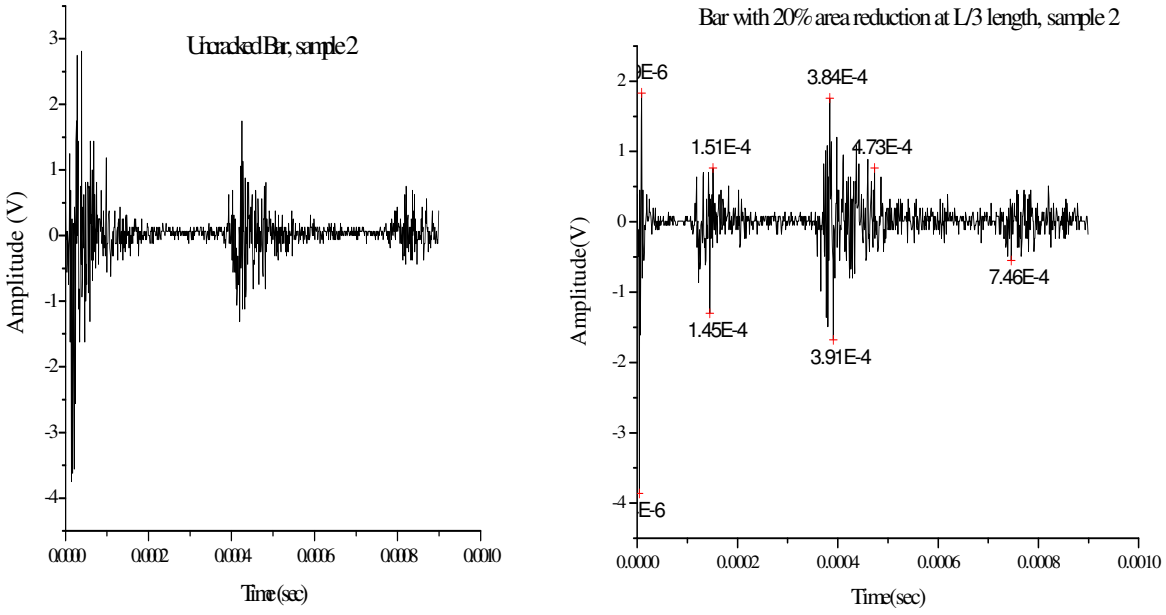

Figure 5.14: Pulse Echo through bar with 0% and 20% area reduction respectively at L/3 location at 3.5 MHz frequency

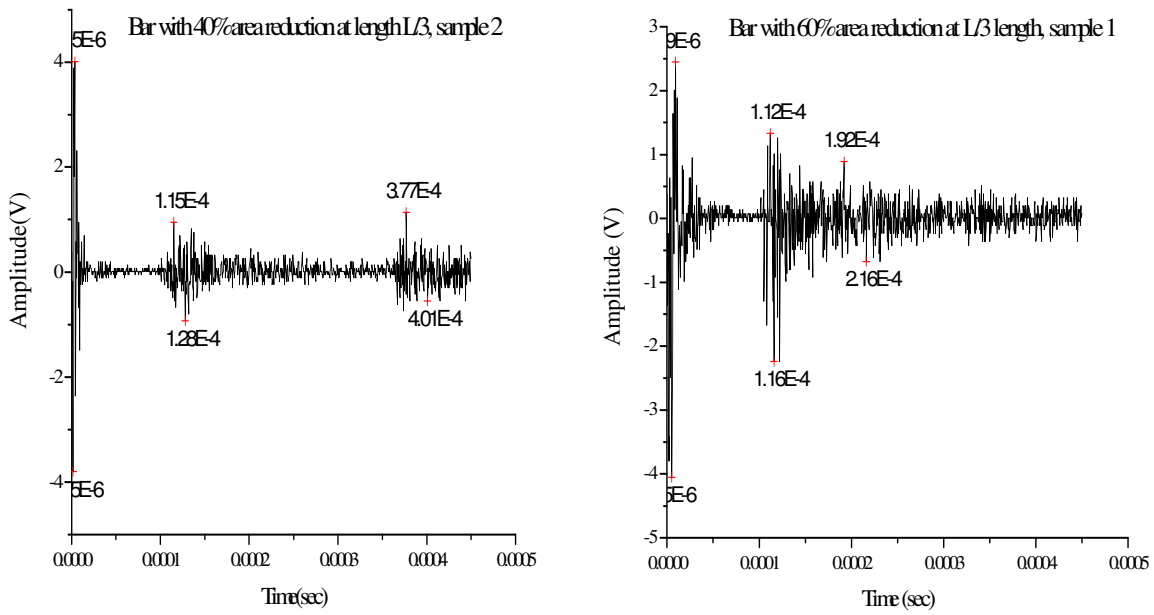

Figure 5.15: Pulse Echo through bar with 40% and 60% area reduction respectively at L/3 location at 3.5 MHz frequency

The velocity of longitudinal wave in steel rod of young's modulus of elasticity as 200 GPa and density as 7800 Kg/m^3 is 5063 m/s. At this velocity the time of travel of wave in healthy specimen of 1m length is 3.95E-4 sec and as per the graphs it is 4E-4 sec. Similarly the time of flight of wave from the crack at L/3 length is 1.32E-4 sec theoretically and we can see from the graph that it comes out be 1.28E-4 sec. Similar results were found when specimens were tested for crack at 2L/3 length.

Table 5.1: Pulse echo through 1.0 m steel bar with damage at L/3 location

Fault location – L/3	
Theoretical results	**Time (sec)**
	1st peak
Healthy specimen	3.95x 10^{-4}
Cracked specimen	1.317x 10^{-4}
Experimental results	
Area Reduction	**1st peak**
Healthy specimen (0 %)	4.0x 10^{-4}
20 %	1.39 x 10^{-4}
40 %	1.15 x 10^{-4}

60 %	1.12 x 10^{-4}

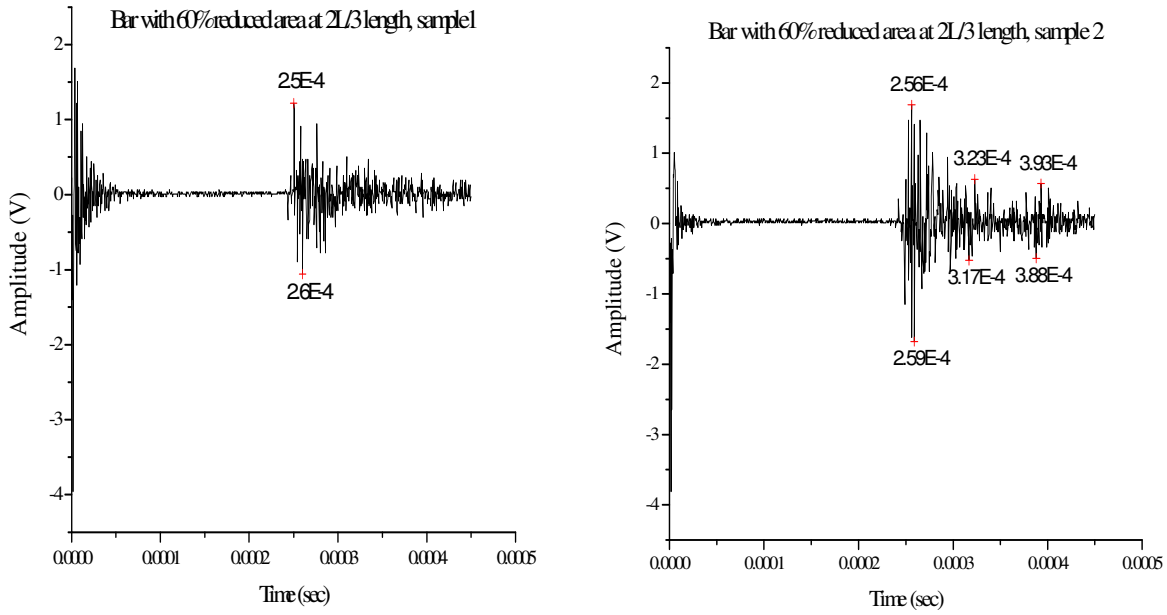

Figure 5.16: Pulse Echo through bar with 60% area reduction at 2 L/3 lengths at 3.5 MHz frequency

Application of 3.5 MHz frequency to steel rod with fault at 2 L/3 locations

Table 5.2: Pulse echo through 1.0 m steel bar with damage at 2L/3 location

Fault location – 2L/3	
Theoretical results	**Time (sec)**
	1st peak
Healthy specimen	3.95x 10^{-4}
Cracked specimen	2.633x 10^{-4}
Experimental results	
	1st peak
Healthy specimen	4.0x 10^{-4}
Cracked specimen	2.60 x 10^{-4}

5.6 Experiments using digitizer card for capturing the wave signature

As stated before, all the above experiments were carried out using mixed-signal oscilloscope. However, due to MSO limitation of storing only 1000 points we were not able to capture the exact waveform. So we shifted from oscilloscope to digitizer card through which we were able to capture 40 lakh points and it gave us the data very much near to the exact signature of waveform. **Figure 5.17** and **figure 5.18** show the image captured using digitizer card and oscilloscope respectively.

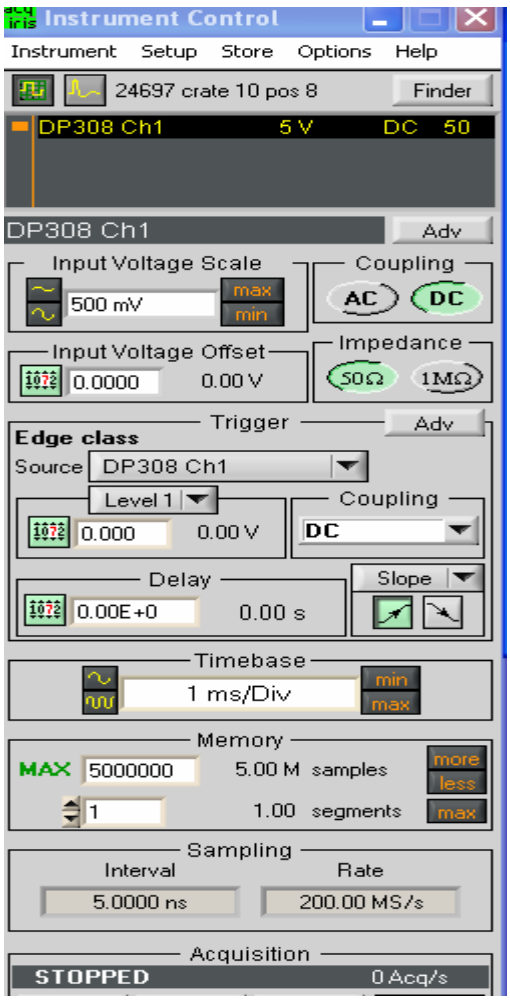

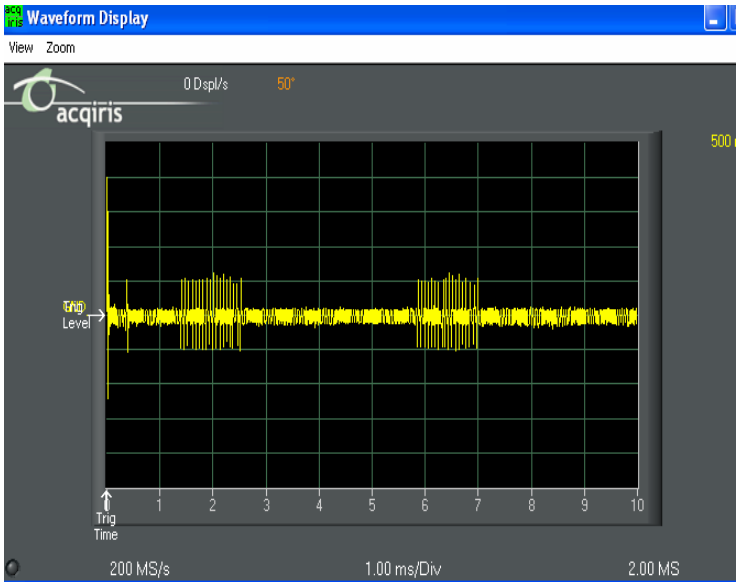

Figure 5.17: Image of waveform captured using digitizer card

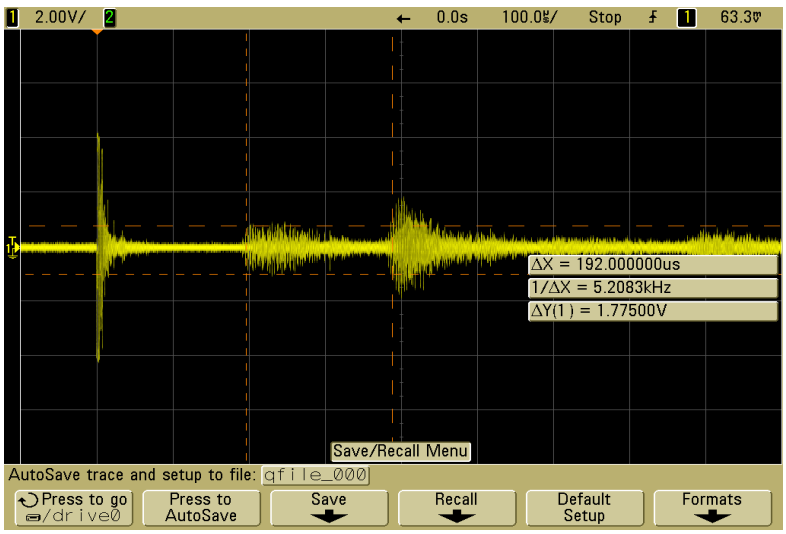

Figure 5.18: Image of waveform captured using mixed-signal oscilloscope

Four sets of specimens were prepared of 0%, 20%, 40% and 60% area reduction at the centre of the bar of length 0.81m, 1.0m, 1.5m and 2.0m at 3.5 MHz frequency. Two samples of each specimen were tested to see the repeatability and precision of the data collected. Parametric study was carried out to analyze the magnitude and time of the first peak received in through transmission and was observed that irrespective of the bar length, the trends were same in all the specimens thus validating our results. The final results were reported in the form of voltage-time curve (v-t).The data obtained experimentally was then compared with the theoretical results and found to be matching. As described earlier pulse echo method was used to locate the area and position of the crack and through transmission was used to find out the magnitude or extent of the crack in a specimen. The experimental results obtained are reported further.

5.6.1 Pulse Echo results for 0.81 m bars at L/2 fault location

JSR DPR 300 Pulser/Receiver settings	
Receiver	
Bandwith	35
Gain [-12 dB-67 dB]	46 dB
High Pass Filter [Out-12.5 MHz]	Out MHz
Low Pass Filter [3 MHz-35 MHz]	7.5 MHz
Pulser	
Damping [331 ohms-30 ohms]	30 ohms
Energy [1-4]	4
PRF [100 Hz-5 KHz]	200 Hz
Voltage [100V-400V]	275 V
Impedance [Low-High]	Low

In pulse echo method, first and second echo was reported in healthy as well as cracked specimen. In healthy specimen the first echo is that obtained after reflecting the other end as shown in

figure 5.19. In cracked specimen the first echo was that obtained from the crack and second is the back wall echo as shown in **figure 20**.

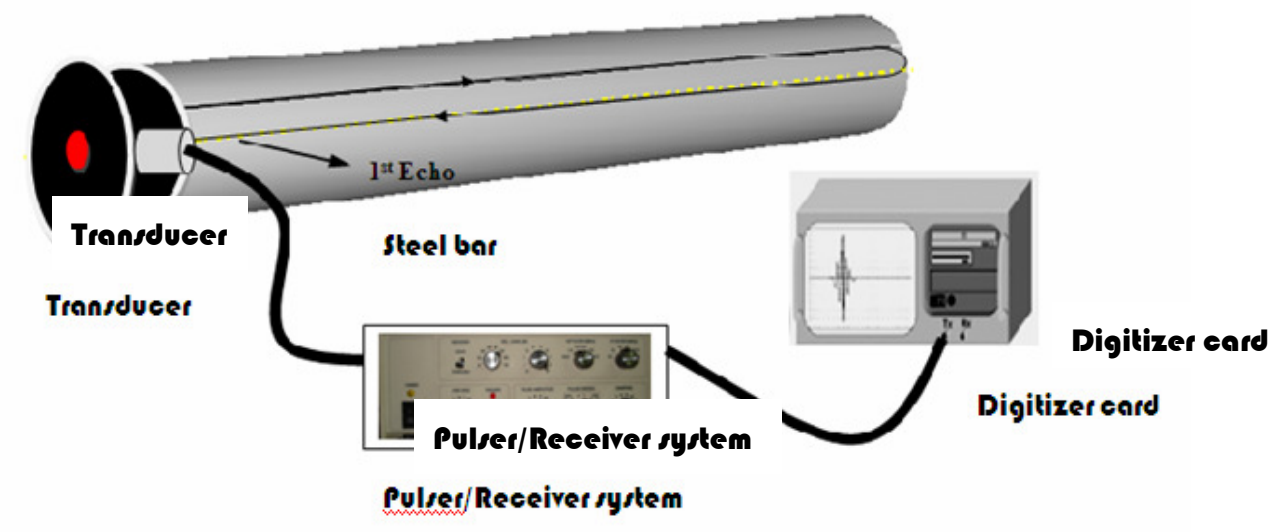

Figure 5.19: Pulse echo through healthy specimen showing the first echo received

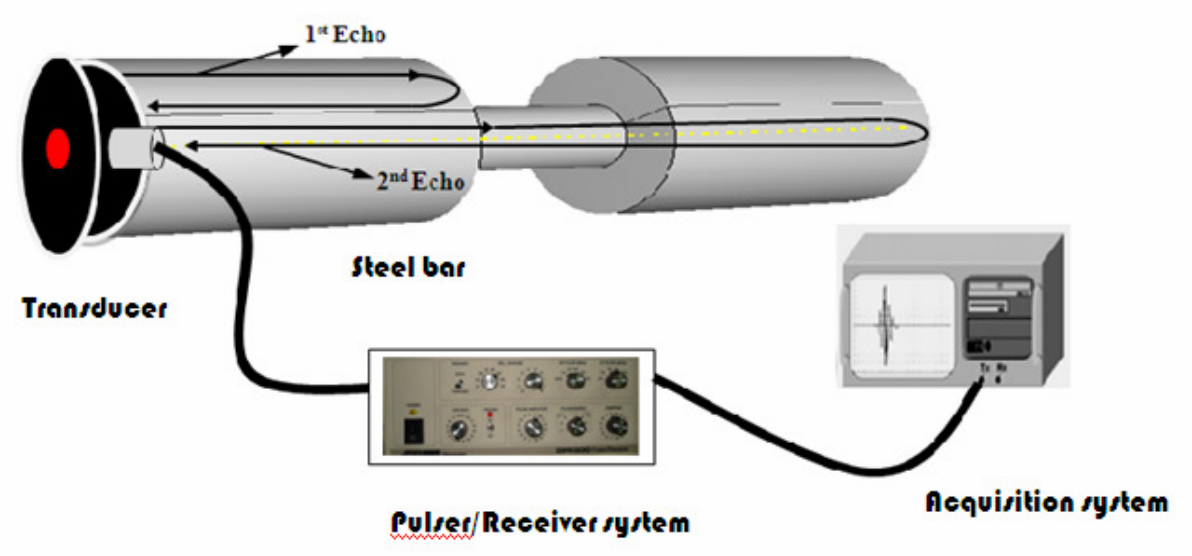

Figure 5.20: Pulse echo through cracked specimen showing the first and second echo received

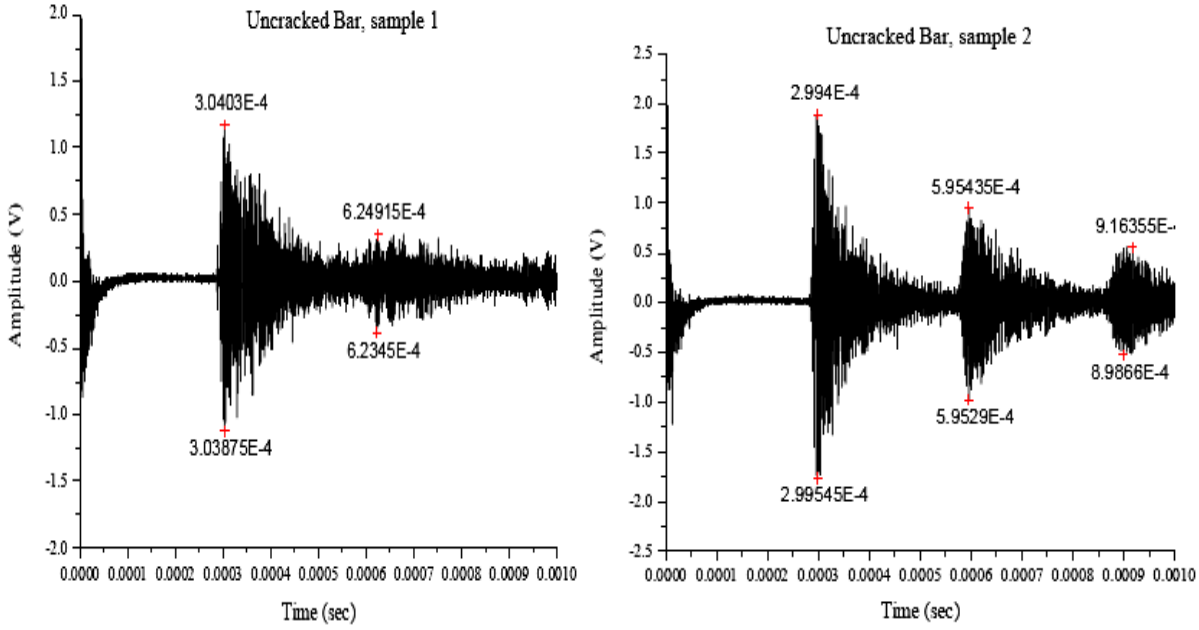

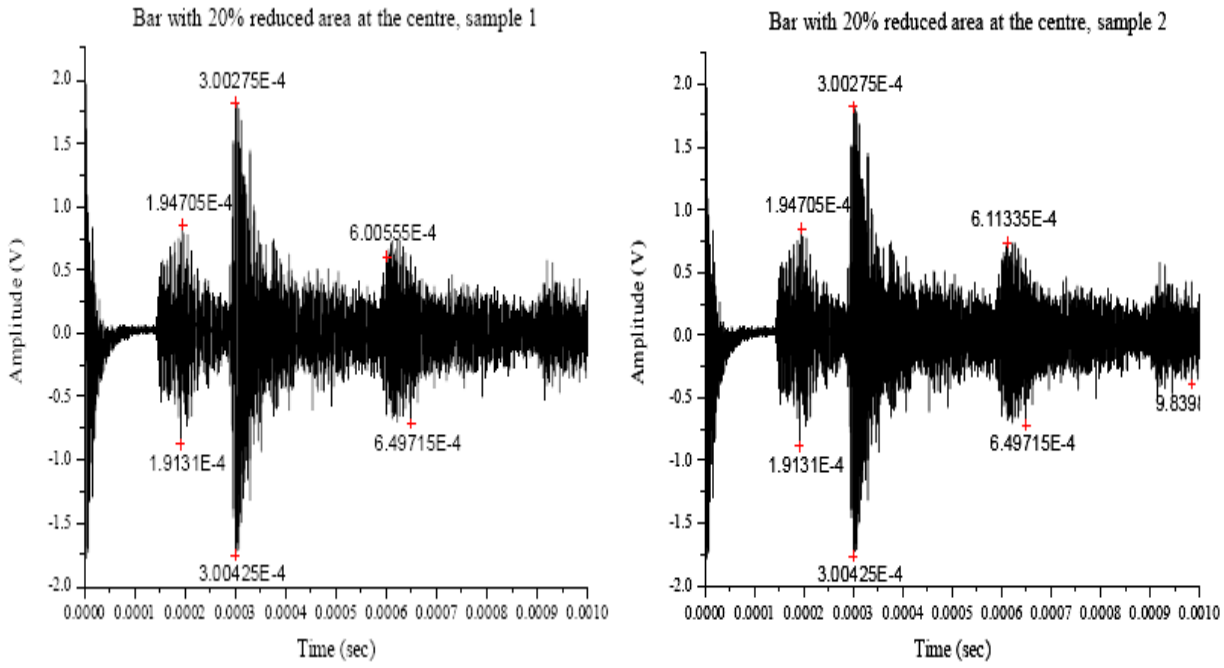

Figure 5.21: Pulse Echo through bar with 0% and 20% area reduction respectively at L/2 fault location at 3.5 MHz frequency

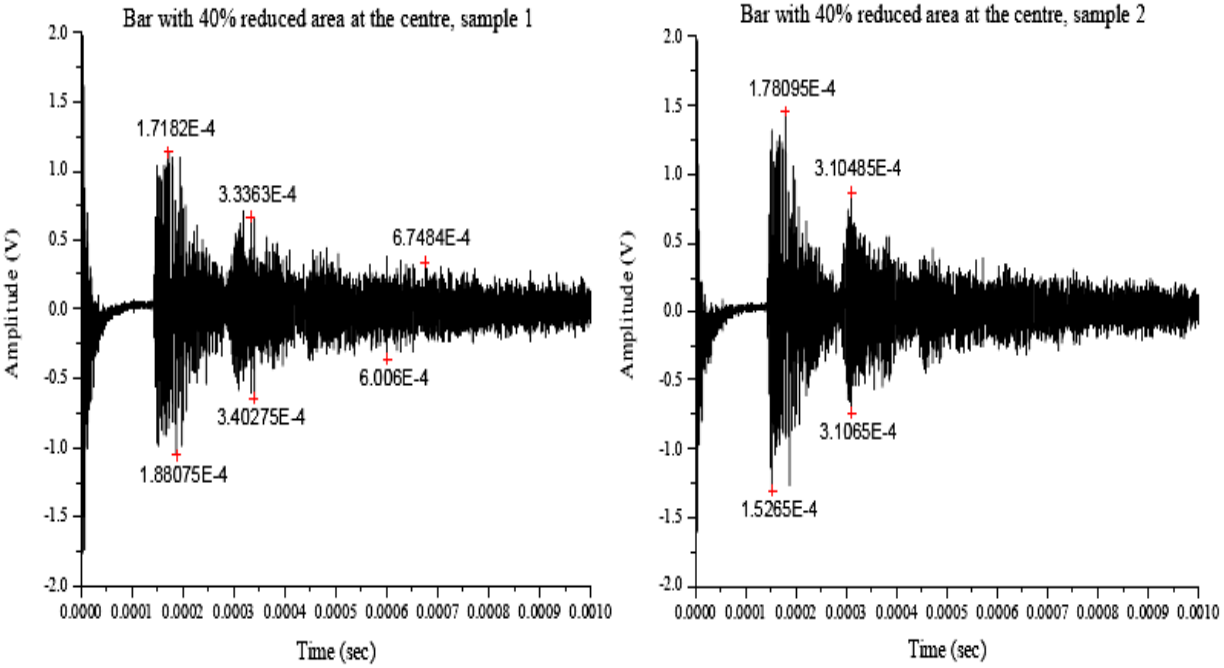

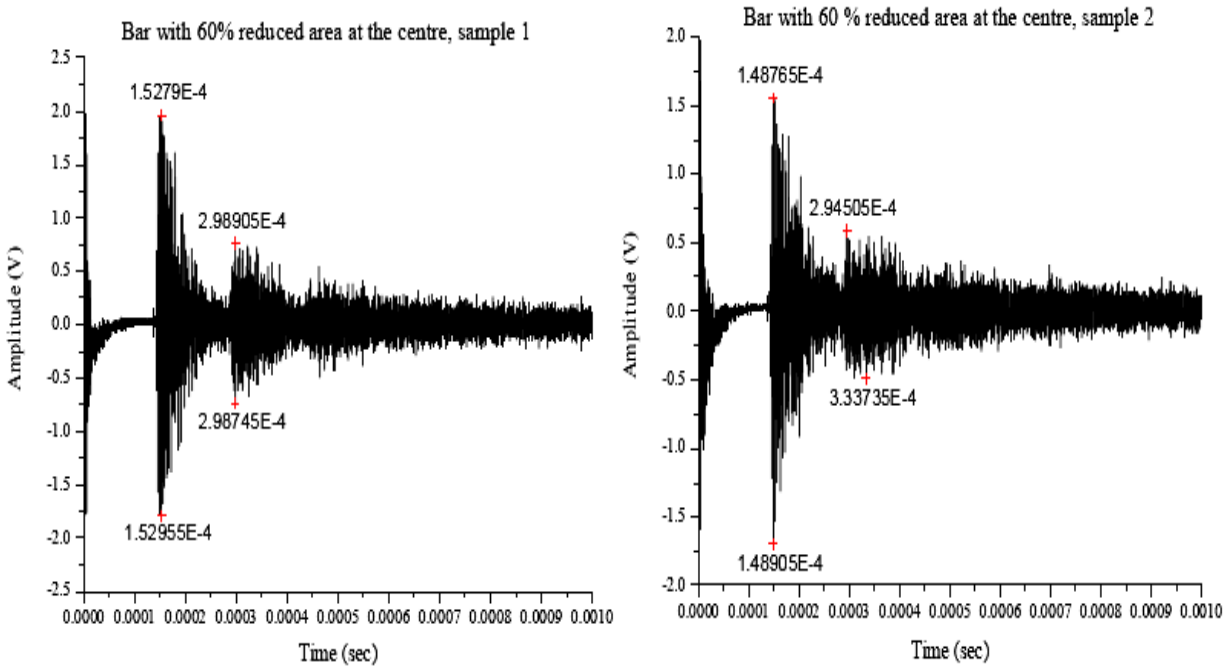

Figure 5.22: Pulse Echo through bar with 40% and 60% area reduction respectively at L/2 fault location at 3.5 MHz frequency

5.6.2 Through Transmission resluts for 0.81 m bars at L/2 fault location

In Through transmission method, first and second peak was reported in healthy as well as cracked specimen. In healthy specimen the first peak is that obtained at the other end as shown in **figure 5.23**. In cracked specimen the first peak was that obtained at the other end just like in healthy specimen and second peak is received after reflecting from the crack as shown in **figure 5.24**

.

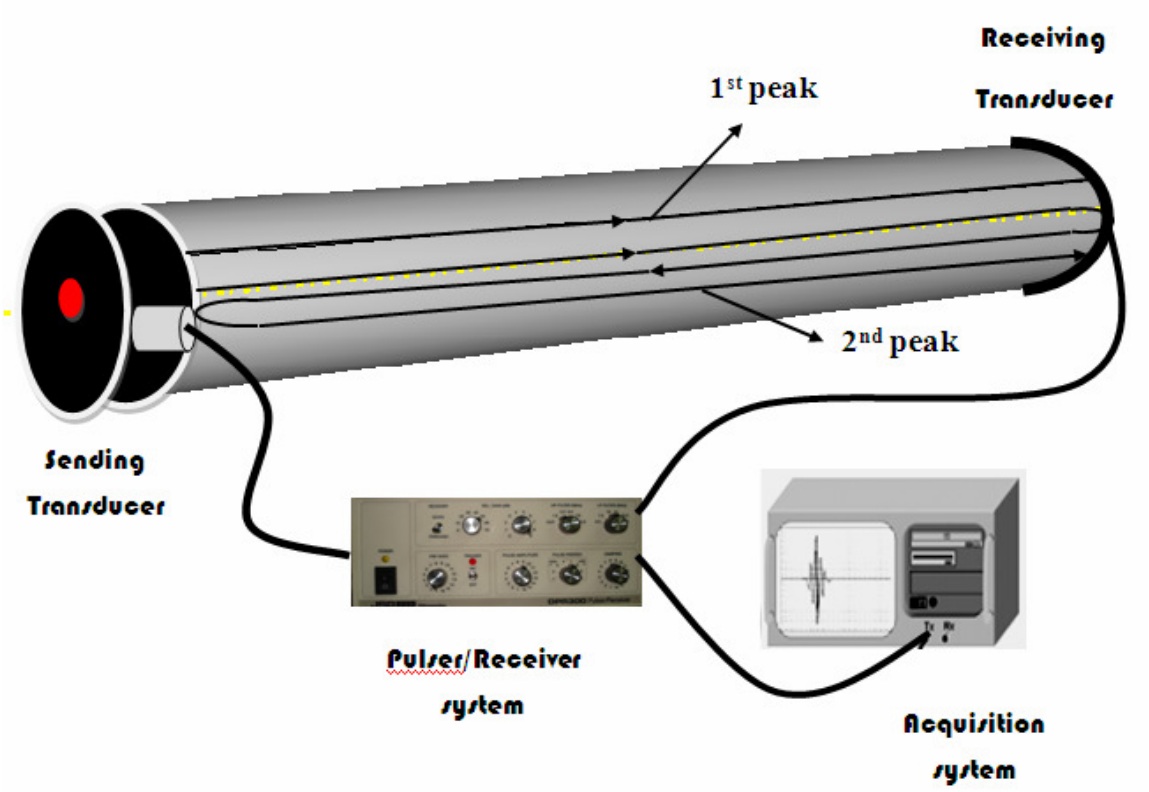

Figure 5.23: Through transmission method through healthy specimen showing the first and second peak received

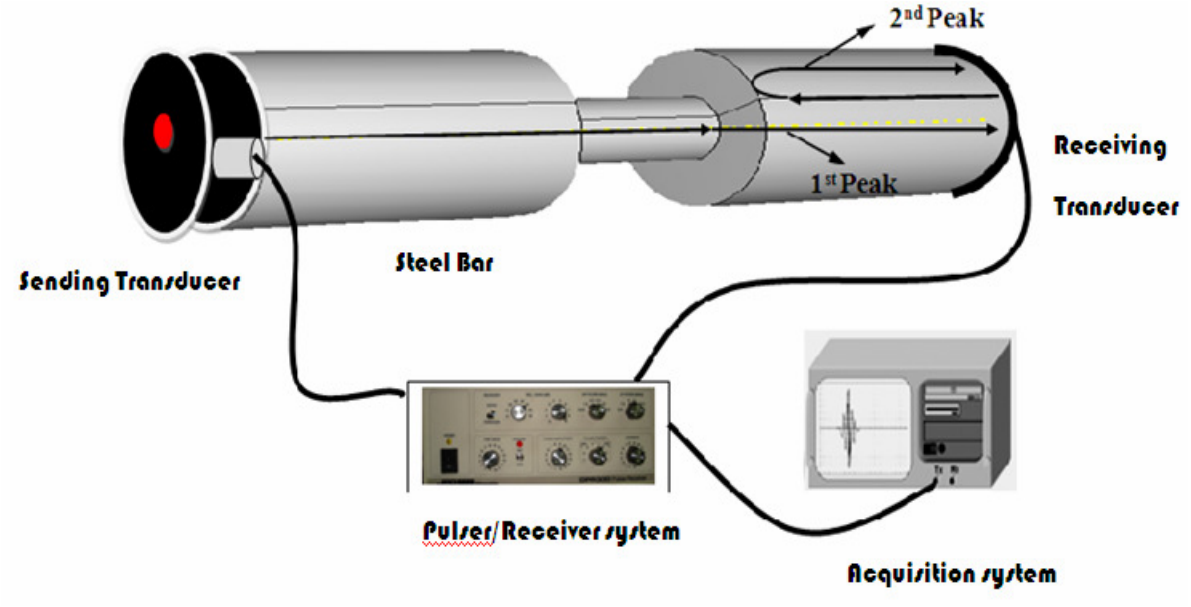

Figure 5.24: Through transmission method through cracked specimen showing the first and second peak received

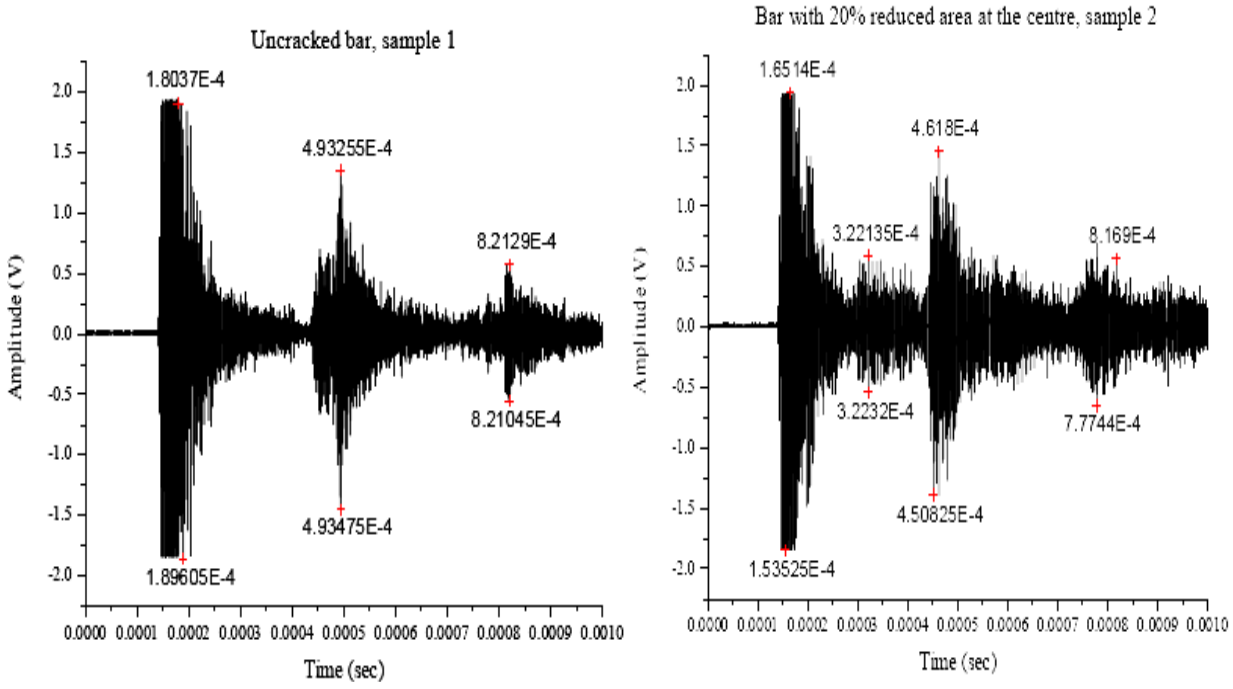

Figure 5.25: Through transmission along bar with 0% and 20% area reduction respectively at L/2 fault location at 3.5 MHz frequency

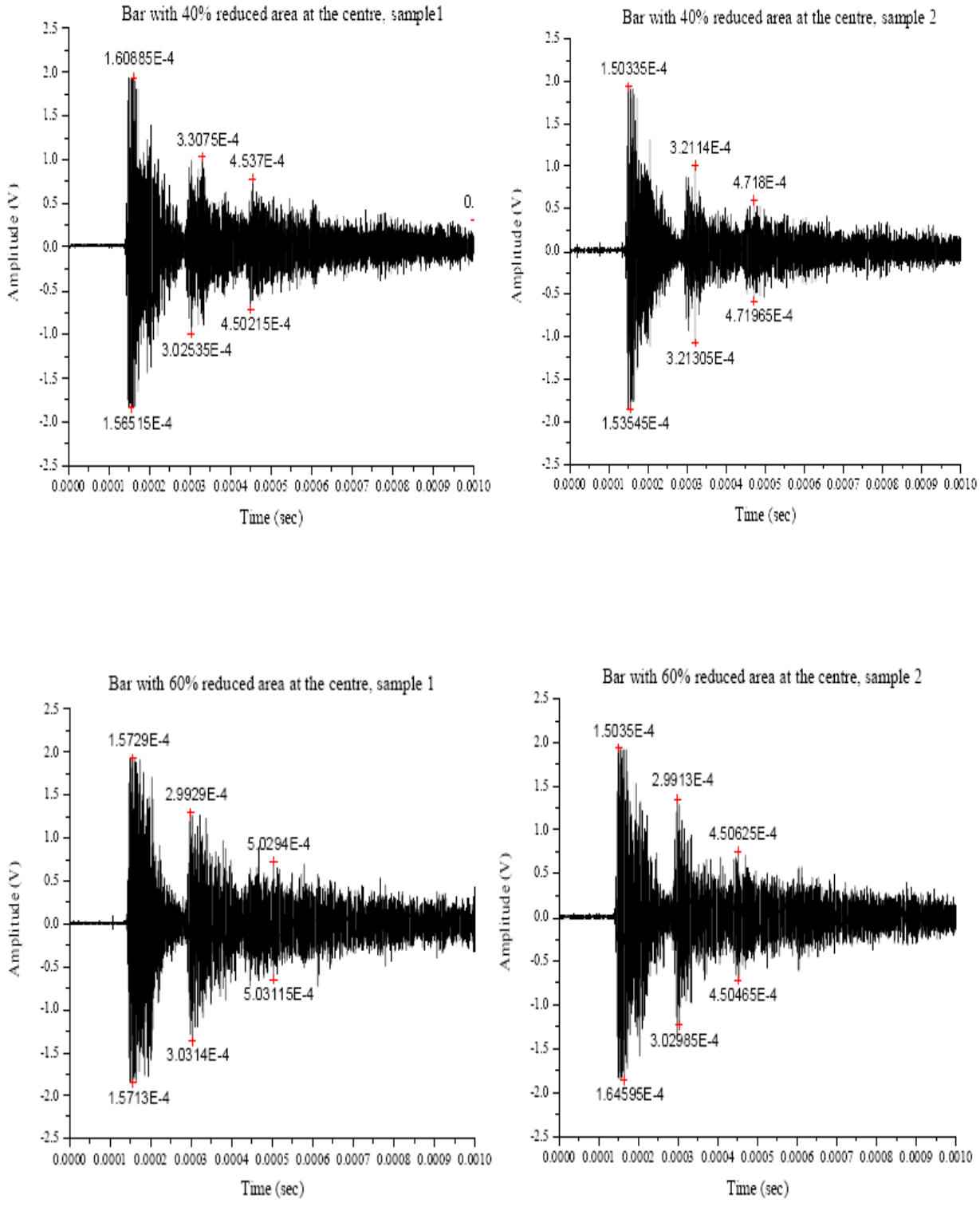

Figure 5.26: Through transmission along bar with 40% and 60% area reduction respectively at L/2 fault location at 3.5 MHz frequency

- **EXPERIMENTAL RESULTS**

0.81 m Bar, Through Transmission, Fault location-L/2, Transducer Frequency-3.5Mhz, Bar Dia-12 mm

Table 5.3: Amplitude of first, second and third peak in through transmission method

	Amplitude (Pk-Pk)		
Area Reduction	**1st peak**	**2nd peak**	**3rd peak**
0% (12 mm) S1	3.782	2.723	0.991
0% (12 mm) S2	3.782	2.844	1.411
20% (9.6 mm) S1	3.782	1.072	2.814
20% (9.6 mm) S2	3.766	1.400	3.511
40% (7.2mm) S1	3.751	1.896	1.437
40% (7.2mm) S2	3.747	2.005	1.173
60% (4.8 mm) S1	3.766	2.457	1.538
60% (4.8 mm) S2	3.738	2.656	1.419

- **THEORETICAL RESULTS**

$$C = \sqrt{\frac{E}{\rho}} = \sqrt{\frac{200 * 10^9 \frac{N}{m^2}}{7800 \frac{Kg}{m^3}}} = 5063.69 \frac{m}{s}$$

Table 5.4: Comparison of experimental and theoretical results for time of flight in through transmission

THEORETICAL RESULTS			
Fault location – L/2	**Time (sec)**		
	1st peak	**2nd peak**	**3rd peak**
Healthy specimen	1.59×10^{-4}	4.79×10^{-4}	7.998×10^{-4}
Cracked specimen	1.59×10^{-4}	3.199×10^{-4}	4.79×10^{-4}
EXPERIMENTAL RESULTS			
Area Reduction	**1st peak**	**2nd peak**	**3rd peak**
Healthy specimen (0 %)	1.572×10^{-4}	4.820×10^{-4}	7.823×10^{-4}
20 %	1.612×10^{-4}	3.187×10^{-4}	4.560×10^{-4}
40 %	1.556×10^{-4}	3.184×10^{-4}	4.625×10^{-4}
60 %	1.519×10^{-4}	3.018×10^{-4}	4.553×10^{-4}

Table 5.5: Amplitude of first and second peak in pulse echo method

Amplitude (Pk-Pk)		
Area Reduction	**1st peak**	**2nd peak**
0% (12 mm) S1	2.263	0.623
0% (12 mm) S2	3.611	1.878
20% (9.6 mm) S1	1.705	3.553
20% (9.6 mm) S2	1.226	2.465
40% (7.2mm) S1	2.079	1.302
40% (7.2mm) S2	2.683	1.548
60% (4.8 mm) S1	3.720	1.452
60% (4.8 mm) S2	3.235	1.081

Table 5.6: Comparison of experimental and theoretical results for time of flight in pulse echo

THEORETICAL RESULTS		
Fault location – L/2	**Time (sec)**	
	1st Echo	**2nd Echo**
Healthy specimen	3.199×10^{-4}	6.398×10^{-4}
Cracked specimen	1.59×10^{-4}	3.199×10^{-4}
EXPERIMENTAL RESULTS		
Area Reduction	**1st Echo**	**2nd Echo**
Healthy specimen (0 %)	3.001×10^{-4}	6.098×10^{-4}
Cracked specimen (20 %)	1.784×10^{-4}	3.042×10^{-4}
40 %	1.63×10^{-4}	3.228×10^{-4}
60 %	1.511×10^{-4}	2.973×10^{-4}

5.6.3 Pulse Echo results for 1.0 m bars at L/2 fault location

JSR DPR 300 Pulser/Receiver settings	
Receiver	
Bandwith	35
Gain [-12 dB-67 dB]	35 dB
High Pass Filter [Out-12.5 MHz]	1 MHz
Low Pass Filter [3 MHz-35 MHz]	7.5 MHz
Pulser	
Damping [331 ohms-30 ohms]	32 ohms
Energy [1-4]	1
PRF [100 Hz-5 KHz]	100 Hz
Voltage [100V-400V]	325 V
Impedance [Low-High]	Low

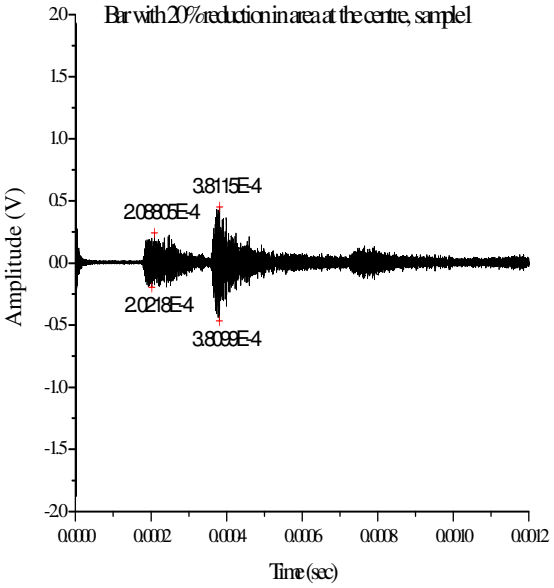
Bar with 20% reduction in area at the centre, sample1
Amplitude (V)
Time (sec)
3.8115E-4
2.0880E-4
2.0218E-4
3.8099E-4

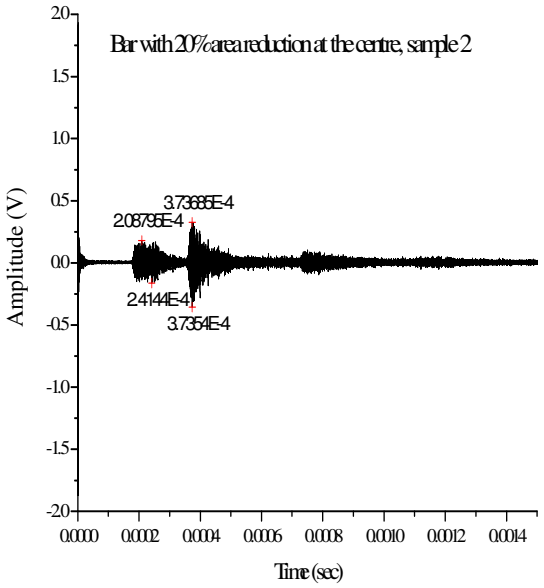
Bar with 20% area reduction at the centre, sample 2
Amplitude (V)
Time (sec)
3.7368E-4
2.0879E-4
2.4144E-4
3.7354E-4

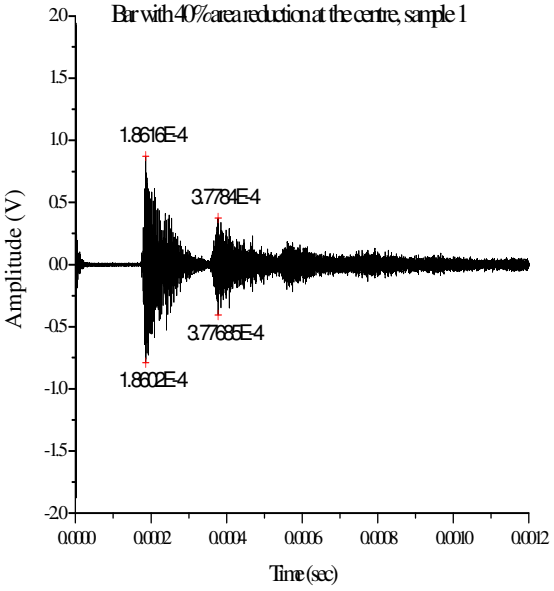
Bar with 40% area reduction at the centre, sample 1
Amplitude (V)
Time (sec)
1.8616E-4
3.7784E-4
3.7685E-4
1.8602E-4

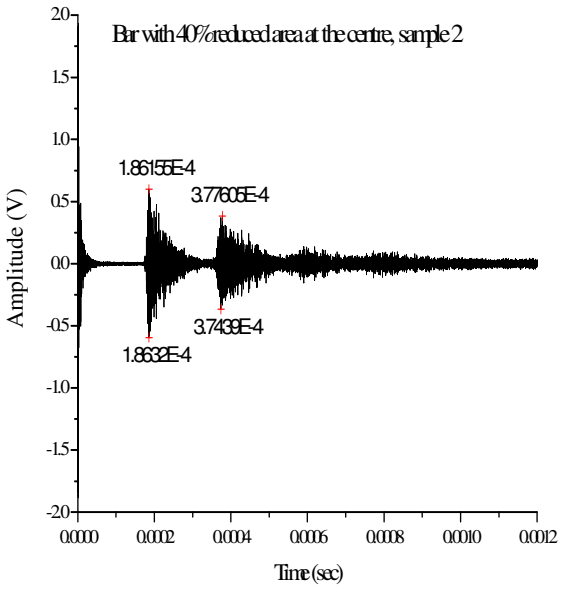
Bar with 40% reduced area at the centre, sample 2
Amplitude (V)
Time (sec)
1.8615E-4
3.7760E-4
3.7439E-4
1.8632E-4

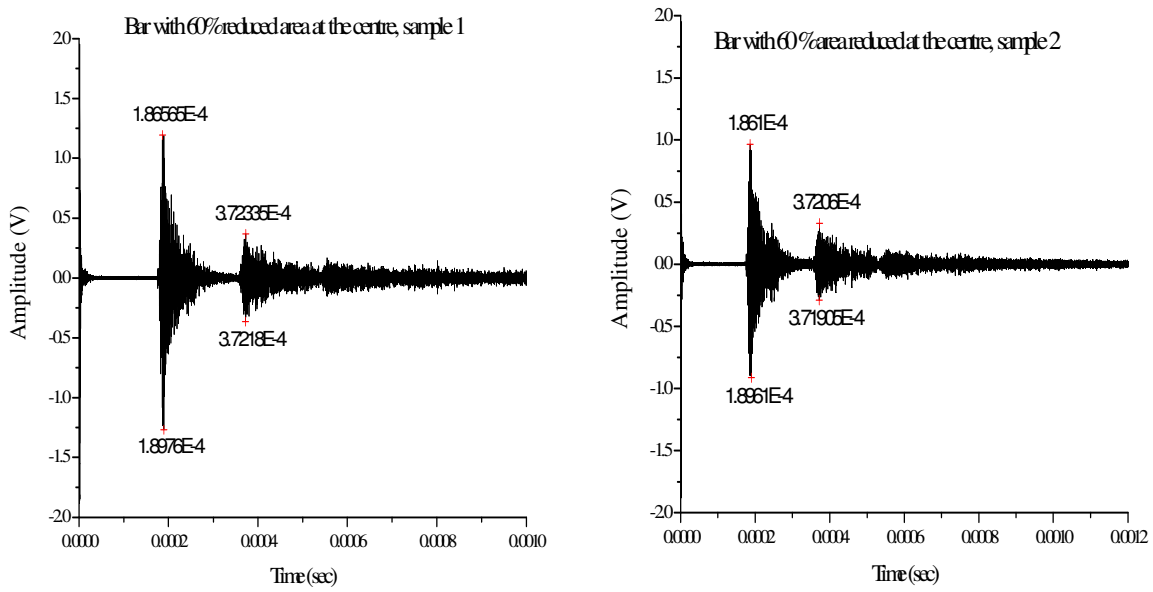

Figure 5.27: Pulse echo through bar with 20%, 40% and 60% area reduction respectively at L/2 fault location at 3.5 MHz frequency

5.6.4 Through Transmission results for 1.0 m bars at L/2 fault location

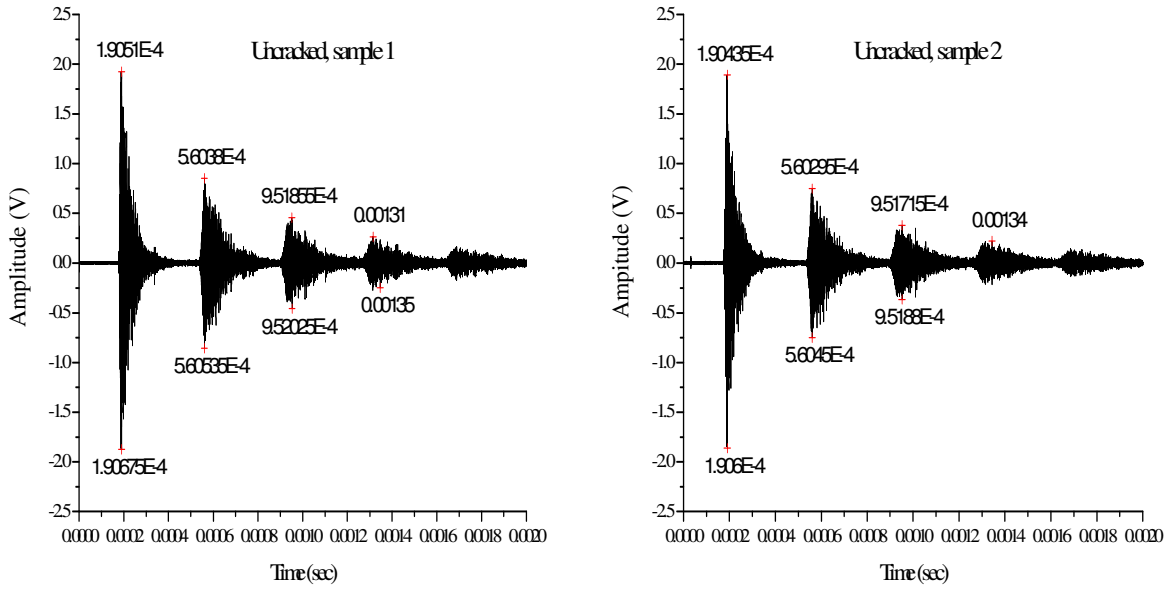

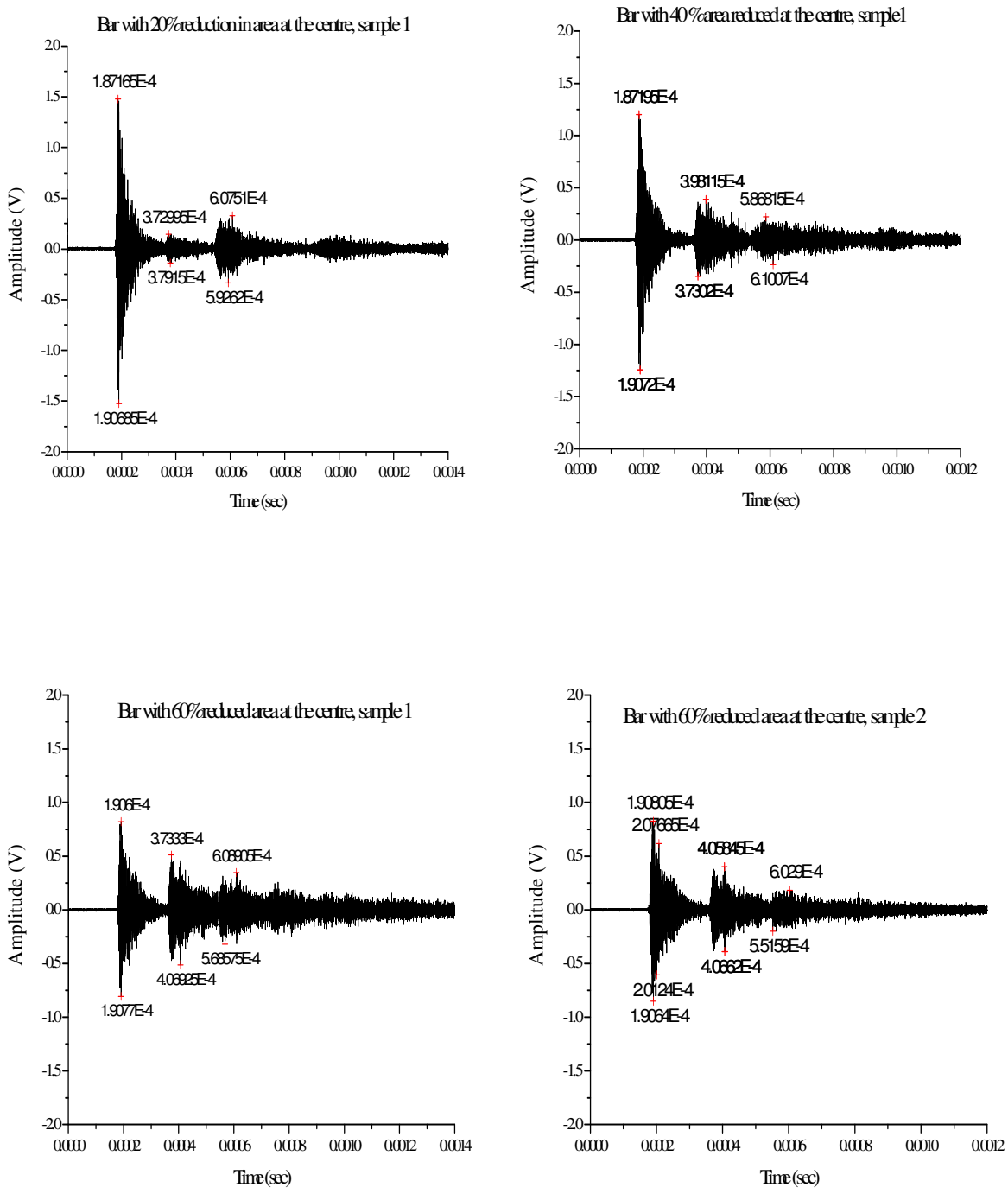

Figure 5.28: Through transmission along bar with 0 %(S_1, S_2), 20%, 40% and 60 %(S_1, S_2) area reduction respectively at L/2 fault location at 3.5 MHz frequency

- **EXPERIMENTAL RESULTS**

1.0 m Bar, Through Transmission, Fault location-L/2, Transducer Frequency-3.5Mhz, Bar Dia-12 mm

Table 5.7: Amplitude of first, second and third peak in through transmission method

	Amplitude (Pk-Pk)		
Area Reduction	**1st peak**	**2nd peak**	**3rd peak**
0% (12 mm) S1	3.797	1.711	0.916
0% (12 mm) S2	3.759	1.498	0.747
20% (9.6 mm) S1	3.005	0.284	0.662
40% (7.2mm) S1	2.446	0.736	0.460
60% (4.8 mm) S1	1.625	1.023	0.668
60% (4.8 mm) S2	1.676	0.791	0.382

Table 5.8: Comparison of experimental and theoretical results for time of flight in through transmission

THEORETICAL RESULTS			
Fault location – L/2	**Time (sec)**		
	1st peak	**2nd peak**	**3rd peak**
Healthy specimen	1.975×10^{-4}	5.925×10^{-4}	9.876×10^{-4}
Cracked specimen	1.975×10^{-4}	3.950×10^{-4}	7.9×10^{-4}
EXPERIMENTAL RESULTS			
Area Reduction	**1st peak**	**2nd peak**	**3rd peak**
Healthy specimen (0 %)	1.905×10^{-4}	5.606×10^{-4}	9.578×10^{-4}
20 %	1.906×10^{-4}	3.792×10^{-4}	6.075×10^{-4}
40 %	1.907×10^{-4}	3.856×10^{-4}	6.10×10^{-4}
60 %	1.907×10^{-4}	4.061×10^{-4}	6.089×10^{-4}

Table 5.9: Amplitude of first and second echo in pulse echo method

Amplitude (Pk-Pk)		
Area Reduction	**1st peak**	**2nd peak**
20% (9.6 mm) S1	0.377	0.857
20% (9.6 mm) S2	0.298	0.665
40% (7.2mm) S1	1.633	0.762
40% (7.2mm) S2	1.197	0.723
60% (4.8 mm) S1	2.423	0.714

60% (4.8 mm) S2	1.882	0.618

Table 5.10: Comparison of experimental and theoretical results for time of flight in pulse echo

THEORETICAL RESULTS		
Fault location – L/2	**Time (sec)**	
	1st Echo	**2nd Echo**
Healthy specimen	3.950×10^{-4}	7.9×10^{-4}
Cracked specimen	1.975×10^{-4}	3.950×10^{-4}
EXPERIMENTAL RESULTS		
Area Reduction	**1st Echo**	**2nd Echo**
Healthy specimen (0 %)	3.787×10^{-4}	7.765×10^{-4}
Cracked specimen (20 %)	1.973×10^{-4}	3.737×10^{-4}
40 %	1.906×10^{-4}	3.770×10^{-4}
60 %	1.864×10^{-4}	3.737×10^{-4}

5.6.5 Through Transmission results for 1.5 m bars at L/2 fault location

JSR DPR 300 Pulser/Receiver settings	
Receiver	
Bandwith	35
Gain [-12 dB-67 dB]	56 dB
High Pass Filter [Out-12.5 MHz]	1 MHz
Low Pass Filter [3 MHz-35 MHz]	7.5 MHz
Pulser	
Damping [331 ohms-30 ohms]	32 ohms
Energy [1-4]	1
PRF [100 Hz-5 KHz]	100 Hz
Voltage [100V-400V]	475 V
Impedance [Low-High]	Low

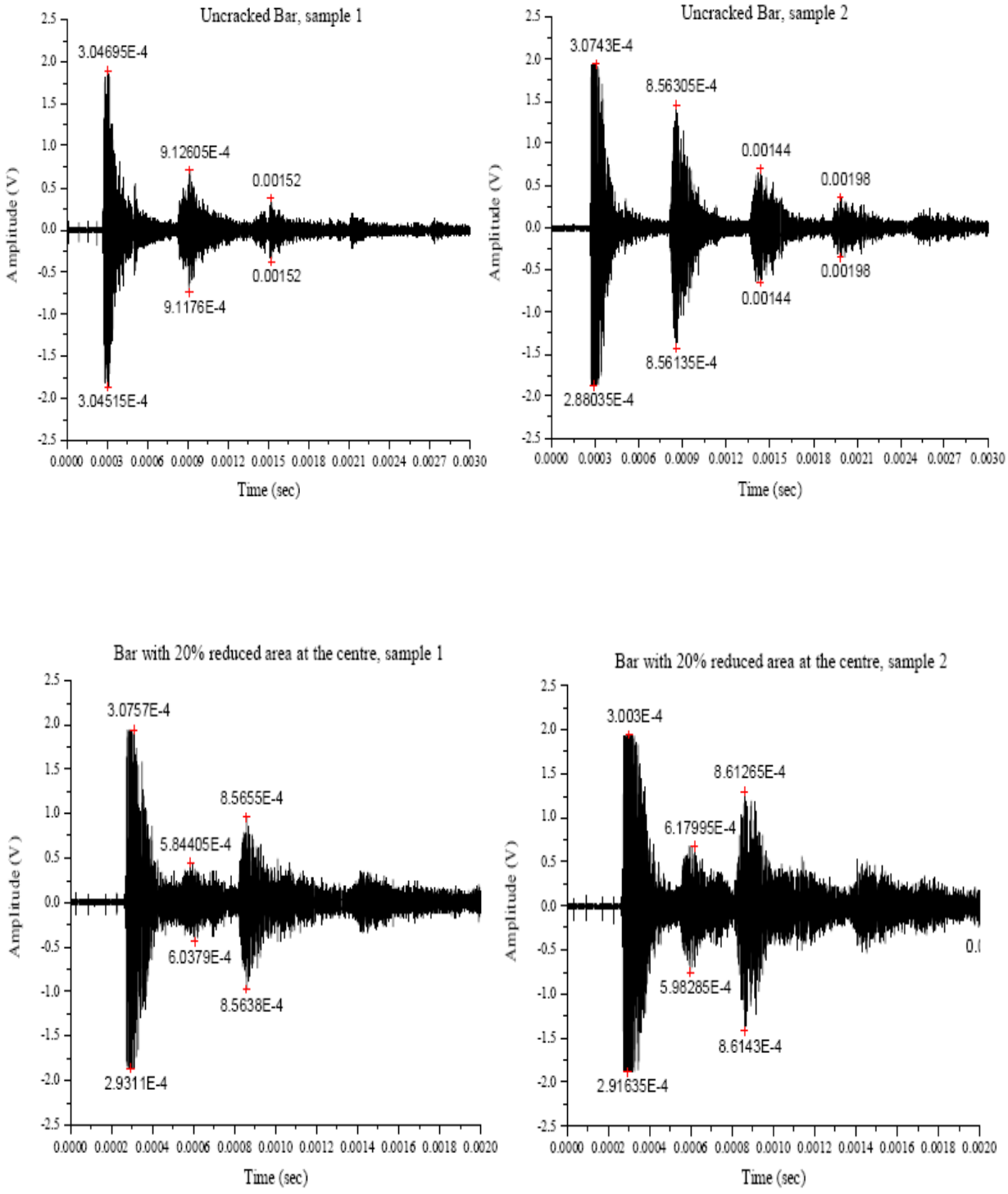

Figure 5.29: Through transmission along bar with 0 %(S_1, S_2) and 20 %(S_1, S_2) area reduction respectively at L/2 fault location at 3.5 MHz frequency

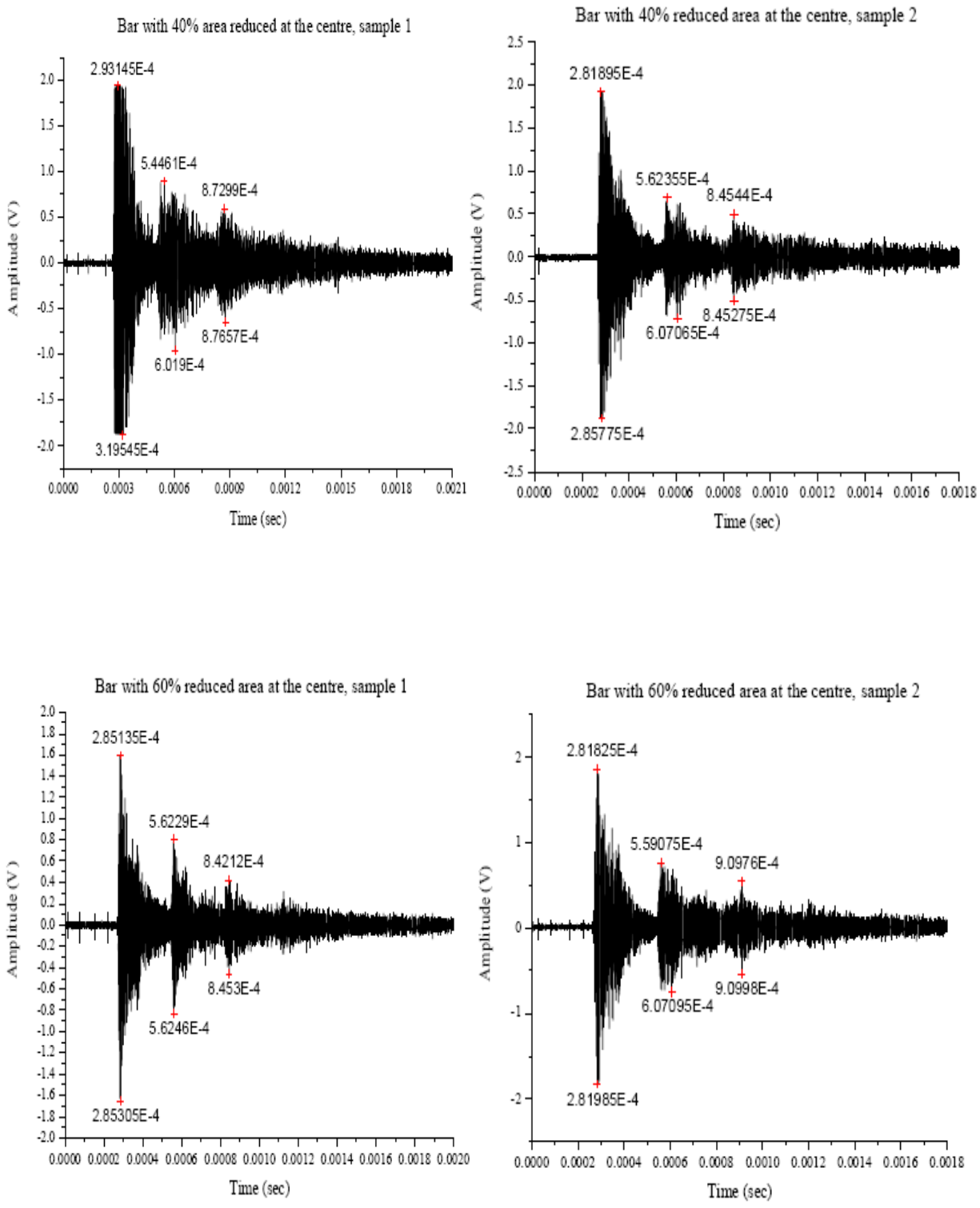

Figure 5.30: Through transmission along bar with 40 %(S_1, S_2) and 60 %(S_1, S_2) area reduction respectively at L/2 fault location at 3.5 MHz frequency

5.6.6 Pulse Echo results for 1.5 m bars at L/2 fault location

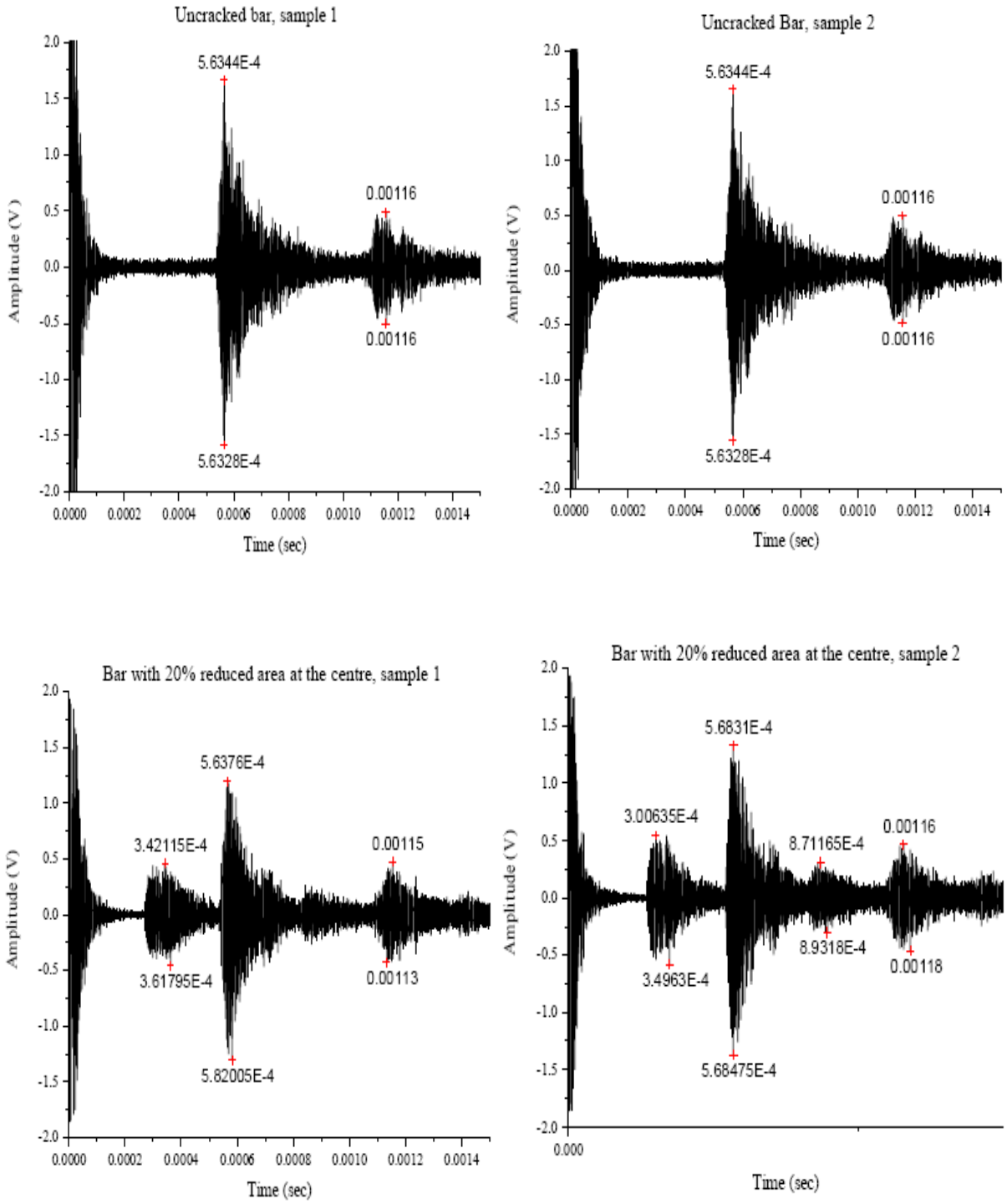

Figure 5.31: Pulse echo through bar with 0 %(S_1, S_2) and 20 %(S_1, S_2) area reduction respectively at L/2 fault location at 3.5 MHz frequency

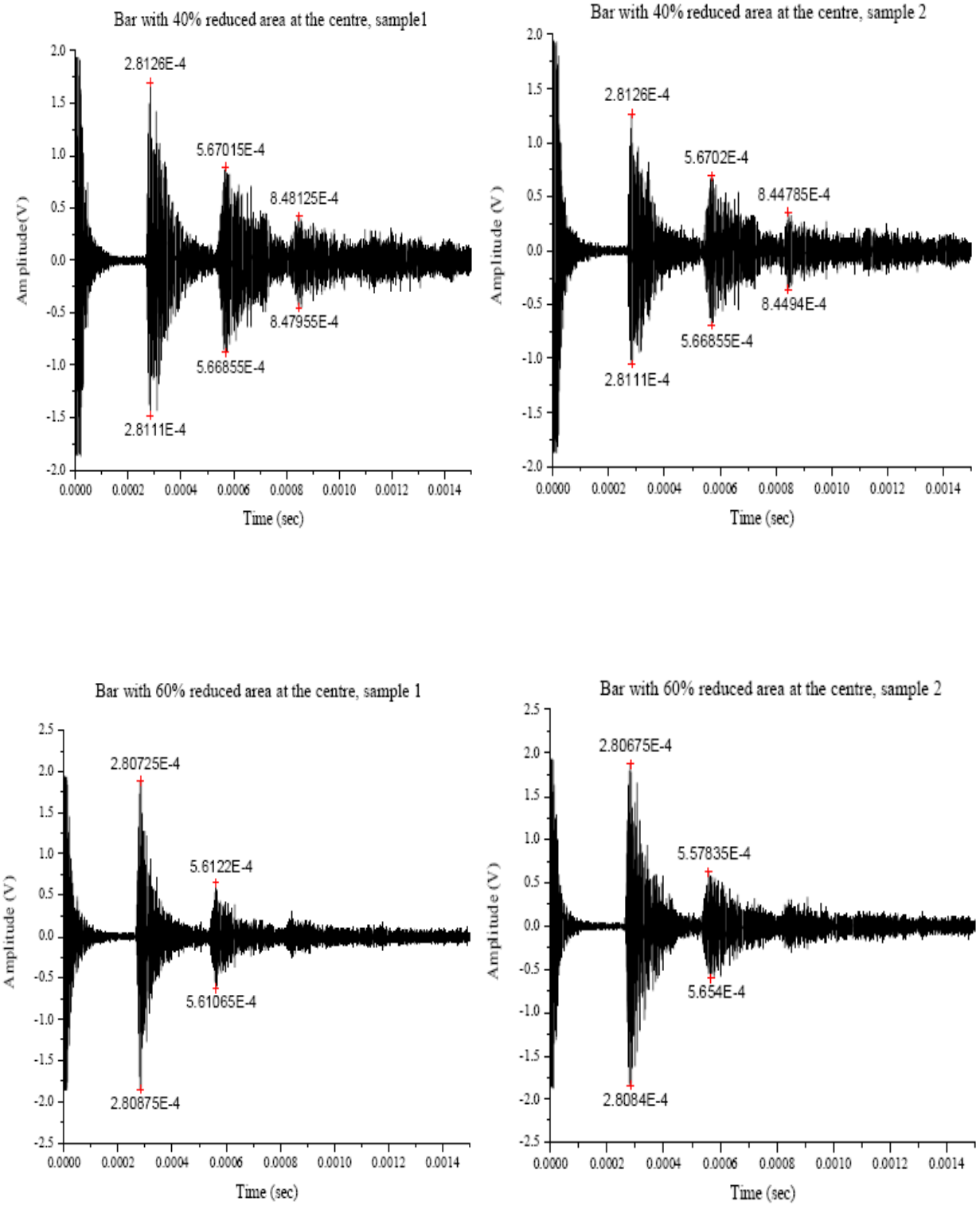

Figure 5.32: Pulse echo through bar with 40 %(S_1, S_2) and 60 %(S_1, S_2) area reduction respectively at L/2 fault location at 3.5 MHz frequency

- **EXPERIMENTAL RESULTS**

1.5 m Bar, Through Transmission, Fault location-L/2, Transducer Frequency-3.5Mhz, Bar Dia-12 mm

Table 5.11: Amplitude of first, second and third peak in through transmission method

	Amplitude (Pk-Pk)		
Area Reduction	**1st peak**	**2nd peak**	**3rd peak**
0% (12 mm) S1	3.753	1.4505	0.763
0% (12 mm) S2	3.820	3.219	1.466
20% (9.6 mm) S1	3.805	0.823	1.739
20% (9.6 mm) S2	3.753	1.036	1.998
40% (7.2mm) S1	3.816	1.548	1.207
40% (7.2mm) S2	3.767	2.5	0.903
60% (4.8 mm) S1	3.131	1.487	0.736
60% (4.8 mm) S2	3.524	1.301	0.862

Table 5.12: Comparison of experimental and theoretical results for time of flight in through transmission

THEORETICAL RESULTS			
Fault location – L/2	Time (sec)		
	1st peak	2nd peak	3rd peak
Healthy specimen(12mm)	2.962×10^{-4}	8.887×10^{-4}	1.481×10^{-3}
Cracked specimen	2.962×10^{-4}	5.925×10^{-4}	8.887×10^{-4}
EXPERIMENTAL RESULTS			
	1st peak	2nd peak	3rd peak
Healthy specimen(12mm)	3.092×10^{-4}	8.843×10^{-4}	1.480×10^{-3}
9.6 mm	2.961×10^{-4}	5.922×10^{-4}	8.795×10^{-4}
7.2 mm	2.941×10^{-4}	5.664×10^{-4}	8.802×10^{-4}
4.8 mm	2.829×10^{-4}	5.611×10^{-4}	8.820×10^{-4}

Table 5.13: Amplitude of first and second echo in pulse echo method

Amplitude (Pk-Pk)		
Area Reduction	**1st peak**	**2nd peak**
0% (12 mm) S1	3.209	0.973
0% (12 mm) S2	3.246	0.998
20% (9.6 mm) S1	0.873	2.468

20% (9.6 mm) S2	1.072	2.590
40% (7.2mm) S1	3.185	1.768
40% (7.2mm) S2	2.321	1.387
60% (4.8 mm) S1	3.731	1.259
60% (4.8 mm) S2	3.697	1.197

Table 5.14: Comparison of experimental and theoretical results for time of flight in pulse echo

THEORETICAL RESULTS		
Fault location – L/2	**Time (sec)**	
	1st Echo	**2nd Echo**
Healthy specimen	5.925×10^{-4}	1.185×10^{-3}
Cracked specimen	2.962×10^{-4}	5.925×10^{-4}
EXPERIMENTAL RESULTS		
Area Reduction	**1st Echo**	**2nd Echo**
Healthy specimen (0 %)	5.634×10^{-4}	1.160×10^{-3}
Cracked specimen (20 %)	3.385×10^{-4}	5.729×10^{-4}
40 %	2.812×10^{-4}	5.673×10^{-4}
60 %	2.807×10^{-4}	5.721×10^{-4}

5.6.7 Through Transmission results for 2.0 m bars at L/2 fault location

JSR DPR 300 Pulser/Receiver settings	
Receiver	
Bandwith	35
Gain [-12 dB-67 dB]	60 dB
High Pass Filter [Out-12.5 MHz]	1 MHz
Low Pass Filter [3 MHz-35 MHz]	7.5 MHz
Pulser	
Damping [331 ohms-30 ohms]	32 ohms
Energy [1-4]	1
PRF [100 Hz-5 KHz]	100 Hz
Voltage [100V-400V]	475 V
Impedance [Low-High]	Low

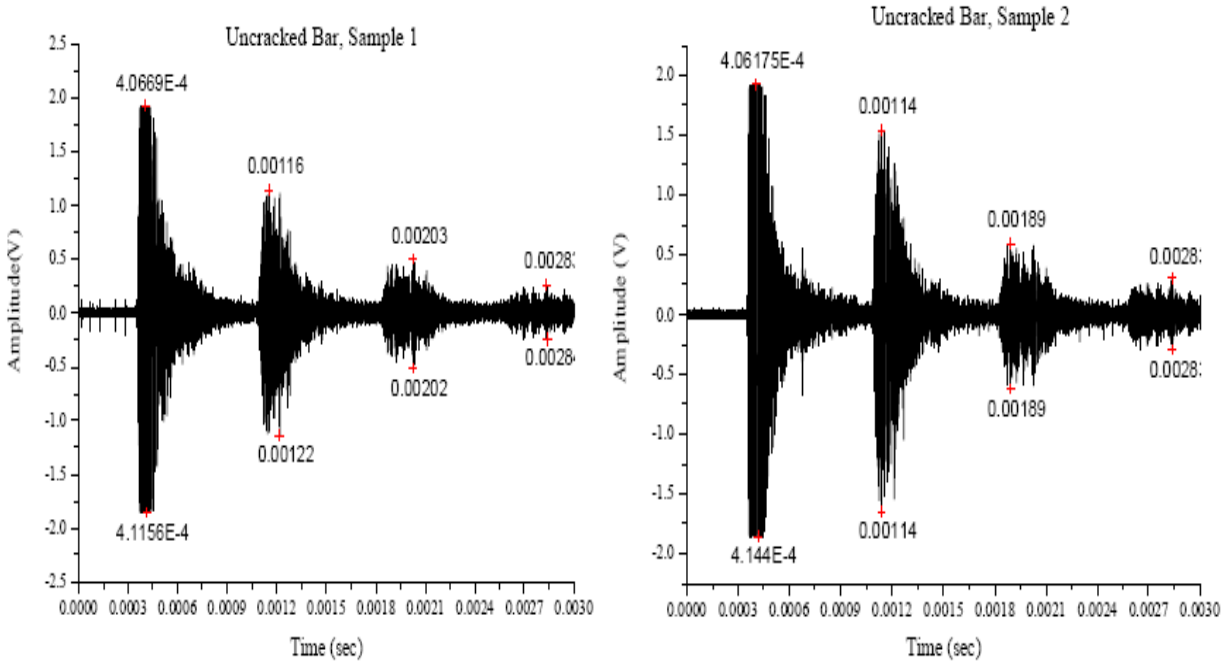

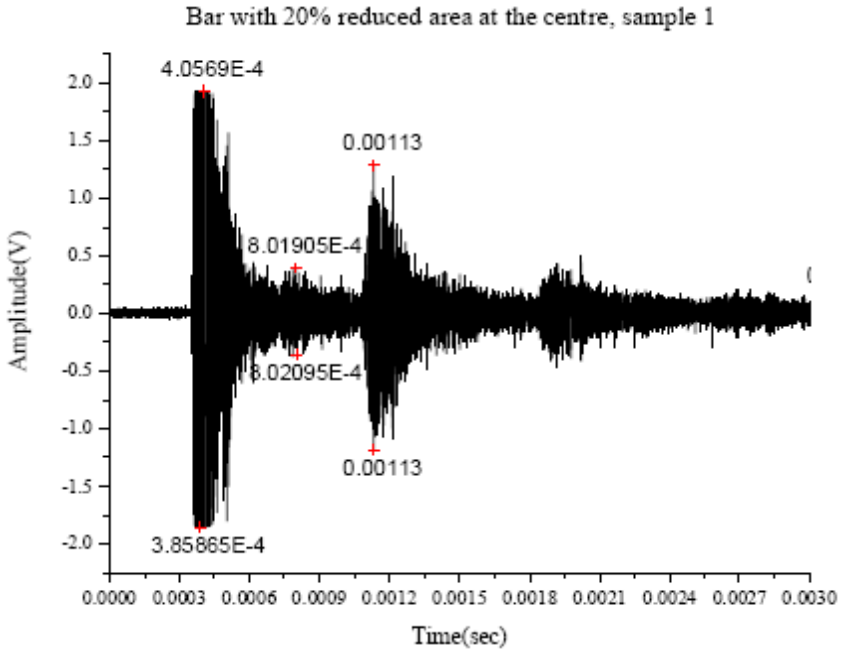

Figure 5.33: Through transmission along bar with 0 %(S_1, S_2) and 20 %(S_1) area reduction respectively at L/2 fault location at 3.5 MHz frequency

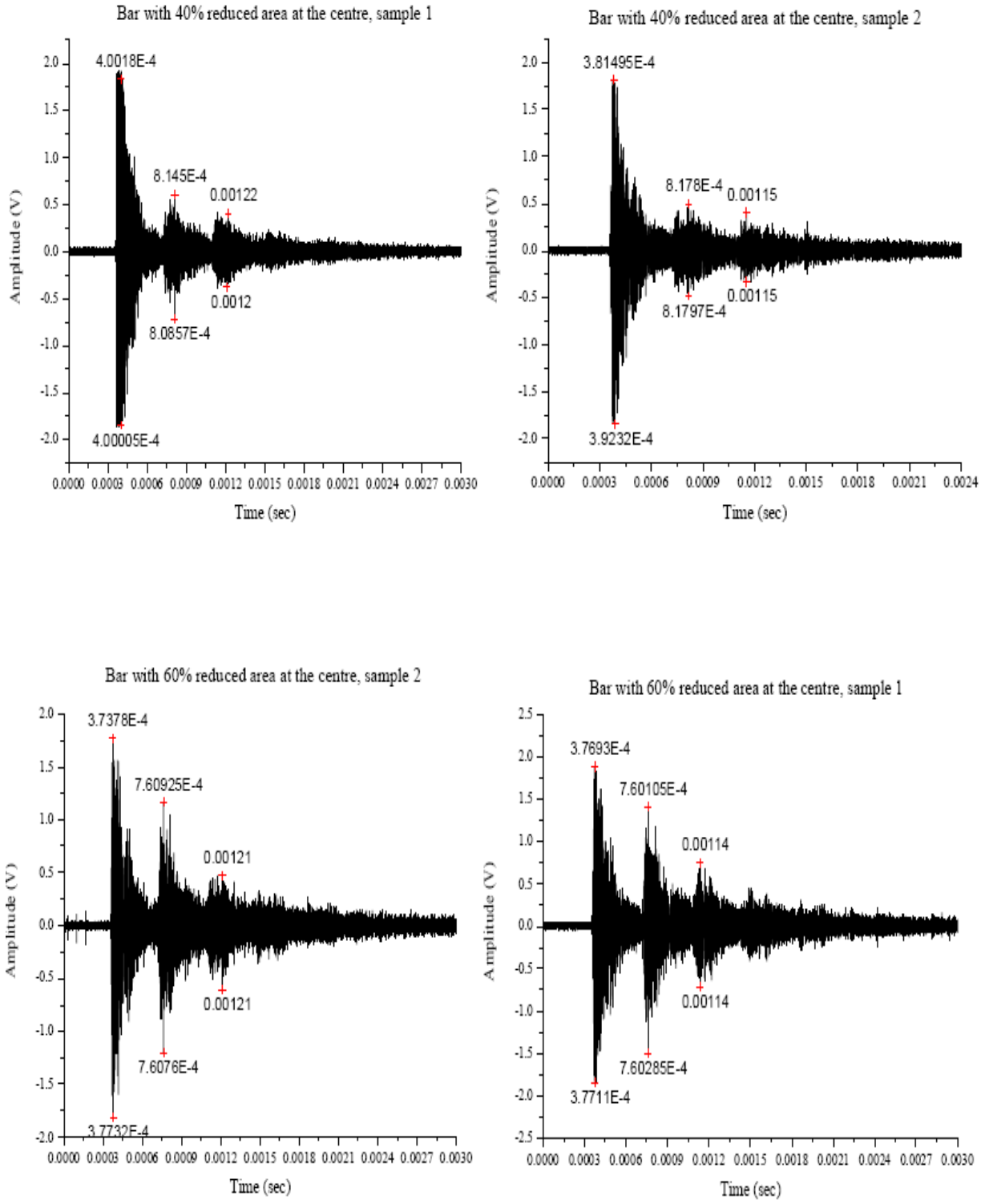

Figure 5.34: Through transmission along bar with 40 %(S_1, S_2) and 60 %(S_1, S_2) area reduction respectively at L/2 fault location at 3.5 MHz frequency

5.6.8 Pulse Echo results for 2.0 m bars at L/2 fault location

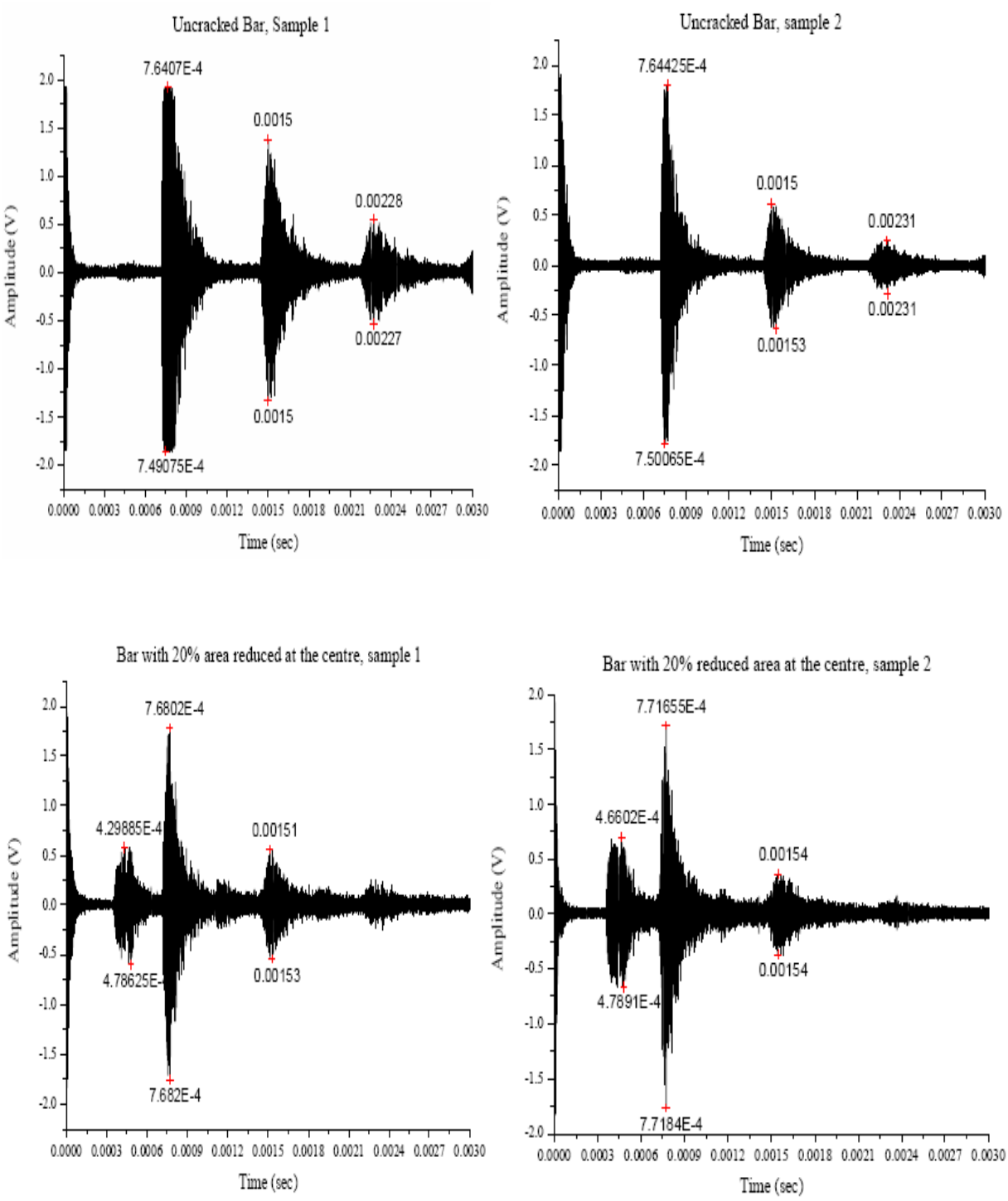

Figure 5.35: Pulse echo through bar with 0 %(S_1, S_2) and 20 %(S_1, S_2) area reduction respectively at L/2 fault location at 3.5 MHz frequency

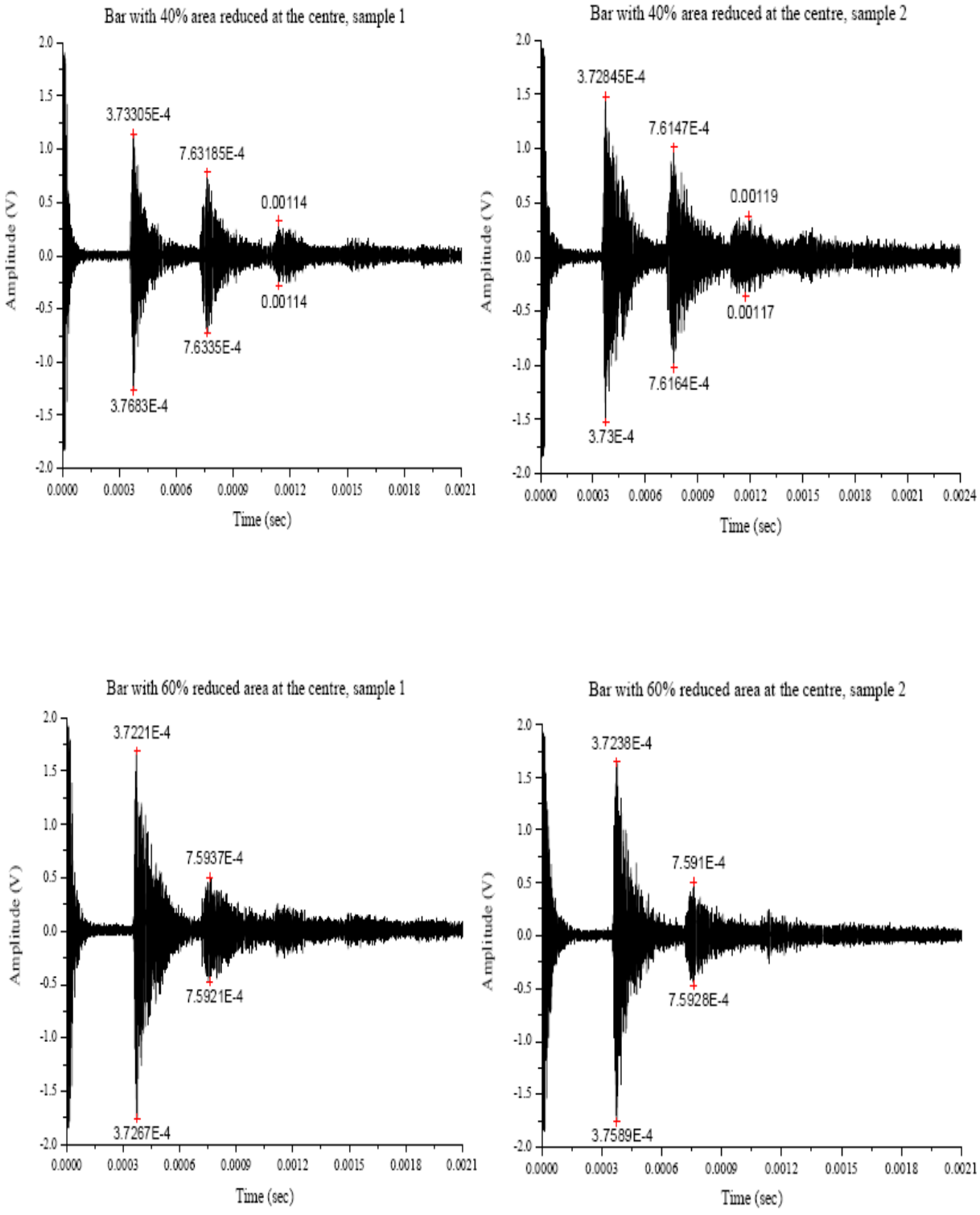

Figure 5.36: Pulse echo through bar with 40 %(S_1, S_2) and 60 %(S_1, S_2) area reduction respectively at L/2 fault location at 3.5 MHz frequency

- **EXPERIMENTAL RESULTS**

2.0 m Bar, Through Transmission, Fault location-L/2, Transducer Frequency-3.5Mhz, Bar Dia-12 mm

Table 5.15: Amplitude of first, second and third peak in through transmission method

	Amplitude (Pk-Pk)		
Area Reduction	**1st peak**	**2nd peak**	**3rd peak**
0% (12 mm) S1	3.781	2.085	0.87
0% (12 mm) S2	3.792	3.488	1.659
20% (9.6 mm) S1	3.776	0.791	2.466
40% (7.2mm) S1	3.763	1.288	0.780
40% (7.2mm) S2	3.706	1.024	0.855
60% (4.8 mm) S1	3.726	2.909	1.466
60% (4.8 mm) S2	3.582	2.372	1.086

Table 5.16: Comparison of experimental and theoretical results for time of flight in through transmission

THEORETICAL RESULTS			
Fault location – L/2	**Time (sec)**		
	1st peak	**2nd peak**	**3rd peak**
Healthy specimen	3.950×10^{-4}	1.185×10^{-3}	1.975×10^{-3}
Cracked specimen	3.950×10^{-4}	7.899×10^{-4}	1.185×10^{-3}
EXPERIMENTAL RESULTS			
Area Reduction	**1st peak**	**2nd peak**	**3rd peak**
Healthy specimen (0 %)	4.080×10^{-4}	1.205×10^{-3}	2.025×10^{-3}
20 %	4.080×10^{-4}	7.883×10^{-4}	1.130×10^{-3}
40 %	3.789×10^{-4}	7.793×10^{-4}	1.150×10^{-3}
60 %	3.772×10^{-4}	7.603×10^{-4}	1.14×10^{-3}

Table 5.17: Amplitude of first and second echo in pulse echo method

Amplitude (Pk-Pk)		
Area Reduction	**1st peak**	**2nd peak**
0% (12 mm) S1	2.684	1.684
0% (12 mm) S2	3.679	1.982
20% (9.6 mm) S1	1.676	3.651
20% (9.6 mm) S2	1.366	3.486
40% (7.2mm) S1	2.586	1.344
40% (7.2mm) S2	2.630	1.870
60% (4.8 mm) S1	3.566	1.167
60% (4.8 mm) S2	3.229	0.940

Table 5.18: Comparison of experimental and theoretical results for time of flight in pulse echo

THEORETICAL RESULTS		
Fault location – L/2	**Time (sec)**	
	1st Echo	**2nd Echo**
Healthy specimen	7.899×10^{-4}	1.580×10^{-3}
Cracked specimen	3.950×10^{-4}	7.899×10^{-4}
EXPERIMENTAL RESULTS		
Area Reduction	**1st Echo**	**2nd Echo**
Healthy specimen (0%)	7.577×10^{-4}	1.514×10^{-3}
Cracked specimen (20%)	4.495×10^{-4}	7.645×10^{-4}
40 %	3.835×10^{-4}	7.626×10^{-4}
60 %	3.783×10^{-4}	7.569×10^{-4}

This chapter details the experimental results obtained for pulse echo and through transmission through extruded mild steel rods of 0.81m, 1.0m, 1.5m and 2.0m bar length. The analytical verification of the results was carried out using ABAQUS/Explicit and is discussed in next chapter.

CHAPTER 6

STRESS WAVES IN ISOTROPIC SOLIDS - MODELING AND ANALYSIS

This chapter discusses about the numerical modelling of the stress waves in isotropic solids. The numerical model is generated using a finite element tool- ABAQUS/Explicit. An isotropic beam is modelled for the simulations. The details of model and elements used are described in the following sections.

6.1 Brief introduction about ABAQUS/Explicit

A complete ABAQUS/Explicit analysis usually consists of three distinct stages: preprocessing, simulation, and post processing. These three stages are linked together by files as shown below:

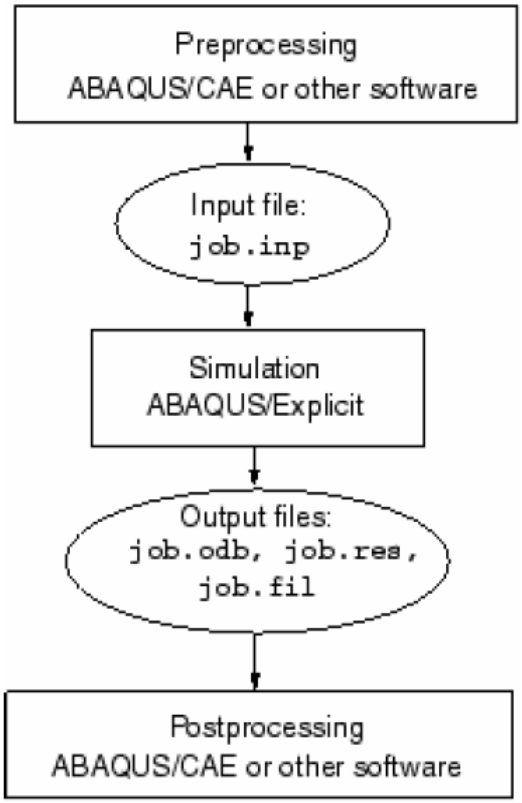

6.2 Types of problems suited in ABAQUS/Explicit

- High-speed dynamic events
- Complex contact problems
- Complex post buckling problems
- Highly nonlinear quasi-static problems
- Materials with degradation and failure

6.3 Finite element method for explicit dynamics

ABAQUS includes two libraries of solid elements, CAX and CGAX, whose geometry is axisymmetric (bodies of revolution) and which can be subjected to axially symmetric loading conditions. In addition, CGAX elements support torsion loading. As a result, CGAX elements will be referred to as generalized axisymmetric elements, and CAX elements as torsionless axisymmetric elements. In both cases, the body of revolution is generated by revolving a plane cross-section about an axis (the symmetry axis) and is readily described in cylindrical polar coordinates r, z, and θ. The radial and axial coordinates of a point on this cross-section are denoted by rand z, respectively. At θ=0, the radial and axial coordinates coincide with the global Cartesian X- and Y-coordinates.

If the loading consists of radial and axial components that are independent of θ and the material is either isotropic or orthotropic, with θ being a principal material direction, the displacement at any point will only have radial (u_r) and axial (u_z) components and the only stress components that will be nonzero are σ_{rr}, σ_{zz}, $\sigma_{\theta\theta}$, and σ_{rz}. Moreover, the deformation of any r–z plane completely defines the state of strain and stress in the body. Consequently, the geometric model is described by discretizing the reference cross-section at θ=0.

If one allows for a circumferential component of loading (which is independent of θ) and for general material anisotropy, displacements and stress fields become three-dimensional, but the problem remains axisymmetric in the sense that the solution does not vary as a function of θ and the deformation of the reference r–z cross-section still characterizes the deformation in the entire body. The motion at any point will have, in addition to the aforementioned radial and axial displacements, a twist φ (in radians) about the z-axis, which is independent of θ.

6.4 Description about continuum axisymmetric elements CAX4R

CAX4R- 4- noded bilinear axisymmetric quadrilateral, reduced integration, hourglass control

Active degree of freedom- u_r, u_z, φ

Node ordering and face numbering on elements

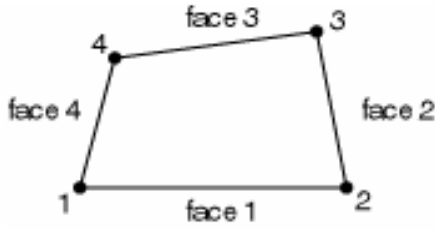

Numbering of integration points for output

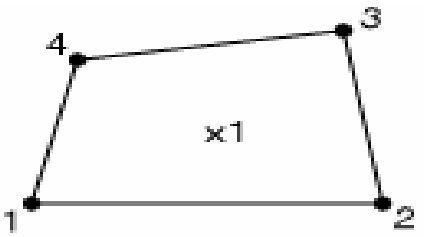

6.5 Type of applied loading

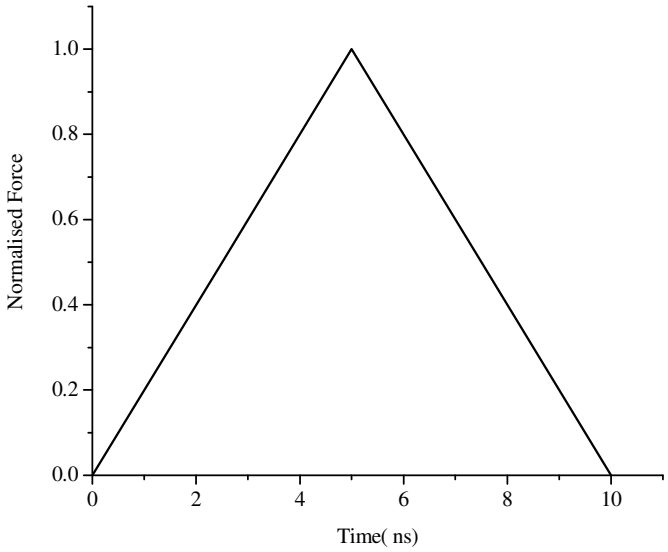

6.6 Finite element modeling

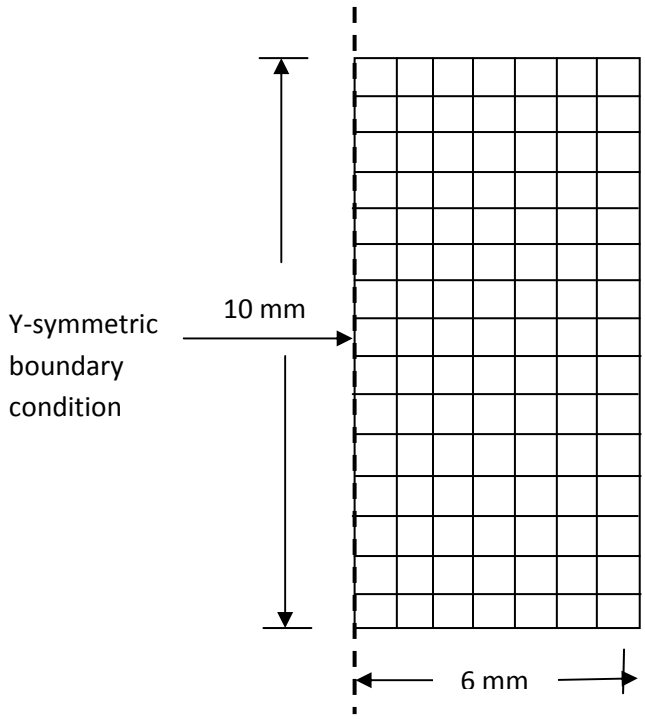

Figure 6.1: Meshing of model (isotropic) used for analysis

As we have discussed in previous chapter a uniform isotropic steel bar is considered for the experimental investigations of wave propagation. The numerical model for this bar is generated for its finite element analysis. A commercial software ABAQUS/Explicit is used to get analytical results. **Figure.6.1** shows the meshed model of steel bar used for numerical analyses. The bar is divided into small elements, square in shape.

6.7 *Details of model*

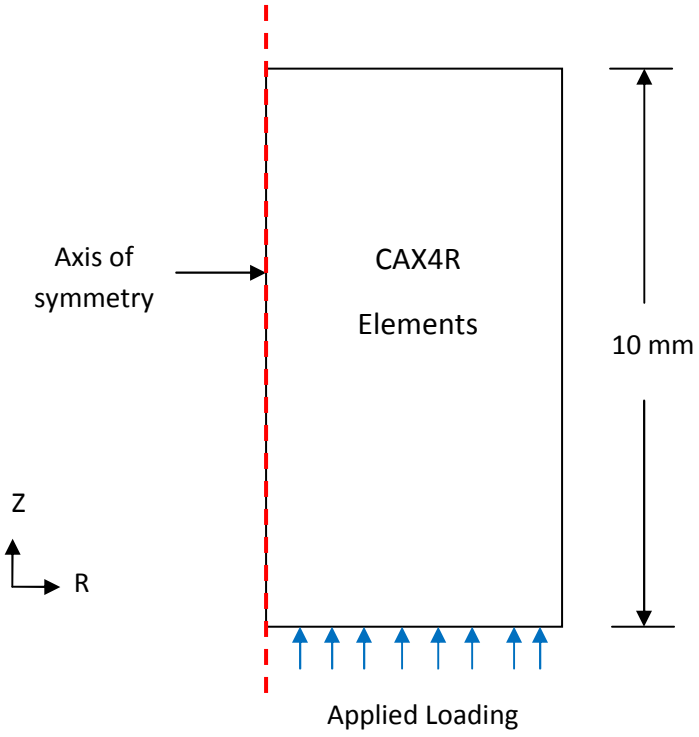

Figure 6.2: Model (isotropic) used for analysis in ABAQUS/Explicit

A uniform rod made of steel is considered for the analysis. The z-axis is made as the axis of symmetry. The model is meshed with axisymmetric four noded elements i.e. CAX4R in ABAQUS/Explicit.

A uniform pressure load is applied to the bar. Variation of the load is triangular considering the rise time and fall time of the signal. The duration of the pulse is set as 10 nS.

Details of the model:

Length of the bar element = 10 mm

Element size = 0.05 mm * 0.05 mm

Depth = 6 mm

Pulse Duration = 10 ns

Pulse Shape = triangular

6.8 Beam with crack

The above model is also analysed for damaged condition. A crack is modeled at the centre of the beam having varying depth. Three different crack depths were modeled with width of 0.05mm. The depth of the crack was varied from 20%-60% of the bar depth. **Figure 6.3** shows the details of the beam model with crack. The crack in this model is 0.05mm wide and 1.2mm deep.

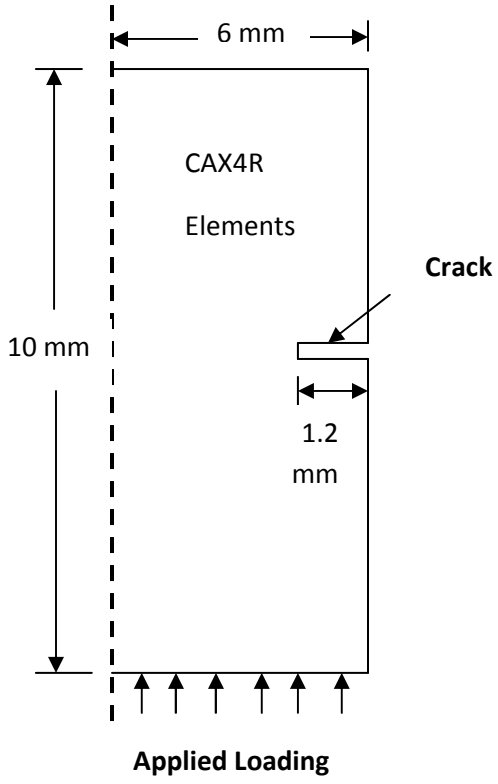

Figure 6.3: Model with crack used for analysis in ABAQUS/Explicit

After the generation of the models the analyses were carried out for different cases and the analytical results were obtained. The signatures obtained are analyzed and studied carefully.

6.9 Analytical results

- **Healthy specimen**

The theory of stress waves of elastic media shows that in an infinite isotropic elastic solid a disturbance is propagated by means of three types of bulk waves, longitudinal (P) waves, shear vertical (SV), and shear horizontal (SH) waves, each traveling with its own constant velocity. Longitudinal waves are fastest of all and hence they reach earlier to the sensor and are sensed first.

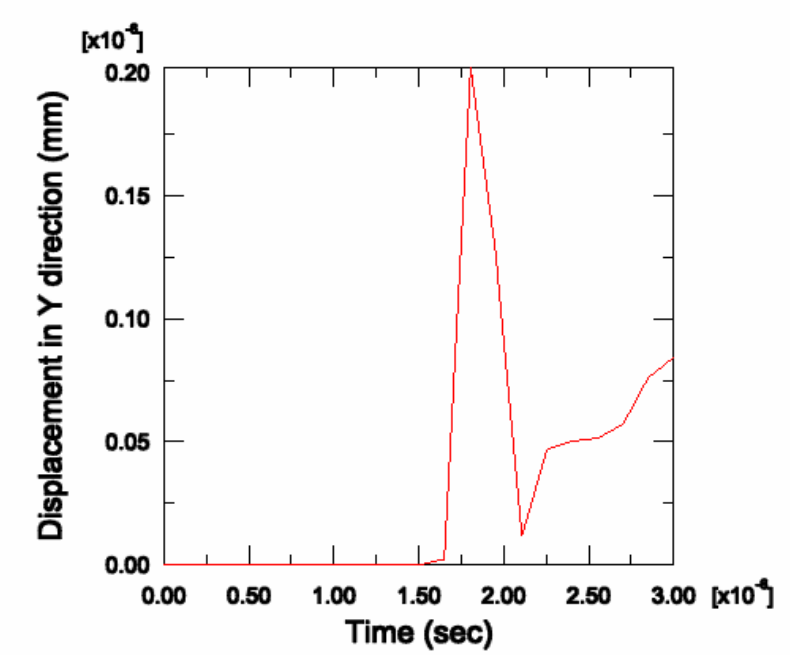

Figure 6.4: Graph of displacement in Y-direction vs time for bar length 10 mm

Here it can be seen from the graph that arrival time of the wave in case of displacement in y-direction is 1.85e-6 S. The wave velocity through steel can be analytically calculated by the following formula

$$C = \sqrt{E/\rho} \qquad (6.1)$$

By this formula the actual velocity of the waves through steel comes out to be 5063 m/s and from this velocity time of flight can be calculated which comes out to be 1.97e-6 S. This approximately matches with the results from graph.

- **Specimen with crack**

Here also one can see from the graph that the arrival time of first peak is same as that in healthy specimen irrespective of the crack depth. This matches with our experimental results of through transmission.

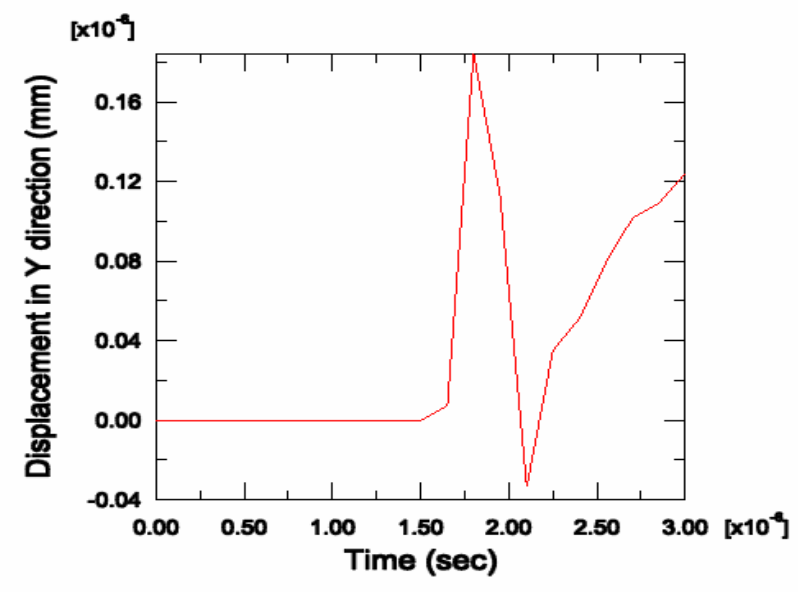

Figure 6.5: Graph of displacement in Y-direction vs time for cracked specimen of 20% area reduction

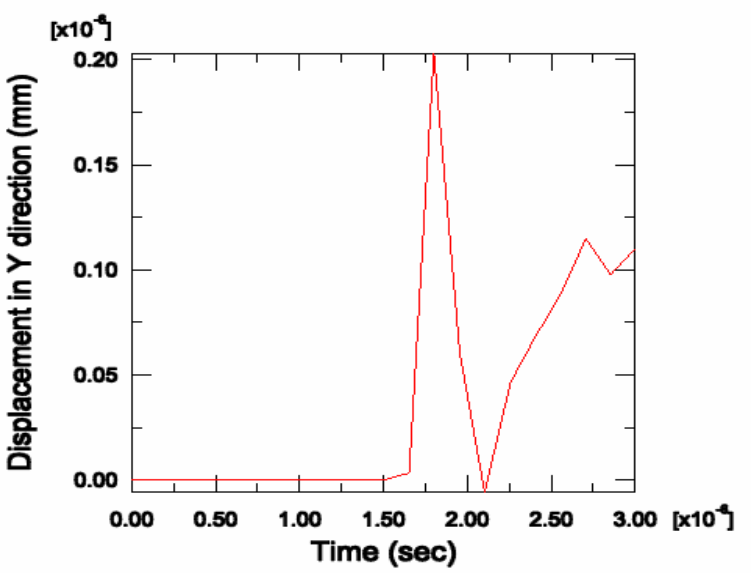

Figure 6.6: Graph of displacement in Y-direction vs time for cracked specimen of 40% area reduction

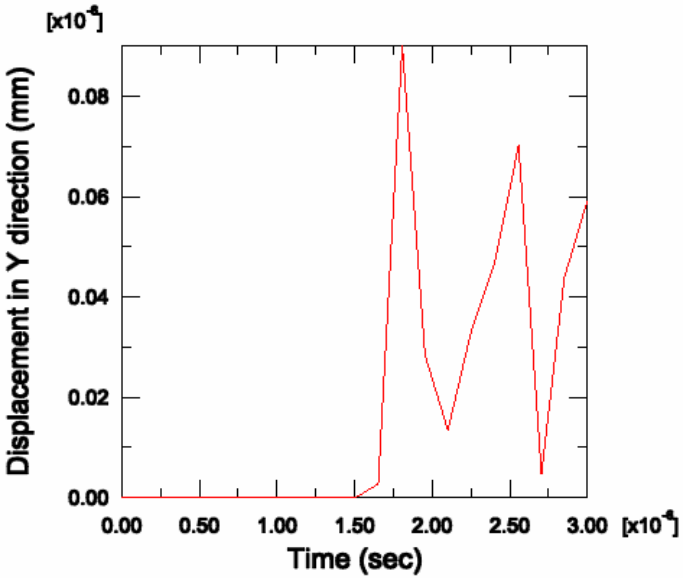

Figure 6.7: Graph of displacement in Y-direction vs time for cracked specimen of 60% area reduction

Table 6.1: Comparison of theoretical results with analytical results

	Time (sec)
Theoretical results	**1st peak**

Healthy specimen	$1.975x\ 10^{-6}$
Cracked specimen	$1.975x\ 10^{-6}$
Analytical results	
Area Reduction	**1^{st} peak**
Healthy specimen (0 %)	$1.80x\ 10^{-6}$
20 %	$1.85x\ 10^{-6}$
40 %	$1.85\ x\ 10^{-6}$
60 %	$1.85\ x\ 10^{-6}$

CHAPTER 7

DISCUSSION OF RESULTS AND CONCLUSIONS

7.1 Observation from Pulse Echo method

The measured amplitude and time of flight in case of Pulse echo method can be used to find the exact location of the crack. The magnitude or amplitude of the peak received after reflecting from the crack boundary relates the amount of defect. It was observed that the amplitude of first peak received from the crack increased with the increase in % of area reduction and the amplitude of first back wall echo (BWE) reduced with the increase in the amount of defect.

The time at which the first echo was received tells us the location at which crack/defect is present in the specimen. The exact location of the crack can be known by knowing the time of flight of first echo irrespective of the location of the crack as it was varied at L/2, L/3 and 2L/3 locations along the specimen.

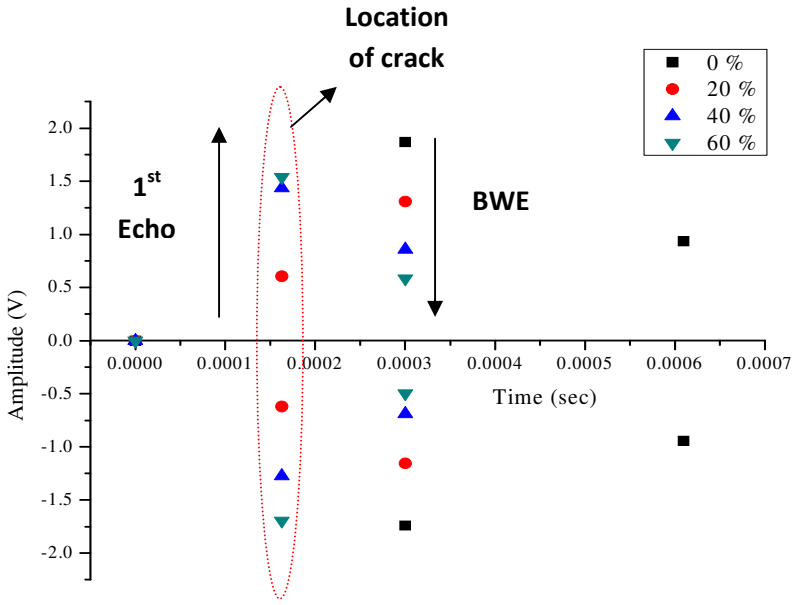

Figure 7.1: Graph showing pick peaks in pulse echo through 0.81m bars

As we can see in the **figure 7.1, figure 7.2** and **figure 7.3** the amplitude of first peak is increasing with the increase in the % area reduction and that of second peak is decreasing. The peaks were obtained by peak picking over the time period. The same trends were seen in 1.0m, 1,5m and 2.0m bars.

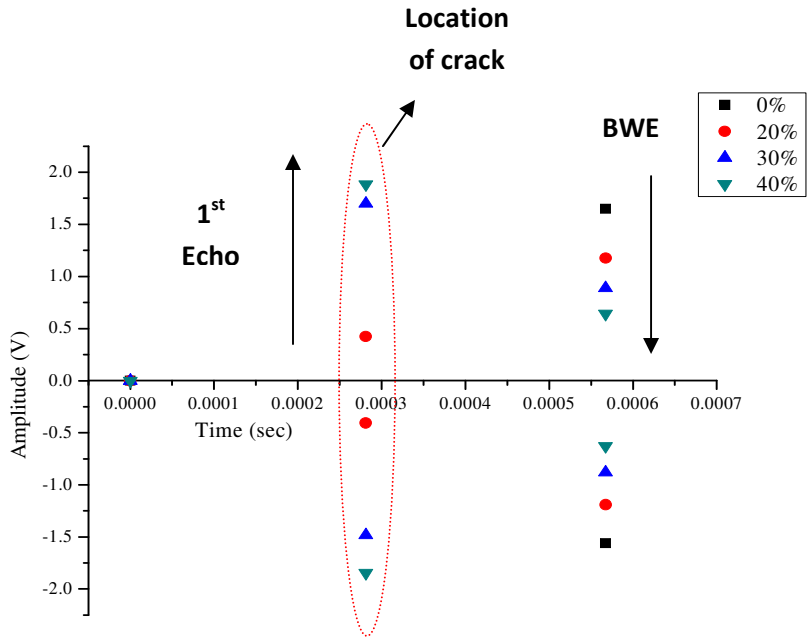

Figure 7.2: Graph showing pick peaks in pulse echo through 1.5 m bars

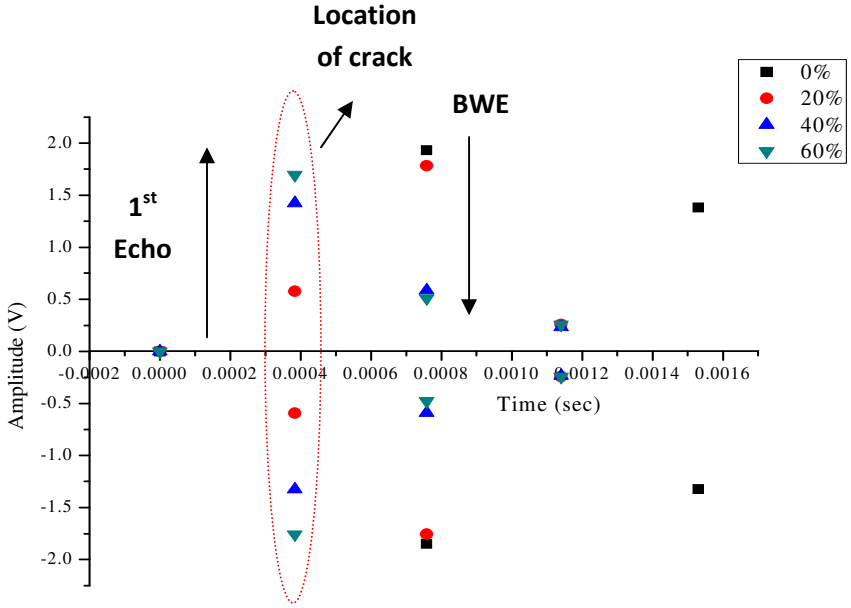

Figure 7.3: Graph showing pick peaks in pulse echo through 2.0 m bars

The parametric study carried out could be justified by the results obtained and as can be seen from the **figure 7.4** below. In case of pulse echo it could be seen that the amplitude of first echo reflected from the crack boundary is increasing with the increase in area reduction and that of BWE decreases with the increase in area reduction as more energy is reflected from the crack itself as compared to back wall.

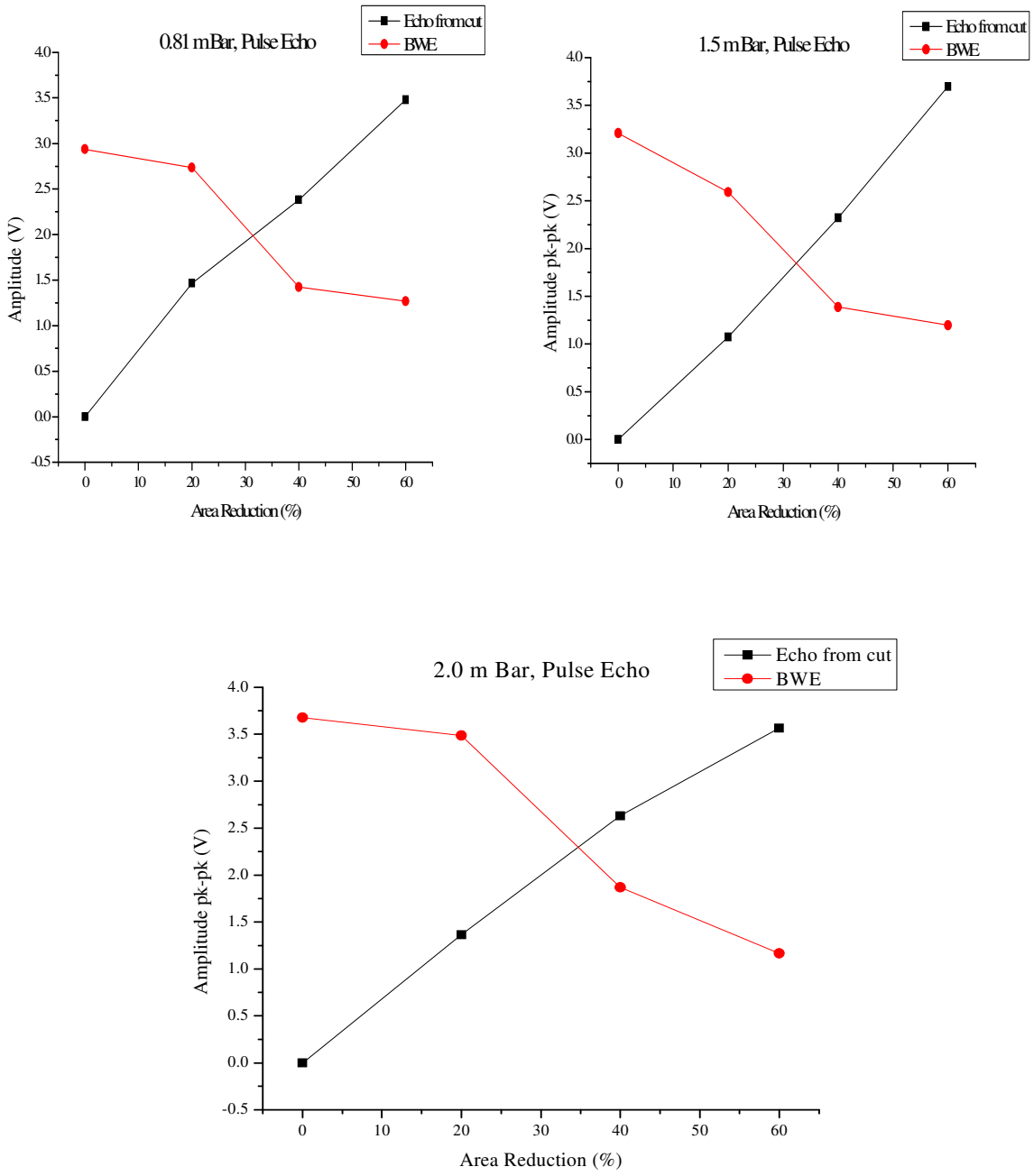

Figure 7.4: Graph showing the trend of 1st and 2nd echo through 0.81m, 1.5m and 2.0 m bars.

7.2 Observation from Through Transmission method

In through transmission the amplitude of the second peak received after reflecting from the crack boundary can be used to define the amount of defect in the specimen. It was observed that amplitude of the second peak increased with the increase in % area reduction signifying the increase in the defect in the specimen as shown in **figure 7.5, figure 7.6** and **figure 7.7**. Also the time flight of first peak can be used to know the length of the specimen and that of second peak the location of defect/damage.

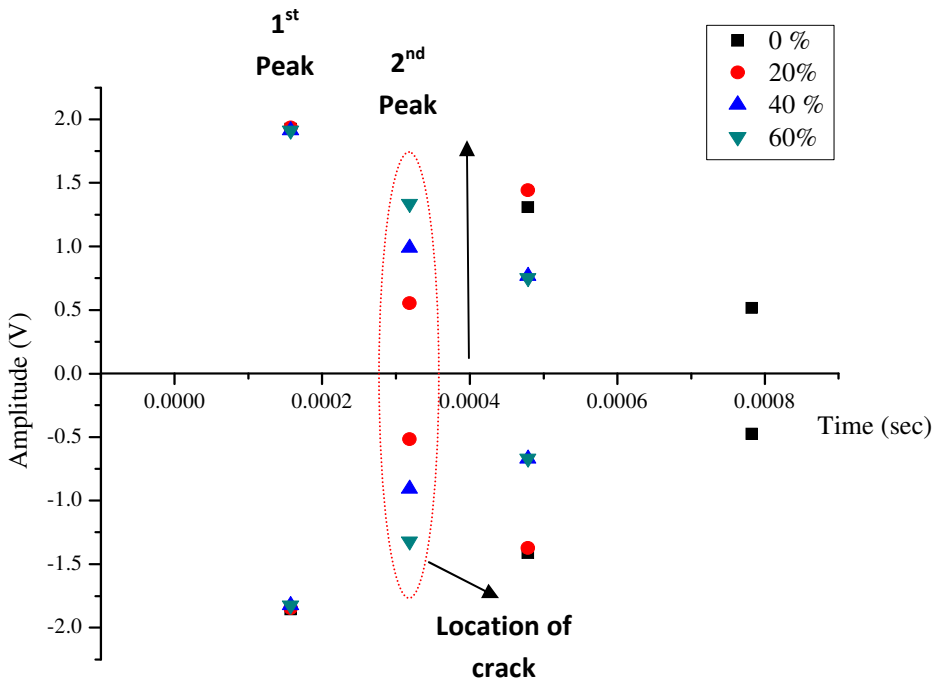

Figure 7.5: Graph showing pick peaks in through transmission along 0.81 m bars

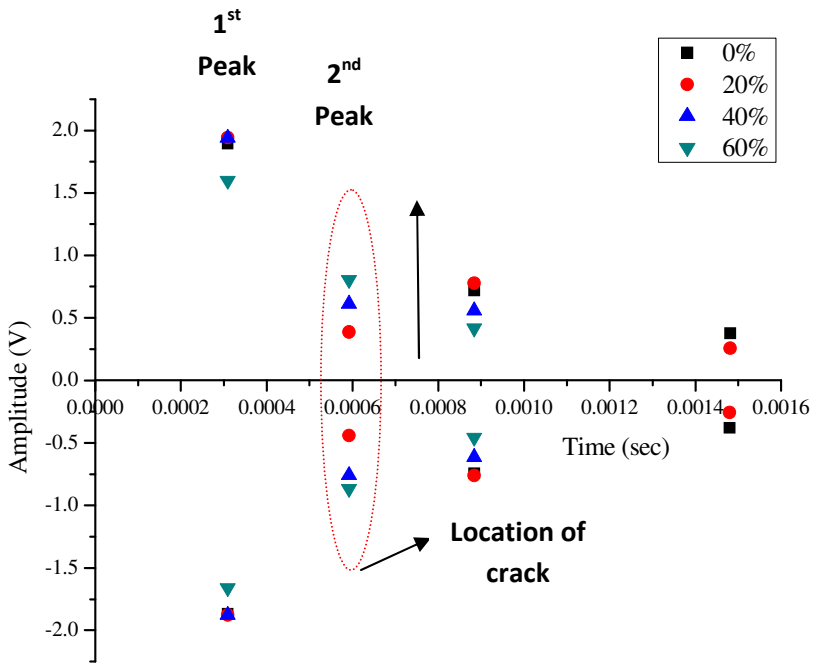

Figure 7.6: Graph showing pick peaks in through transmission along 1.5 m bars

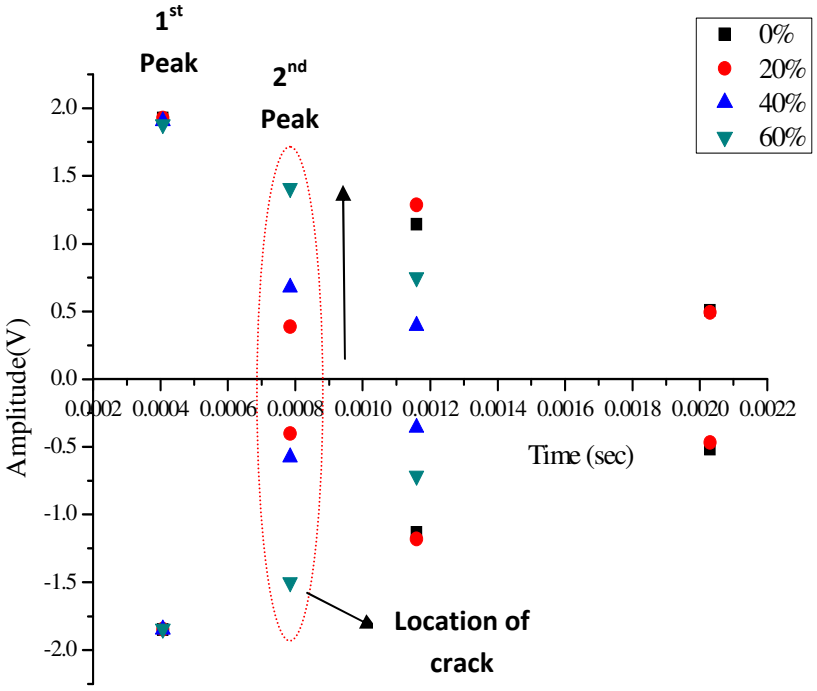

Figure 7.7: Graph showing pick peaks in through transmission along 2.0 m bars

In through transmission it was observed that the amplitude of the first peak remained almost same for all the specimens irrespective of the length and area reduction of the crack as shown in **figure 7.8**. The amplitude of the second peak increased with increase in area reduction as described earlier.

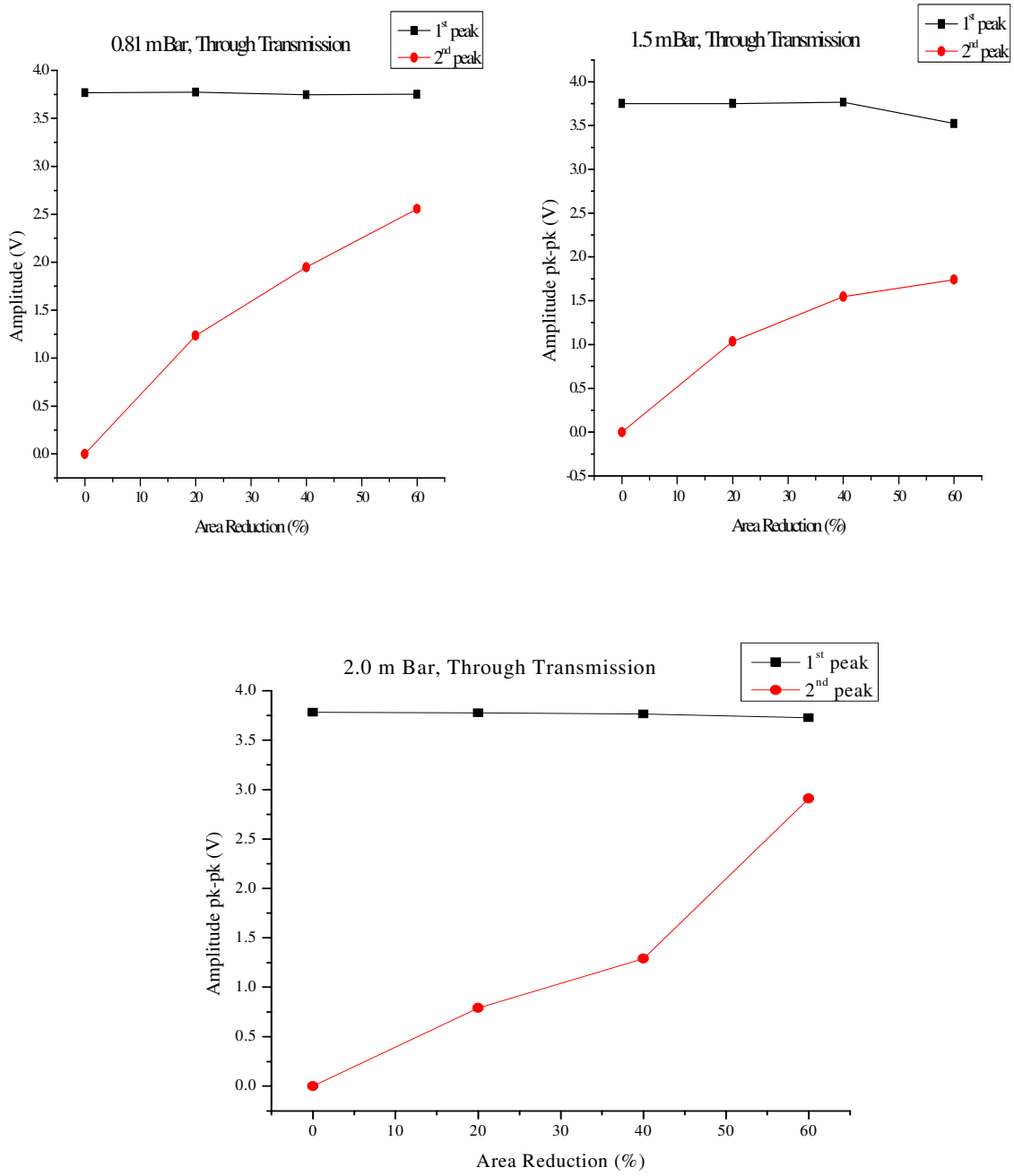

Figure 7.8: Graph showing the trend of 1st and 2nd peak through 0.81m, 1.5m and 2.0 m bars.

7.3 Future scope of work

The area of nondestructive testing and damage detection constitutes the extremely important and challenging area of study where wave propagation provides an efficient means of characterizing defects in structures. As the topic of wave propagation is very wide spread and has utilities in many areas of human endeavor, there is much scope for future work.

The experimentation carried out can be extended for:

- The reinforcing bars embedded in concrete to model the real life problem of corrosion
- The rolled mild steel bars instead of extruded bars as used in present study
- To detect the effect on wave propagation due to delamination or disbonding between concrete and reinforcing bars
- The detection of multiple cracks in reinforcing bars and also in pretensioning tendons

REFERENCES

Abrahams, I. D., Wickham, G. R., (1992), "*Scattering of elastic waves by a small inclined surface-breaking crack",* Journal of Mech. Phys. Solids, 40(8), 1707-1733

B.A. Auld, "*Acoustic Fields and Waves in Solids"*, Vols. I & II, Krieger Publishing Company, Malabar, FL, 1990.

Beard M.D., Lowe M.J.S. (2003) "*Non-destructive testing of rock bolts using guided ultrasonic waves",* International Journal of Rock Mechanics & Mining Sciences 40 (2003) 527–536

Boller C., "*Structural health management of ageing aircraft and other infrastructure*", Monograph on structural health monitoring, Institute of smart structures and systems (ISSS), pp. 1-59.

Bertram, A**.** A., Dale, E. C., Peter, J. S., (1996), "*Shear horizontal wave propagation in periodically layered composites"*, IEEE transactions on ultrasonics, ferroelectrics, and frequency control, 43(2), 319-325

Biwa, S., Yamamoto, S., Kobayashi, F., Ohno, N., (2004), "*Computational multiple scattering analysis for shear wave propagation in unidirectional composites*", International Journal of Solids and Structures, 41, 435–457

Bruck, H. A., (2000), "*A one-dimensional model for designing functionally graded materials to manage stress waves*", International Journal of Solids and Structures, 37, 6383-6395.

Bhalla, S., Soh, C.K., Liu, Z., "*Wave propagation approach for NDE using surface bonded piezoceramics*", NDT&E International 38 (2005) 143-150.

Baranio, Giulia. Berra, Mario. Bertolini, Luca. Pastore, Tommaso., (1996,a),Steel corrosion monitoring in normal and total lightweight concretes exposed to chloride and sulphate solutions Part I : Potential Measurements, C*ement and Concrete Research*, Vol 26, No 5,683-689

Baranio, Giulia. Berra, Mario. Bertolini, Luca. Pastore, Tommaso., (1996,b), Steel corrosion monitoring in normal and total lightweight concretes exposed to chloride and sulphate solutions Part II : Polarisation Resistance Measurements, *Cement and Concrete Research*, Vol 26,No 5, 683-689.

Biwa, S., Yamamoto, S., Kobayashi, F., Ohno, N., (2004), Computational multiple scattering analysis for shear wave propagation in unidirectional composites, *International Journal of Solids and Structures*, 41, 435–457

Broomfield, John., Davies, Kevin,. Hladky, Karel., (2002),The use of permanent corrosion monitoring in new and existing reinforced concrete structures,*Cement and Concrete Composites*, 24, 27-34.

Bruck, H. A., (2000), A one-dimensional model for designing functionally graded materials to manage stress waves, *International Journal of Solids and Structures*, 37, 6383-6395

Deng, X., Wang,Q., Giurgiutiu,V., "*Structural health monitoring using active sensors and wavelet transforms*", SPIE's 6th Annual international symposium on smart structures and materials,1-5 march 1999.

Doyle, J. F., (1989) Wave propagation in structures, Springer, New York.

E, Scarpetta and M.A. Sumbatyan, "*Wave penetration through elastic solids with a periodic array of rectangular flaws"*, *Meccanica* 36, 191-199, (2001).

E. Scarpetta and M. A. Sumbatyan, "*On wave propagation in elastic solids with a doubly periodic array of cracks"*, *Wave Motion* 25 (1997) 61–72.

Elsener,B.,(2002), Macrocell corrosion of steel in concrete-implications for corrosion monitoring, *Cement and Concrete Composites*, 24, 65-72.

Fromme.P, Wilcox, P.D. and Lowe, M.J.S., "*On the sensitivity of corrosion and fatigue damage detection using guided ultrasonic waves*", 2004 IEEE Ultrasonics Symposium.

G.R. Liu, J.D. Achenbach, *"Strip element method for stress analysis of anisotropic linearly elastic solids"*, ASME Journal of Applied Mechanics 61 (1994) 270–277.

Glass, G.K. Page, C.L. Short, N.R. Yu, S.W.,(1993) An Investigation of Galvanostatic Transient Methods to monitor corrosion rate of steel in concrete, *Corrosion Science*, Vol 35,No 5, 1585-1592

Gandhe, D.,Mukherjee, A(2006) "*Detection of surface crack by stress wave propagation"* (M.Tech Thesis, IIT Mumbai)

Gilchrist, M. D., (1999), "*Attenuation of ultrasonic Rayleigh-Lamb waves by small horizontal defects in thin aluminium plates*", International Journal of Mechanical Sciences, 41, 581-594

Giurgiutiu, V., "*Lamb wave generation with piezoelectric wafer active sensors for structural health monitoring*", proceedings of the SPIE's 10th International Symposium on smart structures and materials, 2-6 March 2002.

Giurgiutiu, V., "*Tuned lamb wave excitation and detection with piezoelectric wafer active sensors for structural health monitoring*", Journal of Intelligent Material Systems and Structures, Vol. 16, April 2005.

Giurgiutiu, V., Bao,J., and Zhao,W.,(2001), "*Active sensor wave propagation health monitoring of beam and plate structures"*, proceedings of the SPIE's 8th International Symposium on smart structures and materials,4-8 March 2001.

Iyer,S.,(2002) *Evaluation of ultrasonic C-scan imaging to detect corrosion and voids in post-tensioning tendon*s, M S.Thesis, The Pennsylvania State University

J. Wang, J. Lin, "*A Two-dimensional theory for surface acoustic wave analysis in finite piezoelectric solids"*, Journal of Intelligent Materials and Structure Systems 16 (2005).

J. Wang, K.-Y. Hashimoto, "*A two-dimensional theory for the analysis of surface acoustic waves in anisotropic elastic solids"*, Proceedings of 2003 IEEE International Ultrasonics Symposium, Honolulu, Hawaii, October 5–8, 2003.

Joshi, S., Mukherjee, A., and Schmauder S., (2003), "*Numerical characterization of functionally graded active materials under electrical and thermal fields*", *Smart Materials and Structures, 12, 571-579.*

K.F. Graff, "*Wave Motion in Elastic Solids"*, Dover, New York, 1991.

Krautkramer J and Krautkramer H, *"Ultasonic Testing of Materials"*, Spinger verlag, Berlin (1993).

Krawczuk, M., Palacz, M., Ostachowicz, W., (2004), "*Wave propagation in plate structures for crack detection"*, Finite Elements in Analysis and Design, 40, 991–1004

Kundu, T.,Ed (2003) "*Ultrasonic Nondestructive Evaluation: Engineering and Biological Material Characterization"* (CRC Press, Boca Raton, Florida)

Lima, W. J. N., Hamilton, M.F., (2003), "*Finite-amplitude waves in isotropic elastic plates"*, Journal of Sound and Vibration, 265, 819–839

Mal, A. K., (1988), "*Guided waves in layered solids with interface zones*", International Journal of Engineering and Science, 26(8), 873-881

Mal, A., (2002), "*Elastic waves from localized sources in composite laminates*", International Journal of Solids and Structures, 39, 5481–5494

Omote R., Kawashima, K., and Ito,T., "*Simulation of Nonlinear Rayleigh Wave Propagation through Minute Surface Crack*", 2001, IEEE Ultrasonics Symposium.

Park. Zin-Taek, Choi. Yoon-Seok, Kim. Jung-Gu, Chung. Lan,(2005) Development of galvanic sensor system for detecting corrosion damage of steel embedded in concrete structures Part 2. Laboratory electrochemical testing of sensors in concrete, Cement and Concrete Research, 35, 1814-1819

R.D. Mindlin, "*An Introduction to the Mathematical Theory of Vibrations of Elastic Plates*", US Army Signal Corps Engineering Laboratories, Fort Monmouth, NJ, 1955.

Rens, K.L., Transue, D.J., Schuller, M.P., (2000), Acoustic tomographic imaging of concrete infrastructure, *ASCE J.Infrastructure System*s, 6(1), 10-23

Samadhiya, R. and Mukherjee,A (2006*)"Functionally graded piezoceramic ultrasonic transducers",* Smart Materials and Structures.

Sathiyanarayanan. S, Natrajan. Panjali, Saravanan. K. Srinivasan. S, Venkatachari. G,(2006), Corrosion Monitoring of steel in concrete by galvanostatic pulse technique, Cement and Concrete Composites, 28, 630-637

Sharma, J. N., Singh, D., Rajneesh Kumar, (2004), "*Propagation of Generalized Viscothermoelastic Rayleigh–Lamb Waves In Homogeneous Isotropic Plates*", Journal of Thermal Stresses, 27, 645–668

Sun, H.M., Wang, J.B., Pan, J., "*An effective algorithm for simulating acoustical wave propagation"*, Computer physics communications 151 (2003) 241-249.

V. N. Bindal, "*Transducers for ultrasonic flaw detection*", NPH, 1999

Y. C. Angel and J. D. Achenbach, "*Harmonic waves in an elastic solid containing a doubly periodic array of cracks"*, *ibid.* 9 (1987).

Yang, S., Yuan, F. G., (2005), "*Transient wave propagation of isotropic plates using a higher-order plate theory*", International Journal of Solids and Structures*,* 42, 4115–4153

Yang, C., Lin Ye, Su,Z., Bannister, M., "*Some aspects of numerical simulation for lamb wave propagation in composite laminates"*, Composite structures 75 (2006) 267-275.

REFERENCES

1. Abrahams, I. D., Wickham, G. R., (1992), "*Scattering of elastic waves by a small inclined surface-breaking crack*", Journal of Mech. Phys. Solids, 40(8), 1707-1733.
2. Alleyne, D.N. (1991), "*The non destructive testing of plates using ultrasonic lamb waves*", PhD dissertation, Imperial college of science, technology and medicine, University of London.
3. Beard, M.D., (2002) "*Guided wave inspection of embedded cylindrical structures"*, PhD. dissertation, Imperial college of science, technology and medicine, University of London.
4. Baranio, Giulia. Berra, Mario. Bertolini, Luca. Pastore, Tommaso, (1996, a),"*Steel corrosion monitoring in normal and total lightweight concretes exposed to chloride and sulphate solutions Part I: Potential Measurements*", Cement and Concrete Research, Vol 26, No 5,683-689.
5. Biwa, S., Yamamoto, S., Kobayashi, F., Ohno, N., (2004), "*Computational multiple scattering analysis for shear wave propagation in unidirectional composites*", International Journal of Solids and Structures, 41, 435–457
6. Bruck, H. A(2000) *"A one-dimensional model for designing functionally graded materials to manage stress waves"*, International Journal of solids and Structures, 37, 6383-6395
7. Deng, X., Wang, Q., Giurgiutiu, V., (1999), "*Structural health monitoring using active sensors and wavelet transforms"*, SPIE's 6th Annual International Symposium on Smart Structures and Materials, 1-5 March.
8. Demma, A., (2003), "*The interaction of guided waves with discontinuities in structures*", Phd. dissertation, Imperial college of science, technology and medicine, University of London.
9. Doyle, J. F(1989), *Wave propagation in structures*, Springer, New York
10. Doyle, P.A., (1978), Scala, C.M., "*Crack depth measurement by ultrasonics- a review*", Ultrasonics, July.

11. E. Scarpetta and M. A. Sumbatyan, (1997), "*On wave propagation in elastic solids with a doubly periodic array of cracks"*, Wave Motion 25, 61–72.
12. Elsener,B.,(2002), "*Macrocell corrosion of steel in concrete-implications for corrosion monitoring"*, Cement and Concrete Composites, 24, 65-72.
13. Gandhe, D., Mukherjee, A(2006) "*Detection of surface crack by stress wave propagation"* (M.Tech Thesis, IIT Mumbai)
14. Glass, G.K. Page, C.L. Short, N.R. Yu, S.W., (1993) "*An Investigation of Galvanostatic Transient Methods to monitor corrosion rate of steel in concrete*", *Corrosion Science*, Vol. 35, No 5, 1585-1592.
15. Giurgiutiu, V., Bao, J., Zhao, W., (2001), "*Active sensor wave propagation health monitoring of beam and plate structures"* SPIE's 8th International Symposium on Smart Structures and Materials, 4-8 March.
16. Iyer,S.,(2002) "*Evaluation of ultrasonic C-scan imaging to detect corrosion and voids in post-tensioning tendon*s", M S.Thesis, The Pennsylvania State University
17. Iyer, S., Schokker, Andrea J., Sinha, SunilK., (2002), "*Ultrasoinc imaging – A novel way to investigate corrosion status in post-tensioned concrete member*s", 197 J. Indian Inst. Sci., 82, 197–217.
18. Joshi, S., Mukherjee, A., and Schmaudar S (2003) *"Numerical characterization of functionally graded active materials under electrical and thermal fields"*, Smart Materials and Structures, 12, 571-579
19. K.F. Graff, "*Wave Motion in Elastic Solids"*, Dover, New York, 1991.
20. Krautkramer J and Krautkramer H, *"Ultasonic Testing of Materials"*, Spinger verlag, Berlin (1993).
21. Kundu, T.,Ed (2003) "*Ultrasonic Nondestructive Evaluation: Engineering and Biological Material Characterization"* (CRC Press, Boca Raton, Florida)
22. Krawczuk, M., Palacz, M., Ostachowicz, W., (2004), "*Wave propagation in plate structures for crack detection*", Finite Elements in Analysis and Design, 40, 991–1004
23. Mukherjee, A., Schmauder, S., Soni, S.S., (2005)"*Stress Waves in Functionally Graded Materials"* M.Tech dissertation at IIT Bombay.

24. Na, W.B., Kundu, T., Ehsani, M.R., (2005), "*Lamb waves for detecting delamination between steel bars and concrete"* Engineering Materials Vols. 293-294, pp 49-62.

25. Na, W.B., Kundu, T., (2003), "*Inspection of interfaces between corroded steel bars and concrete using the combination of a piezoelectric-zirconate titanate transducer and an electromagnetic acoustic transducer*", Society for Experimental Mechanics, Vol. 43, No. 1, March.

26. Omote, R., Kawashima K., Ito, T., (2001), "*Simulation of non linear Rayleigh wave propagation through minute surface cracks*", IEEE ultrasonic symposium 717-720.

27. Pavlakovik, B.N., Lowe, M.J.S., Cawley, P., (2001), "*High frequency low loss ultrasonic modes in imbedded bars",* Journal of Applied Mechanics, January, Vol. 68.

28. Park. Zin-Taek, Choi. Yoon-Seok, Kim. Jung-Gu, Chung. Lan, (2005) "*Development of galvanic sensor system for detecting corrosion damage of steel embedded in concrete structures Part 2. Laboratory electrochemical testing of sensors in concrete*," Cement and Concrete Research, 35, 1814-1819

29. Reis, H., Ervin, B.L., Kuchma, D.A., Bernhard, J.T., (2005), "*Estimation of corrosion damage in steel reinforced mortar using guided waves"*, Journal of Pressure Vessel Technology, August, Vol. 127 / 255.

30. Rose, J.L., (2004), "*Ultrasonic guided wave in structural health monitoring",* Engineering Materials Vols. 270-273, pp 14-21.

31. Samadhiya, R. and Mukherjee,A (2006*)"Functionally graded piezoceramic ultrasonic transducers",* Smart Materials and Structures

32. Sathiyanarayanan. S, Natrajan. Panjali, Saravanan. K. Srinivasan. S, Venkatachari. G, (2006), "*Corrosion Monitoring of steel in concrete by galvanostatic pulse technique*", Cement and Concrete Composites, 28, 630-637.

33. Sekhar, A.S., (2008), "*Multiple crack effects and identification*", Mechanical Systems and Signal Processing 22, 845–878.

34. Siqueira, M.H.S., Gatts, C.E.N., Silva, R.R., Rebello, J.M.A., (2004), "*The use of ultrasonic guided waves and wavelet analysis in pipe inspection"*, Ultrasonics 41, 785–797.

35. Schmerr, L. W (1998) "*Fundamental of Ultrasonic Nondestructive Evaluation-A Modeling Approach"* (Plenum Press, New York)

36. Staszewsky, W.J., (2005), "*Ultasonic/Guided waves for structural health monitoring"*, Engineering Materials Vols. 293-294, pp 49-62

37. Song, H.W., Saraswathy, V., (2007), "*Corrosion monitoring of reinforces structures-A review",* International journal of Electrochemical science, 2, 1- 28.